Studies for Io's Extended Atmosphere and Neutral Clouds and Their Impact on the Local Satellite Atmosphere and on the Planetary Magnetosphere

William H. Smyth

Atmospheric and Environmental Research, Inc.

840 Memorial Drive

Cambridge, Massachusetts 02139-3794

December 9, 1993

Final Report for the Period

December 10, 1992 to December 9, 1993

Prepared for

NASA Headquarters

TECHNICAL REPORT STANDARD TITLE PAGE

1. Report No	2. Government Accession No	3. Recipient's Catalog No.

4. Title and Subtitle	5. Report Date
Studies for Io's Extended Atmosphere and Neutral Clouds and Their Impact on the Local Satellite Atmosphere and on the Planetary Magnetosphere	December 1993
	6. Performing Organization Code
7. Author(s)	8. Performing Organization Report No
William H. Smyth	
9. Performing Organization Name and Address	10. Work Unit No.
Atmospheric and Environmental Research, Inc. 840 Memorial Drive Cambridge, MA 02139-3794	11. Contract or Grant No. NASW-4771
	13. Type of Report and Period Covered Final Report 12/10/92 - 12/9/93
12. Sponsoring Agency Name and Address	14. Sponsoring Agency Code
NASA Headquarters Headquarters Division Washington, DC 20546	
15. Supplementary Notes	

16. Abstract

The research performed in this project is divided in two main investigations: (1) the synthesis and analysis of a collection of independent observations for Io's sodium corona, its sodium extended atmosphere, and the sodium cloud, and (2) the analysis of a (System III longitude correlated) space-time "bite-out" near western elongation in the 1981 sodium cloud images from the JPL Table Mountain Sodium Cloud Data Set. For the first investigation, modeling analysis of the collective observed spatial profiles has shown that they are reproduced by adopting at Io's exobase a modified sputtering flux speed distribution function which is peaked near 0.5 km/s and has a small high-speed (15-20 km/s) nonisotropic component. The nonisotropic high-speed component is consistent with earlier modeling of the trailing directional feature. For the second investigation, modeling analysis of the "bite-out" observed near western elongation (but not eastern elongation) has shown that it is reproduced in model calculation by adopting a plasma torus description for the sodium lifetime that is inherently asymmetric in System III longitudes of the active sector and that also has an east-west asymmetry. The east-west and System III longitude asymmetries were determined from independent observations for the plasma torus in 1981. The presence of the "bite-out" feature only near western elongation may be understood in terms of the relative value for sodium of its lifetime and its transport time through the System III enhanced plasma torus region.

17. Key Words (Selected by Author(s))	18. Distribution Statement
satellite corona and extended atmospheres, plasma-neutral interactions in magnetospheres	

19. Security Classif. (of this report)	20. Security Classif. (of this page)	21. No. of Pages	22. Price*
Unclassified	Unclassified	10	

*For sale by the Clearinghouse for Federal Scientific and Technical Information, Springfield, Virginia 22151.

TABLE OF CONTENTS

I. INTRODUCTION

The overall objective of this research has been to undertake certain studies for the sodium corona, its spatial extension, and the more distance sodium cloud by analysis of their ground-based observations. The major objectives of these studies have been to improve significantly our understanding of the nature of the escape of sodium from Io, the nature of the space-time variabilities of the extended sodium atmosphere beyond the immediate corona, and also the nature of Io's sodium cloud and its interactions with the plasma torus. The interactions of Io's extended atmosphere/neutral clouds and the plasma torus are coupled in interesting ways that have yet to be fully understood, but which are recognized as being fundamentally important in both the atmosphere and magnetospheric disciplines. Because atomic sodium is brighter in its emission lines than the much more abundant atomic oxygen and atomic sulfur by a factor of several orders of magnitudes and has therefore been observed almost exclusively in the past two decades, studies for sodium provide the primary avenue for probing the behavior of neutrals in the Io-Jupiter system.

In this report, studies for sodium are divided into two different investigations which are discussed in Section II and Section III. In Section II, the major objectives are (1) the synthesis of a number of different and independent sodium observations covering a radial range from Io's nominal exobase of ~1.4 satellite radii to east-west distances from Io of ~100 satellite radii and (2) the determination from this collective data set of a consistent flux speed distribution for sodium at the satellite exobase. This investigation is discussed in detail in a recently submitted paper entitled "Io's Corona and Spatial Extended Cloud: A Consistent Flux Speed Distribution" which is included in Appendix A. In Section III, the major objective is the analysis and explanation of a System III longitude correlated "bite-out" in the south portion of the sodium cloud when Io is near western elongation. This "bite-out" was previously documented in the JPL Table Mountain Io Sodium Cloud Data Set (Goldberg et al. 1984). This investigation is discussed in detail in a preliminary version of a paper entitled "Correlating System III Asymmetries in the Jovian Magnetosphere and the Sodium Cloud" which is included in Appendix B. Because of the two papers in the Appendices, the text of the annual report will be limited to an overview summary of these two investigations.

II. IO'S SODIUM CORONA AND SPATIALLY EXTENDED CLOUD

2.1 Observational Data for Sodium

A data set, composed of different ground-based observations for Io's sodium corona and spatially extended sodium cloud and covering the spatial range from Io's nominal exobase of 1.4 satellite radii to east-west distances from Io of ±100 satellite radii, is assembled and found to be internally consistent. The data set is composed of three parts: (1) the novel 1985 eclipse measurements of Schneider *et al.* (1991) acquired from ~1.4 to ~10 satellite radii from Io, (2) the 1985 east-west emission data of Schneider *et al.* (1991) acquired from ~4 to ~40 satellite radii from Io, and (3) sodium cloud image data acquired from ~10 to ~100 satellite radii from Io by a number of different observers in the 1976 to 1983 time frame.

The interleaved novel ground-based observations of Io's sodium corona and the near extended cloud were obtained in 1985 by Schneider (1988; Schneider *et al.* 1987, 1991) when the Galilean satellites of Jupiter underwent mutual eclipse. These observations provide for the first time valuable information about the density gradient of atomic sodium within the Lagrange sphere of Io (i.e., a radius of 5.85 satellite radii, R_{Io}) and also provide spatial information beyond this boundary that extends into the nearer portion (i.e., 6-40 R_{Io} from Io's center) of the sodium cloud. Two different types of observations were acquired: eclipse observations and emission observations. Eclipse observations measured the absorption feature at the D-line wavelengths as seen from Earth in the spectra of the reflected sunlight from the disk of another Galilean satellite (either Europa or Ganymede for measurements of interest here) that was produced by sodium in Io's atmosphere as Io eclipsed the sun from the viewpoint of the other Galilean satellite. Since the equivalent width of each absorption profile can be directly converted to a column abundance of sodium along the optical path, successive measurements during one solar eclipse of either Europa or Ganymede by Io produce a spatial profile of the column density near Io. The column density distributions determined from the different eclipse measurements are essentially symmetric about Io within the Lagrange sphere radius (5.85 R_{Io}, i.e., the gravitational grasp of the satellite), providing a one-dimensional (time independent) radial profile as noted earlier by Schneider *et al.* (1991). Emission observations measured the solar resonance scattered D-line intensity emitted by sodium

atoms in the near cloud environment of Io. In additional to spectral information, which will be only briefly considered here, these observations provide a one-dimensional spatial profile of the D-line emission brightnesses along a slit that is oriented east-west (i.e., perpendicular to the spin axis of Jupiter) and that contains (or very nearly contains) Io's disk. The east-west sodium brightness profiles for the emission data are distinctly different in front of Io and behind Io and are time-dependent. Eclipse data yield the most accurate information very near Io (i.e., 1.4 to 6 R_{Io} from Io's center), while emission data yield the most accurate information at larger distances (i.e., 4 to 40 R_{Io}) as discussed in detail by Schneider *et al.* (1991).

In order to extend the spatial range coverage of the 1985 emission data, spatially-extended east-west D_2 emission profiles for sodium from ~10 to ~100 satellite radii from Io were extracted from sodium cloud image observations. This was accomplished by using a number of the sodium cloud images in D_2 emission lines which were acquired in the 1975-1984 time interval (Murcray 1978; Murcray and Goody 1978; Matson *et al.* 1978; Goldberg *et al.* 1980, 1984; Morgan 1984, private communication; Goldberg and Smyth 1993) where Io was centered behind an occulting mask typically 10 to 12 arc sec across (i.e., covering a radial distance from the center of Io of about 10 R_{Io}) in order to block the bright disk-reflected sunlight from the satellite. Brightnesses in the immediate vicinity of the mask were usually spatially distorted in the resulting image but were consistently measured to be a few kiloRayleigh (kR), similar to the brightnesses of the 1985 emission data at 10 R_{Io}.

A comparison of the space-time behavior of the 1985 emission data and the sodium cloud image data was undertaken. They were found to be consistent. The east-west sodium brightness profiles as determined from the emission data are distinctly different in front of Io and behind Io and exhibit the time-dependent behaviors of the forward cloud and the trailing north-south oscillating directional features, which are correlated with the Io geocentric phase angle, the Io System III longitude, and the east-west asymmetry of the plasma torus. In this regard and of particular interest, an observed brightness enhancement of the trailing cloud portion of the east-west emission data profile, which is also correlated with an observed enhancement in the full width half maximum of the measured spectral line shape, is identified as occurring when the (higher-speed) trailing directional feature crossed the east-west position of the observing slit (i.e., the null position between north and south).

2.2 Analysis of the Sodium Observations

The spatial sodium profiles acquired in the 1985 eclipse and emission data are analyzed together with the more spatially-extended east-west profiles extracted from earlier sodium cloud image observations in order to investigate the nature of the flux speed distribution of sodium atoms at Io exobase. The combined data set is analyzed using the sodium cloud model of Smyth and Combi (1988a,b). At the satellite exobase, the speed dispersion of either an isotropic Maxwell-Boltzmann flux speed distribution or an isotropic classical sputtering flux speed distribution (which has a broader dispersion) is shown to be inadequate in fitting the combined data set. In the absence of the trailing cloud enhancement at the null condition, an isotropic modified sputtering flux speed distribution provides an excellent fit to the combined data set for a sodium source of 1.7 x 10^{26} atoms sec^{-1} (see Figures 11b and 12b, in Appendix A). To fit also the enhanced trailing cloud profile at the null condition, an additional enhanced high-speed (~15-20 km sec^{-1}) sodium population is required which is nonisotropically ejected from the satellite exobase so as to preferentially populate the trailing cloud rather than the forward cloud. Such a nonisotropic high-speed population of sodium is consistent with the earlier modeling analysis of the directional features by Pilcher *et al.* (1984). The two-dimensional distribution of the sodium about Io determined by the model for the isotropic modified sputtering flux speed distribution is presented (see Figure 15, in Appendix A). A complete sodium source rate speed distribution function at the satellite exobase, which also includes the even higher-speed (~20-100 km sec^{-1}) charge-exchange source (Smyth and Combi 1991) at Io that populates the sodium zenocorona (or magneto-nebula) far from Jupiter, is also presented (see Figure 16, in Appendix A).

III. SYSTEM III ASYMMETRY IN IO'S SODIUM CLOUD

3.1 Observational Data for Sodium

The "bite-out" of the sodium cloud near western elongation was discovered in the 1981 Region B/C image data reported by Goldberg et al. (1984), which are part of the larger JPL Table Mountain Io Sodium Cloud Data Set. The time evolution of this "bite-out" was excellently documented in a sequence of these images acquired on May 13, 1981 which were included in a 16 mm movie showing the changing D_2 cloud image on the sky plane as Io moved about Jupiter (Goldberg et al. 1982; Goldberg 1983). The entire 1981 Region B/C data set consists of 263 images of the sodium cloud which were

recorded simultaneously in both the D_2 (5890Å) and D_1 (5896Å) wavelength emission lines over 14 nights with an image integration time of approximately 10 minutes. Three consecutive images were usually added to improve signal to noise. These co-added images produced a time–averaged picture of the sodium cloud over an Io geocentric phase angle of about 4° and an Io System III magnetic longitude angle of about 14° and, therefore, approximate reasonably well instantaneous snapshots of the Io sodium cloud. The range of the geocentric phase angles and System III magnetic longitude angles of Io covered by the entire 1981 Region B/C data set is summarized in Appendix B graphically in Figure 1 and numerically in Table 2. Most of the 263 images comprising this coverage have undergone some type of partial data processing so that the time evolution of the cloud can be followed qualitatively. The dots and squares in Figure 1 show the midpoint conditions for 34 images that have undergone complete data reduction and calibration. Observational conditions and Image ID Numbers for these 34 images are summarized in Appendix B in Table 3.

The time evolution of the "bite-out" in the south portion of the sodium cloud near western elongation is illustrated in Appendix B in Figure 2 for a sequence of four images on May 13, 1981 and in Figure 3 for a sequence of four images with nearly the same Io geocentric phase angle but different Io System III longitudes. In the top image of Figure 2 for which Io has a System III magnetic longitude angles of about 168°, the "bite-out" was not present. For System III magnetic longitude angles of about 180°, the "bite-out" however, began to appear in the form of a deficiency of sodium south of Io and to the outside of its orbit that slices across the image at an angle of positive slope, as is illustrated in the second image of Figure 2. The "bite-out" became more pronounced as the System III longitudinal angle increases. The same general pattern is repeated in other 1981 west cloud data. Examination of a number of other sodium cloud images obtained in the 1977 to 1984 time frame indicates that the "bite-out" is a long-term and stable feature of the sodium cloud near western elongation.

Examination of sodium cloud images for Io east of Jupiter, when the satellite is in the same System III longitude angle range for which the "bite-out" occurs in the west cloud, however, does not reveal a corresponding bite-out" feature. In fact, little or no change is observed in the east cloud, as illustrated in Figure 3 of Appendix B. Because the excitation mechanism for sodium emission in the D-lines is solar resonance scattering, the deficiency of sodium brightness in the "bite-out" represents a deficiency in the sodium abundance. This suggests that the "bite-out" may be caused by an east-west

asymmetry in the plasma torus together with a longitudinally asymmetry in the "so-called" active sector (~200-300 degrees System III longitude) of the plasma torus (Hill, Dessler and Goertz 1983) in which the electron-impact ionization lifetime of sodium would then have to be enhanced. Such an enhancement would require an increase in some combination of the electron density and temperature in the active sector and also in the plasma torus west of Jupiter. Any increase in electron density would increase the emission brightness in the plasma torus of the S^+ ions (6716 Å and 6731 Å) and the S^{++} ions (9531 Å), since their electron impact excitation mechanism is primarily sensitive to the electron density for the electron temperatures in the plasma torus near Io. The sodium cloud images in the JPL data set have indeed recently been shown by Goldberg and Smyth (1993) to be brighter east of Jupiter and hence exhibit an east-west asymmetry which is anticorrelated with the well-documented east-west asymmetry of the plasma torus emission brightness. The presence of the "bite-out" feature then suggests that the brightness of the sodium emission lines and ion emission lines should also be naturally anticorrelated in System III longitude.

3.2 Observational Data for The Io Plasma Torus

A review of observations for ion emissions from the plasma torus indicates that a physically corresponding System III brightness enhancement in these plasma torus S^+ emission lines, which is anticorrelated with the "bite-out" sodium brightness, has indeed been observed in the active sector from ground-based telescopes since 1976. A comparison of these plasma observations for the System III asymmetry indicates that generally two separate longitudinally asymmetric brightness components appear to exist in the torus. The first component is centered at ~170 to 200 degrees, with an angular width of ~ 90 degrees or more, and is a permanent feature of the torus. When compared to the normal brightness of the plasma torus at the diametrically opposite magnetic longitude angle, the first component is typically 2-5 times brighter (and at extremes, 10 times brighter) with significant brightness changes occurring on a time scale of months to years. The second component is centered at ~280-290 degrees, has a comparable angular width to the first component, and is sometimes present and sometimes absence in the torus. The brightness of the second component may be comparable to or less than brightness of the first component.

For our immediate purpose of understanding the "bite-out" in the sodium image data, the presence of both a longitudinal and east-west brightness asymmetry in the plasma torus is fortunately reasonably well documented in the winter to spring of 1981 by the extension amount of ground-based observations acquired by Morgan (1983) and his analysis and modeling of these data (Morgan 1985 a,b). The System III longitudinal variation of the SII (6716Å, 6731Å) emissions was time dependent in the measurements of Morgan (1983; 1985 a,b). It changed from an ordered single peak ~ 2.5 times brighter in a broad region centered near 180° System III longitude in run 1 (Feb 14-17) and run 2 (Mar 20-23) to a double-peaked structure with peaks located near 180° and 290° in run 3 (April 21 - 24) and run 4 (May 2-4). In Figure 4 of Appendix B, the longitudinal asymmetry for run 4 is shown and reveals that near 180° and 300° system III longitude the two intensity peaks west of Jupiter were brighter and vary by about a factor of 2 while the intensity peaks east of Jupiter were much dimmer and had a smaller amplitude variation. This double-peaked structure west of Jupiter was also independently verified in the April 1981 SII image data of Pilcher et al. (1985).

3.3 Analysis of the Sodium Observations

To study the time-variable "bite-out" signatures of the sodium cloud, it is necessary to have a model that contains, to a reasonable level of accuracy, a description of the atom dynamics, the atom sink processes, the atom excitation mechanism, and the atom source velocity distribution at the satellite exobase. An updated version of the sodium cloud model of Smyth and Combi (1988a,b) is adopted here for this purpose. The sodium cloud model of Smyth and Combi (1988b) includes the dominant electron impact ionization sink for sodium which is based upon a three-dimensional space-time dependent description of the plasma torus for a tilted and offset magnetic dipole field in the presence of an east-west electric field. The east-west electric field provides an east-west asymmetry in the plasma properties which is required to explain the anticorrelated east-west brightness asymmetry of the sodium and ion emissions. The sodium cloud model has been improved (see Appendix B) to include an inherently asymmetric plasma torus description based upon the 1981 plasma torus data of Morgan (1985 a,b). The sodium source at Io's exobase has recently been shown by Smyth and Combi (1993) to be well represented by a modified sputtering flux speed distribution function which has its maximum value at ~0.5 km sec^{-1} (i.e., a sub-escape speed from Io's exobase). For atoms in the sodium cloud of which all have already escaped from Io, previous modeling efforts (Smyth and Combi 1988b) have shown, however, that the basic nature of the forward cloud and also the escaped sodium within

about one half Jupiter radii north and south of Io can be reasonably well reproduced by assuming a monoenergetic 2.6 km sec^{-1} source at a nominal Io's exobase of 2600 km, where the escape speed is ~2.0 km sec^{-1}. This source is quite adequate for our present purposes of investigating the "bite-out" feature but will understandably (see Pilcher et al. 1984) not reproduce the trailing-cloud directional feature due to its absences of higher-velocity components (i.e., ~10-20 km sec^{-1}) or the brightness gradient in the more distance portions of the forward cloud (Smyth and Combi 1993).

To analyze the "bite-out" in the sodium cloud image data, model calculations were performed for select sodium cloud images both east and west of Jupiter. For sodium cloud images west of Jupiter, the "bite-out" feature was not produced when an inherently symmetric description of the plasma torus was adopted. The "bite-out" feature was, however, produced with its proper System III longitude correlation when the inherently asymmetric description of the plasma torus based upon the 1981 plasma measurements of Morgan (1985 a,b) was adopted. For sodium cloud images east of Jupiter, the "bite-out" feature was not produced for either the inherently symmetric or inherently asymmetric description of the plasma torus. The "bite-out" feature occurs for images west of Jupiter because the sodium lifetime within the enhanced System III longitude region is sufficiently reduced so as to become smaller than or comparable to the transport time for sodium atoms to pass through this region. The "bite-out" feature does not occur for images east of Jupiter because the sodium lifetime within the enhanced System III longitude region is somewhat larger than the transport time for sodium atoms to pass through this region. East of Jupiter, the sodium lifetime near Io is larger because of the outward radial displacement (by the east-west electric field) of the sharply decreasing inward radial gradient of both the plasma torus properties and the radial structure of the System III longitudinal enhancement.

REFERENCES

Goldberg, B. A., Y. Mekler, R. W. Carlson, T. V. Johnson, and D. L. Matson (1980). Io's Sodium Emission Cloud and the Voyager 1 Encounter. *Icarus* **44**, 305-317.

Goldberg, B. A., R. W. Carlson, G. W. Garneau, T. V.Johnson, S. K. LaVoie, J. J. Lorre and D. L. Matson (1982). Dynamics of the Io Sodium Cloud. *BAAS* **14**, 762.

Goldberg, B. A. (1983). Dynamics of the Io Sodium Cloud, 16 mm movie produced for display at the National Air and Space Museum, Smithsonian Institute, Washington, D. C.

Goldberg, B. A., Garneau, G. W. and LaVoie, S.K. (1984) Io's Sodium Cloud. *Science*, **226**, 512-516.

Goldberg, B. A. and W. H. Smyth (1993). The JPL Table Mountain Io Sodium Cloud Data Set, paper in preparation.

Hill, T. W., A. J. Dessler and C. K. Goertz (1983). Magnetospheric Models, In *Physics of the Jovian Magnetosphere*, (A. J. Dessler, Ed.), pp 106-156, Cambridge Press, N. Y.

Matson, D. L. , B. A. Goldberg, T. V. Johnson, and R. W. Carlson (1978). Images of Io's Sodium Cloud. *Science* **199**, 531-533.

Morgan, J. S. (1983). Low Resolution Spectroscopy of the Io Torus, Ph.D. thesis, Dept of Astronomy, Univ. of Hawaii.

Morgan, J.S. (1985a). Temporal and Spatial Variations in the Io Torus, *Icarus* **62**, 389-414.

Morgan, J.S. (1985b). Models of the Io Torus, *Icarus* **63**, 243-265.

Murcray, F. J. (1978). Observations of Io's sodium cloud. Ph.D. Thesis, Dept. of Physics, Harvard University, Cambridge, Massachusetts.

Murcray, F. J., and R. Goody (1978). Pictures of the Sodium Cloud. *Ap. J.* **226**, 327-335.

Pilcher, C. B., Smyth, W. H., Combi, M. R., and Fertel, J. H. (1984) Io's Sodium Directional Features: Evidence for a Magnetospheric-Wind-Driven Gas Escape Mechanism. *Ap. J.*, **287**, 427-444.

Pilcher, C. B., J. H. Fertel and J. S. Morgan (1985). [SII] Images of the Torus. *Ap. J.* **291**, 377-393.

Schneider, N. M. (1988) Sodium in Io's extended atmosphere. Ph.D. Thesis, Department of Planetary Science, The University of Arizona.

Schneider, N. M., Hunten, D. M., Wells, W. K., and Trafton, L. M. (1987) Eclipse measurements of Io's sodium atmosphere. *Science*, **238**, 55-58.

Schneider, N.M., Hunten, D.M., Wells, W.K., Schultz, A.B., and Fink, U. (1991) The Structure of Io's Corona, *Ap.J.*, **368,** 298-315.

Smyth, W. H., and Combi, M. R. (1988a) A general model for Io's neutral gas cloud. I. Mathematical description. *Ap. J. Supp.*, **66,** 397-411.

Smyth, W.H., and Combi, M.R. (1988b) A General Model for Io's Neutral Gas Cloud. II. Application to the Sodium Cloud. *Ap. J.* **328**, 888-918.

Smyth, W.H., and Combi, M.R. (1991) The Sodium Zenocorona, *J. Geophys. Res.* **96**, 22711-22727.

Smyth, W.H. and M. R. Combi (1993). Io's Sodium Corona and Spatially Extended Cloud: a Consistent Flux Speed Distribution. *Icarus*, submitted.

Appendix A

Io's Sodium Corona and Spatially Extended Cloud: A Consistent Flux Speed Distribution

Io's Sodium Corona and Spatially Extended Cloud :

A Consistent Flux Speed Distribution

William H. Smyth[1]

Michael R. Combi[2]

Submitted to Icarus

October 29, 1993

1. Atmospheric and Environmental Research, Inc., Cambridge, MA 02139

2. Space Physics Research Laboratory, University of Michigan, Ann Arbor, Michigan 48109

Number of manuscript pages : 46

Number of Figures : 16

Number of Tables : 5

Key words : Io, satellite exospheres, gas tori

Running heading : Io's Sodium Corona and Spatially Extended Cloud

For editorial correspondence and proofs please contact:

William H. Smyth

Atmospheric and Environmental Research, Inc.

840 Memorial Drive

Cambridge, MA 02139

Telephone number : (617) 547-6207

Fax number : (617) 661-6479

Internet : smyth@aer.com

ABSTRACT

A data set, composed of different ground-based observations for Io's sodium corona and spatially extended sodium cloud and covering the spatial range from Io's nominal exobase of 1.4 satellite radii to east-west distances from Io of ±100 satellite radii, is analyzed collectively to investigate the velocity distribution of sodium at the exobase. The data set is composed of the novel 1985 eclipse measurements of Schneider *et al.* (1991) acquired from 1.4 to ~10 satellite radii from Io, the 1985 east-west emission data of Schneider *et al.* (1991) acquired from ~4 to ~40 satellite radii from Io, and sodium cloud image data acquired from ~10 to ~100 satellite radii from Io by a number of different observers in the 1976 to 1983 time frame. The column density distributions determined from the different eclipse measurements are essentially symmetric about Io within the Lagrange sphere radius (5.85 satellite radii, i.e., the gravitational grasp of the satellite), providing an one-dimensional radial profile as noted earlier by Schneider *et al.* (1991). At distances beyond the Lagrange sphere radius, however, the apparent change in the observed column density slope is shown in model calculations to occur in the forward cloud, but not trailing cloud portion, of the column density profile. The east-west sodium brightness profiles as determined from the emission data are distinctly different in front of Io and behind Io and are shown to exhibit the time-dependent behaviors of the forward cloud and the trailing north-south oscillating directional features, which are correlated with the Io geocentric phase angle, the Io System III longitude, and the east-west asymmetry of the plasma torus. In this regard and of particular interest, an observed brightness enhancement of the trailing cloud portion of the east-west emission data profile, which is also correlated with an observed enhancement in the full width half maximum of the measured spectral line shape, is identified as occurring when the (higher-speed) trailing directional feature crossed the east-west position of the observing slit (i.e., the null position

between north and south). The combined data set is analyzed using the sodium cloud model of Smyth and Combi (1988a,b). At the satellite exobase, the speed dispersion of either an isotropic Maxwell-Boltzmann flux speed distribution or an isotropic classical sputtering flux speed distribution (which has a broader dispersion) is shown to be inadequate in fitting the combined data set. In the absence of the trailing cloud enhancement at the null condition, an isotropic modified sputtering flux speed distribution provides an excellent fit to the combined data set for a sodium source of 1.7×10^{26} atoms sec^{-1}. To fit also the enhanced trailing cloud profile at the null condition, an additional enhanced high-speed (~15-20 km sec^{-1}) sodium population is required which is nonisotropically ejected from the satellite exobase so as to preferentially populate the trailing cloud rather than the forward cloud. Such a nonisotropic high-speed population of sodium is consistent with the earlier modeling analysis of the directional features by Pilcher *et al.* (1984). A complete sodium source rate speed distribution function at the satellite exobase, which also includes the even higher-speed (~20-100 km sec^{-1}) charge-exchange source (Smyth and Combi 1991) at Io that populates the sodium zenocorona (or magneto-nebula) far from Jupiter, is presented.

1. INTRODUCTION

Novel ground-based observations of Io's sodium corona and near extended cloud were obtained in 1985 by Schneider (1988; Schneider *et al.* 1987, 1991) when the Galilean satellites of Jupiter underwent mutual eclipse. These observations provide for the first time valuable information about the density gradient of atomic sodium within the Lagrange sphere of Io (i.e., a radius of 5.85 satellite radii, R_{Io}) and also provide spatial information beyond this boundary that extends into the nearer portion (i.e., 6-40 R_{Io} from Io's center) of the sodium cloud. Two different types of observations were acquired: eclipse observations and emission observations. Eclipse observations measured the absorption feature at the D-line wavelengths as seen from Earth in the spectra of the reflected sunlight from the disk of another Galilean satellite (either Europa or Ganymede for measurements of interest here) that was produced by sodium in Io's atmosphere as Io eclipsed the sun from the viewpoint of the other Galilean satellite. Since the equivalent width of each absorption profile can be directly converted to a column abundance of sodium along the optical path, successive measurements during one solar eclipse of either Europa or Ganymede by Io produce a spatial profile of the column density near Io. Emission observations measured the solar resonance scattered D-line intensity emitted by sodium atoms in the near cloud environment of Io. In additional to spectral information, which will be only briefly considered here, these observations provide a one-dimensional spatial profile of the D-line emission brightnesses along a slit that is oriented east-west (i.e., perpendicular to the spin axis of Jupiter) and that contains (or very nearly contains) Io's disk. Eclipse data yield the most accurate information very near Io (i.e., 1.4 to 6 R_{Io} from Io's center), while emission

data yield the most accurate information at larger distances (i.e., 4 to 40 R_{Io}) as discussed in detail by Schneider *et al.* (1991).

In this paper, the spatial sodium profiles acquired in the 1985 eclipse and emission data are analyzed together with more spatially-extended east-west profiles extracted from earlier sodium cloud image observations in order to investigate the nature of the flux speed distribution of sodium atoms at Io exobase. The observational information is presented, compared, and evaluated in section 2. Modeling of the spatial profiles of the sodium data is undertaken in section 3. Discussion and conclusions are presented in section 4.

2. OBSERVATIONS

Of particular interest in this paper are the five higher quality eclipse measurements and the nine higher quality emission observations obtained at the Catalina Observatory 1.5 meter telescope using the LPL echelle spectrograph that were presented by Schneider *et al.*(1991). The dates, times, orbital angular parameters of Io, spectral ID numbers, and the numbering of these observations adopted in this paper are summarized in Table 1. Four of the five eclipse observations were acquired when Io was east of Jupiter (i.e., an Io geocentric phase angle within 90 ± 90 degrees), and only one was acquired when Io was west of Jupiter (i.e. , within 270 ± 90 degrees). Seven of the emission observations were obtained when Io was east of Jupiter, and only two were obtained when Io was west of Jupiter. In addition, select sodium cloud image observations for Io near its orbital elongation points, which were acquired in 1976 by Murcray (1978; Murcray and Goody 1978), in 1981 by Goldberg *et al.* (1984; Goldberg and Smyth 1993), and in 1983 by Morgan (1984, private communication), are used to extract east-west D_2 brightness profiles that overlap the spatial range of the emission data and extend it to ±100 R_{Io}.

2.1 Eclipse Observations

The column density profiles for all five of the eclipse observations are presented collectively in Figure 1 and follow directly from the information given by Schneider *et al.* (1991) in their Table 3. Only one lower-bound data point from eclipse 4 at a distance from the center of Io of 1.17 R_{Io} is excluded since it is well within the nominally exobase radius of 1.4. R_{Io}. The spatial profile for eclipse 2 obtained on September when Io was very near eastern elongation (i.e., 90 degrees Io phase angle) is highlighted in Figure 1 and seen to be similar to the other four spatial profiles. A comparison of the two sides of each eclipse measurement shows no detectable difference in the slopes of their separate profiles within the Lagrange sphere radius of Io. This was noted earlier by Schneider *et al.* (1991) and thus effectively reduces the eclipse data to a radially symmetric profile. The dashed line shows the power law fit to the data points contained within the Lagrange radius and has the form

$$N\ (1.4 \leq r \leq 5.85) = 2.55 \times 10^{12}\, r^{-2.48}$$

where N is the column density in units of atoms cm^{-2} and r is the distance from the center of Io in units of the R_{Io} (i.e., 1815 km). This is the same power law obtained earlier by Schneider *et al.* and undercuts the data points outside the Lagrange radius where the eclipse observations are deemed to be less reliable. Although the eclipse data beyond the Lagrange sphere contain more vertical scatter, they also appear to have possibly a reduced slope Such a change in slope might be caused by the domination of the planetary gravitational field beyond the Lagrange radius of Io and will be discussed further in the modeling analysis section.

2.2 Emission Observations

The D_2 brightness profiles for the nine emission observations are shown collectively in Figure 2. This information, which was previously published only in a graphical format (Schneider *et al.* 1991), is summarized numerically in Table 2 as provided by Schneider (1990, private communication). The spatial profile for Emission 4, which was obtained on September 14 when Io was nearest eastern elongation, is highlighted, and its east and west profiles are identified separately. Excluding all data points inside of 4 R_{Io} where the seeing and instrumental effects artificially flatten the profile, the power law fit to the remaining emission brightness data in Figure 2 is given by

$$I_{D_2}(r \geq 4) = 101\, r^{-1.45}$$

where I_{D_2} is the D_2 brightness in kiloRayleighs (kR) and r is the distance from the center of Io in R_{Io} units. This D_2 brightness of ~ 100 kR as r approaches Io's surface is consistent (Brown and Yung 1976) with the maximum sodium column density of ~1 x 10^{12} atoms cm^{-2} deduced from the eclipse data in Figure 1.

For more insight into the emission data, it is instructive to make a direct comparison of the relative behavior of the nine emission observations. Since the spatial coverage of the D_2 brightness is very nonuniform, this comparison can be readily accomplished by simply inspecting the columns in Table 2. The nonuniform spatial coverage in Table 2 occurs because of different distance intervals adopted to obtain an average brightness value (given different signal to noise ratios) for each data point in the profile and because of signal drop-out associated with constraints imposed on positioning the slit profile on the CCD detector

during interleaved eclipse and emission measurements. Using the emission data for Io east of Jupiter (i.e., seven out of the nine emission observations) and for Io west of Jupiter (i.e., the remaining two emission observations), the relative brightness of the forward and trailing sodium cloud near Io may be monitored as a function of the Io geocentric phase angle by comparing in each observation the two brightness profiles east and west of Io. In this comparison, it will be seen that systematic changes in the D_2 brightness are generally consistent with the Io phase angle dependence observed in Io sodium cloud image data over the last two decades.

When Io is east of Jupiter and has a phase angles less than about 65 degrees, a brighter forward sodium cloud is observed to the east of Io and a dimmer trailing cloud is observed to the west of Io (Goldberg *et al.* 1984). This is the pattern exhibited by the emission 1 observation on August 27 which has an average Io phase angle of 61.4 degrees.

When Io is east of Jupiter and has phase angle between about 65 and 85 to 90 degrees, east and west profiles are observed (Goldberg *et al.* 1984) to be very similar since the brighter forward sodium cloud is now swinging through and approximately aligned along the observer's line of sight. This is the pattern exhibited by the emission 2 observation on August 27 which has an average Io phase angle of 72.2 degrees. For the emission 4 observation acquired 18 days later on September 14 for an average Io phase angle of 87.7 degrees, the reverse pattern, however, is present with the trailing cloud being brighter than the forward cloud. Inspection of the line profile shapes for each data point of the emission 4 observation on September 14 indicates that its full width half maximum (FWHM) is highly asymmetric east and west of Io with a much larger FWHM present at larger distances from Io in the east profile (i.e., in the trailing cloud). The emission 3 observation acquired a day earlier for Io west of Jupiter (and essentially a mirror

geometric observation to that on September 14) and the emission 6 observation acquired for Io west of Jupiter a day later on September 15, also both exhibit a similar highly asymmetric values for the FWHM which are larger in the trailing cloud. This reversal of the normal pattern by the emission 3, the emission 4, and the emission 6 observations therefore all occur when additional high speed sodium was present in the trailing portion of the cloud outside of Io's orbit. The Doppler signature of this additional high speed sodium was, however, not seen in the trailing portion of the cloud in the emission 5 observation which was also acquired on September 14 only about one and one-half hours after the emission 4 observation (i.e., an increase in the Io phase angle and hence the cloud's sky-plane projection angle of only about 13 degrees).

When Io is east of Jupiter and has a phase angle greater than about 85 to 90 degrees, the forward sodium cloud is observed in image data to be brighter to the west of Io and the trailing cloud to be dimmer and to the east of Io (Goldberg *et al.* 1984). This is the pattern exhibited by the emission 7, emission 8, and emission 9 observations which have average Io phase angle of about 117, 122, and 143 degrees, respectively. A comparison of the forward and trailing cloud profiles for the emission 5 observation, which has an average Io phase angle of about 101 degrees, is not possible because there is only one data point west of Io.

When Io is west of Jupiter and has a phase angle greater than about 235 degrees, the forward sodium cloud is generally observed to be brighter and to the east of Io, and the trailing cloud is generally observed to be dimmer and to the west of Io (Goldberg *et al.* 1984). Examination of the profiles for the two out of the nine emission observations for Io west of Jupiter (i.e., emission 3 and emission 6 with Io phase angles of about 277 and 295 degrees, respectively), shows, however, the reverse pattern. As noted above, these two

observations, together with the eastern emission 4 observation, all exhibit this reverse pattern and also have a highly asymmetric spatial profiles east and west of Io for their FWHM values, with much larger FWHM values present at larger distances from Io in the trailing cloud . These asymmetric spatial profiles of the FWHM suggest additional high speed sodium in the cloud outside of Io's orbit may be responsible for this reverse pattern.

A final comparison in Table 2 can be made for the nearly mirror geometric measurements for the emission 7 observation with an Io phase angle of about 117 degrees and the emission 6 observation with an Io phase angle of about 295 degrees. From Table 2, the brightness of the forward cloud at a distance of 10-16 R_{Io} can be seen to be larger for Io east of Jupiter. This is consistent with the well known east-west intensity asymmetry first discovered near Io by Bergstralh *et al.*(1975, 1977) and identified at larger distances from Io by Goldberg and Smyth (1993). A similar comparison between the approximately mirror geometric measurements for the emission 4 observation with an Io phase angle of about 88 degrees and the emission 3 observation with an Io phase angle of about 277 degrees has not been considered since the absolute calibration of the emission 3 observation is in question (Schneider 1990, private communication).

A closer graphical examination of each of the nine profiles in Figure 2 shows that the vertical spread of the whole data set, particularly for $r > 10$, is a result of the superposition of the separate emission observations, where for each observation the slit profiles east and west of Io have two well defined but generally different slopes and different absolute brightnesses. This can readily be shown by a power-law fit analysis [$I_{D_2}(r \geq 4) = A\, r^{-\beta}$] of the separate east and west profiles for each emission observation for Io east of Jupiter, where the exponent, β, and amplitude, A, are summarized in Table 3. These fits omit data points inside four satellite radii of Io's center, where they are

artificially flattened, and thus depict the decay in the brightness profile primarily outside of the Lagrange radius. In Table 3, the emission observations are arranged in increasing Io phase angle, and the spatially-projected location of the forward cloud (F), the symmetric turning point (S) of the cloud, and the trailing cloud (T) are identified for the east and west profiles. The power law slopes of all the forward clouds are similar and have an exponent value of ~ 1.6. The power law slopes of the trailing clouds after the symmetric turning point, excluding the September 14 emission observation at a phase angle of 100.6 degrees, are also similar and have an exponent value of ~ 2.0. The power law slopes of the clouds at the symmetric turning point, excluding the September 14 emission observation of the trailing cloud at a phase angle of 87.7 degrees, are similar and have an exponent value of ~ 1.8. The two power law slopes of the trailing clouds on September 14 do not follow the pattern and have smaller exponent values of ~ 1.23 and 1.27. Not including the two emission observations on August 27 for Io east of Jupiter, which are at or before the symmetric turning point and have the reverse east-west projection orientation for their forward and trailing clouds, the remaining five profiles for Io east of Jupiter are presented graphically in Figure 3 along with their power law fits.

The brightness profiles for the forward cloud (i.e. west of Io) in Figure 3 are very tightly confined. The brightness profiles for the trailing cloud (i.e., east of Io) in Figure 3, however, are significantly different and drop off more rapidly with increasing Io phase angle. The brightest (i.e., least steep) of these profiles is for the emission 4 observation (87.7 degrees Io phase angle) that exhibited a much larger FWHM value in the trailing cloud for the data points at these larger distances from Io. The next brightest profile is for the emission 5 observation (100.6 degrees Io phase angle) acquired ~1.5 hours later on the same day which does not show the asymmetry in the FWHM values. The remaining three rather tightly confined trailing cloud profiles in Figure 3 are for the emission 7, emission 8,

and emission 9 observations that have a very similar slope of β~2 as noted earlier. This behavior of the trailing clouds suggests that both the presents of higher speed sodium atoms as well as rapidly changing projection effects of the cloud on the sky plane as the Io phase angle increases are likely involved in its explanation. This behavior will be examined further and explained in the next section. In contrast, the well confined behavior of the forward sodium cloud and the absence of high speed sodium atom signatures suggest that the forward cloud is, as expected, primarily associated with the escape of low speed sodium from Io. A comparison of the brightness profiles in Figure 3 with other observations of the sodium cloud is undertaken below.

2.3 Sodium Cloud Image Observations

A large number of sodium cloud images in the D_1 and D_2 emission lines were acquired in the 1975-1984 time interval (Murcray 1978; Murcray and Goody 1978; Matson *et al.* 1978; Goldberg *et al.* 1980, 1984; Morgan 1984, private communication; Goldberg and Smyth 1993) where Io was centered behind an occulting mask typically 10 to 12 arc sec across (i.e., covering a radial distance from the center of Io of about 10 R_{Io}) in order to block the bright disk-reflected sunlight from the satellite. Brightnesses in the immediate vicinity of the mask were usually spatially distorted in the resulting image but were consistently measured to be a few kiloRayleigh (kR). These brightness are similar to those of the emission data at 10 R_{Io} in Figure 2.

A simple review of these sodium cloud images shows that the forward sodium cloud is generally more spatially extended and brighter than the trailing cloud. An exception to this occurs, however, when the high-speed trailing directional-feature, which oscillates north and south behind the satellite with its inclination correlated (Pilcher *et al.*

1984) with the System III longitude angle of Io, passes through the east-west line drawn through Io (i.e., the null location of the directional feature). The observed correlations of the north inclination, the south inclination, and the null locations of the directional feature with the System III longitude of Io are shown in Figure 4 as determined by Goldberg and Smyth (1993) and are consistent with those obtained earlier by Pilcher *et al.* (1984). The directional feature changes from a south to north inclination for a null System III longitude angle of Io near 165 degrees and change from north to south for a rather poorly defined null System III longitude angle of Io somewhere between about 320 and 25 degrees. This changing north-south orientation of the trailing directional feature is illustrated in Figure 5 by three sodium cloud images, where an east-west oriented scale centered on Io of length ± 100 R_{Io} is shown for reference. In Figure 5, a north directional feature is present in image A (247 degrees Io System III longitude), a south directional feature is present in image B (104 degrees Io System III longitude), and a slightly north but near-null directional feature is present in image C (178 degrees Io System III longitude). The spatial extension and brightening of the trailing cloud profile along the east-west oriented (dashed) line, when the directional feature is near the null location, are readily apparent.

The forward cloud has been observed in images to distances of 100 satellite radii and more ahead of Io, where the cloud brightness levels are then only a few hundred Rayleighs. Analysis of the D_2 images of Murcray (1978) by Smyth and McElroy (1978 see their Fig. 4) indicated that when Io was near eastern elongation the one kR brightness level in the forward cloud occurred about 60 R_{Io} ahead of Io. Examination of a number of additional images indicates that the observed brightnesses of the forward cloud at this distance appear many times to be lower, although generally it has been difficult to be precise because the cloud is usually not measured to brightnesses less than about 0.2 to 0.5 kR. Using fourteen images of the sodium cloud for Io near its orbital elongation points that

are summarized in Table 4, a range (or an bounding envelope) of values for the D_2 east-west brightness profile of the forward and trailing clouds has been determined and is shown in Figure 3 by different shaded area.

For the forward cloud profile in Figure 3, the shaded area determined from the sodium cloud images occurs for radial distances greater than about 20 R_{Io} and can be seen to be brighter and to have a less steep slope than the emission data profiles. The lower boundary of the forward sodium cloud image profile area intersects the emission data just inside of 10 R_{Io}, which is near the Lagrange radius of Io and is where the slope of the eclipse data in Figure 1 appears to become less steep. For Io near the elongation point, only two emission profiles occur and are too short to overlap the sodium cloud image data, with the one for an Io phase angle of 87.7 degrees extending only to a radial distance of ~10 R_{Io} and the other for an Io phase angle of 100.6 degrees containing only one point at a radial distance of ~15 R_{Io}. For Io somewhat beyond eastern elongation, the remaining three emission data profiles (i.e., for Io phase angles of 117.2, 121.6, and 143.1 degrees) extend radially to ~30 R_{Io} and fall below the sodium cloud image profile area, which is more representative of conditions near elongation. For Io near elongation, the question of consistency of the forward cloud brightness profiles from the emission data and the sodium cloud image data will be addressed in the modeling analysis section.

For the trailing cloud profile in Figure 3, two different shaded areas have been extracted from the sodium cloud image information in Table 4 to quantify its D_2 east-west brightness profile . The extracted profile areas represent the two basic orientations for the directional feature : (1) when the directional feature is either north or south (lower area) and (2) when the directional feature is at the null or near null location (upper area). These two areas establish a range (or an bounding envelope) for the values of the D_2 east-west

brightness profile of the trailing sodium cloud for Io near its orbital elongation point. As expected, the shaded area for the directional feature at the null location is both brighter and less steep than the shaded area for the directional feature with either a north or south inclination. As noted in Figure 5, the D_2 east-west brightness profile of the trailing sodium cloud is more closely confined to Io than the forward cloud when the trailing directional feature is inclined either north or south and has a less steep brightness gradient when the directional feature is at the null location.

The Io System III longitude correlated inclination of the directional feature is thought to be produced by high speed (~15-20 km sec^{-1}) sodium atoms escaping from Io in a nonisotropic manner. From the analysis of Pilcher *et al.* (1984), the nonisotropic escape flux is diminished at the poles relative to the equator and is also diminished in the forward and backward directions of the satellite's motion in comparison to the perpendicular direction of motion to Io's orbit in the satellite orbit plane . For these high speed sodium atoms, the Io System III longitude correlation is produced because atom trajectories, upon reaching the spatial region behind Io, are synchronized in such a way with the time-dependent sodium electron impact ionization sink of the oscillating plasma torus, so as to either go under it, go through it, or go over it, thereby producing an alternating north-south reduction in the sodium density.

In comparing the trailing emission profiles in Figure 3 with the trailing sodium cloud image data, it is important to identify the orientation of the directional feature in the emission data as classified by Figure 4 and also to note if there were enhancements in the measured Doppler signature of the trailing D_2 east-west brightness profiles. This information is summarized in Table 5. For the three emission profiles where an enhanced Doppler spectral profile (i.e., FWHM) was measured, the directional feature was at a null

or near null location, and also the trailing D_2 east-west brightness spatial profile was either similar or dominant (i.e., brighter and less steep) when compared to the forward cloud spatial profile. Two of these emission profiles occurred when Io was west of Jupiter and are not included in Figure 3. The third profile occurred for Io at a phase angle of 87.7 degrees. This is the brightest and least steep of all the profiles in Figure 3 and has a power law fit that is along the top boundary of the upper area for the sodium cloud image data which corresponds to the null condition. The presence of this brightest trailing profile is thus explained as a case where the directional feature was at a null condition. In Figure 3, the trailing emission profile for an Io phase angle of 100.6 degrees, acquired only about 1.5 hours later on the same night and having a south inclined directional feature, has a power law fit that is essentially along the top boundary of the lower area for sodium cloud image data which corresponds to a north or south inclined directional features. The remaining three emission profiles (i.e., for Io phase angles of 117.2, 121.6, and 143.1 degrees) are for Io somewhat beyond eastern elongation and lie near or just below the lower boundary of the lower area for sodium cloud images. The trailing emission profile data are therefore quite consistent with the sodium trailing cloud image data.

3. ANALYSIS OF THE OBSERVATIONS

Modeling analysis of the one-dimensional sodium distribution described in the previous section by the eclipse data, the emission data, and the sodium cloud image data will now be undertaken. One-dimensional profiles are calculated using the numerical sodium cloud model of Smyth and Combi (1988 a,b), where the electron impact ionization sink for sodium is determined for a 7 degree tilted corotating plasma torus with an offset-dipole planetary magnetic field in the presence of a nominal (i.e., ~2.8 mV m^{-1} in Io's frame) east-west electric field. Preliminary modeling reported earlier by Smyth and Combi

(1987) for the first radial profile published by Schneider *et al.* (1987) for the sodium column density determined by two eclipse measurements showed that it could be fit very well from ~4 to 10 R_{Io} by adopting a escaping, monoenergetic (2.6 km sec^{-1}), and isotropic sodium flux from the satellite exobase (assumed 1.4 R_{Io}, where the escape speed is ~2 km sec^{-1}), which was determined independently from modeling typical forward cloud image data in the D_2 emission brightness range of ~1-3 kR. A similar conclusion is reached from a comparison in Figure 6 of this monoenergetic model run with the complete set of eclipse data from Figure 1. In the radial interval from ~2 to 15 R_{Io}, the effect of the sodium lifetime on the calculated profile for this monoenergetic source is illustrated in Figure 7, where it is seen to alter primarily the absolute magnitude rather than the slope of the column density profile. To fit in addition the eclipse data in Figure 6 between the nominal exobase (1.4 R_{Io}) and ~4 R_{Io}, a properly chosen dispersion of initial velocities for the source flux distribution with non-escaping components is required. For the larger spatial distances beyond the Lagrange radius, covered by the east-west profiles for the emission data and the sodium cloud image data, the dispersion of initial velocities in the source for speed components greater than 2.6 km sec^{-1} may also need to be included. Indeed, the eclipse measurements for the corona near Io, the emission measurements that extend into the near sodium cloud, and the sodium cloud image derived profiles that reach to distances of ± 100 R_{Io}, provide a set of spatially overlapping observations that will be used to study and constrain the initial velocity dispersion of the sodium source atoms at the exobase.

To investigate the nature of the initial velocity dispersion of the sodium source, two different source flux speed distributions discussed by Smyth and Combi (1988b; see their Appendix D) are considered: (1) a Maxwell-Boltzmann flux distribution and (2) a modified-

sputtering flux distribution. The Maxwell-Boltzmann flux distribution $\phi(v;T)$ is based on the Maxwell-Boltzmann velocity distribution and is defined as follows:

$$\phi(v;T) = \phi_0 (\frac{R_S}{R_E})^2 \frac{2}{v_T} (\frac{v}{v_T})^3 e^{-(\frac{v}{v_T})^2}$$

where

$$v_T = (\frac{2kT}{m})^{1/2}$$

is the most probable speed of the velocity distribution for an atom of mass m. The Maxwell-Boltzmann flux distribution is proportional to the local velocity integrated flux ϕ_0 referenced here to the satellite radius R_S not the exobase radius R_E and depends upon one parameter, the exobase temperature T (or alternatively v_T), which determines both the most probable speed v_m

$$v_m = (\frac{3kT}{m})^{1/2}$$

and the speed dispersion of the flux distribution. The modified-sputtering flux distribution $\phi(v;\alpha, v_M, v_b)$ is proportional to the local velocity integrated flux ϕ_0 and depends upon three parameters: an exponent α, a velocity parameter v_b, and the velocity parameter v_M:

$$\phi(v;\alpha, v_M, v_b) = \phi_0 (\frac{R_S}{R_E})^2 \frac{1}{v_b D(\alpha, v_M/v_b)} (\frac{v}{v_b})^3 (\frac{v_b^2}{v^2 + v_b^2})^\alpha \left[1 - (\frac{v^2 + v_b^2}{v_M^2})^{1/2} \right],$$

where $D(\alpha, v_M/v_b)$ is a normalization constant (see Smyth and Combi 1988b). The exponent α primarily determines the dispersion of the distribution, which has a greater high-speed population as α decreases. The exponent α has a value of 3 for a classical sputtering distribution (i.e., representing a complete collisional cascade process) and a value of 7/3 for a Thomas-Fermi modified-sputtering flux distribution (i.e., representing the limit of a single elastic collisional ejection process), where the latter distribution is based upon a Thomas-Fermi differential scattering cross section. The velocity parameter v_b is related nonlinearly to the most probable speed v_m of the flux speed distribution and primarily determines v_m (see Smyth and Combi 1988b, Appendix D). The velocity parameter v_M primarily determines the maximum speed for the flux distribution and depends upon the maximum relative speed (and masses) of the plasma torus ion and sodium atom. The Maxwell-Boltzmann flux distribution and the modified-sputtering flux distribution, normalized to unit area, are each shown in Figure 8 for two different values of their parameters. The four flux distributions in Figure 8 will be utilized in the subsequent modeling analysis.

In calculating the column density and the D_2 emission brightness in the numerical sodium cloud model, a smaller two-dimensional sky-plane grid centered on Io (± 15 R_{Io}) is used to cover a spatial scale near the satellite more appropriate to the eclipse data while a much larger two-dimensional sky-plane grid centered on Io is used to cover a larger spatial scale more appropriate for the emission data and the sodium cloud image data. A one-dimensional profile for the eclipse data is obtained from the smaller two-dimensional sky-plane grid by extracting an average radial profile. This average radial profile will be called the calculated eclipse profile and will be denoted by the filled circles in Figures 9-14. A one-dimensional east-west D_2 brightness profile (and also a corresponding column density

profile) for the emission data and the sodium cloud image data is obtained from the larger two-dimensional sky-plane grid by selecting only the east-west grid elements that occur in the grid row containing Io. In Figures 9-14, the calculated east-west brightness and column density profiles are denoted by filled triangles for the forward cloud profile and by filled squares for the trailing cloud profile. To construct an eclipse or east-west profile, monoenergetic model calculations are performed for 18 different nonuniformly-spaced speeds ranging from 0.4 km sec^{-1} to 10 km sec^{-1}. Profiles for speeds beyond 10 km sec^{-1} are determined by a inverse speed extrapolation of the model results. The individual profiles for the different speeds are appropriately weighted for a given source flux speed distribution and then added to obtain the final spatial profile. Model calculations are performed for an Io geocentric phase angle of 92.9 degrees and an Io System III longitude angle of 48.6 degrees. These satellite conditions are similar to those for the emission 4 and eclipse 2 observations of Table 1, which are the observation closest to the eastern elongation point. This choice is also appropriate for all the eclipse data within the Lagrange sphere, which has no discernible dependence on these two Io related angles, and for the Io sodium cloud image data which have east-west profile areas in Figure 3 that are representative of the satellite near its orbital elongation points.

Model calculations for a Maxwell-Boltzmann flux distribution are presented in Figure 9 and Figure 10. In Figure 9a and Figure 9b, the calculated and measured sodium column density for the eclipse observations are compared for two different exobase temperatures. In Figure 10a and Figure 10b, the calculated D_2 emission brightness profiles for the forward and trailing clouds are compared to the emission 4 measurement profiles and to the sodium cloud image data profile areas for the same two exobase temperatures adopted, respectively, in Figures 9a and 9b.

For a Maxwell-Boltzmann flux distribution with a most probable speed of v_m = 1.3 km sec^{-1} (i.e., an exobase temperature of ~1600 K, see Figure 8) and a total flux ϕ_0 (referenced to Io's surface area) of 3.0 x 10^8 atoms cm^{-2} sec^{-1} (i.e., a total source of ~1.2 x 10^{26} atoms sec^{-1}), the model calculated column density and D_2 emission brightness profiles are shown in Figure 9a and Figure 10a, respectively. In Figure 9a for radial distances from the exobase to the Lagrange sphere, the model column density for the calculated eclipse profile (filled circles) provides an excellent fit to the eclipse observations (open circles) and also compares very favorably with the east-west column density profiles calculated for the forward (filled triangle) and trailing cloud (filled squares). In Figure 9a beyond the Lagrange sphere, however, all three of these calculated profiles fall below the eclipse observations. At and beyond about 8 R_{Io}, the calculated east-west forward and trailing profiles rise above the calculated eclipse profile (because the column density is no longer spherically symmetric about Io), with the forward cloud profile having the largest column density and showing a distinct change in its slope compared to the trailing cloud profile. The corresponding model profiles for the D_2 emission brightness are given in Figure 10a. For both the forward and trailing profiles, the calculated eclipse and calculated east-west profiles are in good agreement with each other inside the Lagrange radius, with a maximum brightness of about 200 kR near the exobase. The calculated east-west profile threads the three emission 4 data points for the forward cloud, but falls well below the emission 4 data points in the trailing cloud. For both the forward and trailing clouds at larger radial distances, the calculated east-west profiles fall well below the areas for both the forward and trailing cloud images. This behavior indicates that there is a deficiency in the high-speed population of this source flux speed distribution at the exobase.

Model calculations were therefore performed for a Maxwell-Boltzmann flux distribution with a higher most probable speed of v_m = 2.0 km sec^{-1} (i.e., a exobase temperature of ~3700 K, see Figure 8) and with a total flux ϕ_0 of 1.8 x 10^8 atoms cm^{-2} sec^{-1} (i.e., a total source of ~0.75 x 10^{26} atoms sec^{-1}) and are shown in Figure 9b and Figure 10b. For the D_2 emission brightness profiles in Figure 10b, the calculated east-west profile now threads the center of the forward cloud image area for a radial distance up to about 70 R_{Io} and the lower trailing cloud image area for a radial distance of about 25 R_{Io} before it falls off too steeply. This improved fit at larger radial distances, however, reduces the D_2 emission brightness at the exobase to about 80 kR in Figure 10b and causes the calculated eclipse profile in Figure 9b to fall below the measured eclipse profile for radial distances inside of about 3 R_{Io}. The Maxwell-Boltzmann flux distribution therefore cannot fit both the corona profile near Io and the sodium cloud east-west profiles at large distances from the satellite. A flux distribution that has a broader dispersion with enhanced populations for both the low-speed and high-speed atoms is required. The modified-sputtering flux distribution, which has a broader dispersion, is therefore considered in the remainder of the paper.

Model calculations for a classical sputtering flux distribution (i.e., α=3) and a modified-sputtering flux distribution (i.e., α=7/3, having even a larger high-speed population) are presented in Figure 11a and Figure 11b for the eclipse observations and in Figure 12a and Figure 12b for the emission 4 and sodium cloud east-west D_2 emission brightness profiles. For the two flux distributions, the most probable speed is, respectively, 1.0 km sec^{-1} and 0.5 km sec^{-1}, and the total flux ϕ_0 is, respectively, 3.2 x 10^8 atoms cm^{-2} sec^{-1} (i.e., a total source of ~1.3 x 10^{26} atoms sec^{-1}) and 4.2 x 10^8 atoms cm^{-2} sec^{-1} (i.e., a total source of ~1.7 x 10^{26} atoms sec^{-1}) . In Figure 11, both sputtering flux distributions provide a reasonably good fit to the observed column density profile from

the exobase to radial distances of ~8 R_{Io}, just beyond the Lagrange radius. A careful comparison of Figure 11a and Figure 11b shows that the calculated sodium column density for the classical sputtering flux distribution is slightly larger within the Lagrange radius and is somewhat smaller beyond the Lagrange radius (as is to be expected), with the largest differences occurring in the trailing cloud profile beyond about 10 R_{Io}.

For these two sputtering flux distributions, the same general behavior is seen in comparing the two calculated D_2 emission brightness profiles in Figure 12a and Figure 12b. For the classical sputtering flux distribution in Figure 12a, the calculated D_2 emission brightness profiles for the forward profile is slightly above the measured data point inside the Lagrange radius, matches the two measured data points beyond the Lagrange radius, and then threads the forward cloud image area nicely between about 20 R_{Io} and 80 R_{Io} before it falls too rapidly and drops below this area. An improved fit for the forward profile is provided by the modified sputtering distribution (α=7/3) in Figure 12b. The calculated D_2 emission brightness profile for the forward profile in Figure 12b matches the measured data point inside the Lagrange radius, matches the two measured data points beyond the Lagrange radius, and then nicely threads the forward cloud image area all the way to 100 R_{Io}. For the trailing profile and the classical sputtering flux distribution in Figure 12a, the calculated D_2 emission brightness profile matches the measured data point inside the Lagrange radius, is slightly below the two measured data point outside the Lagrange radius, and then threads the lower of the two trailing cloud image areas nicely between about 15 R_{Io} and 35 R_{Io} before it falls too rapidly and drops below this area. An improved fit is also provided for the trailing profile by the modified sputtering distribution in Figure 12b. The calculated D_2 emission brightness profile for the trailing profile in Figure 12b matches the measured data point inside the Lagrange radius, is slightly below

the two measured data point outside the Lagrange radius, and then threads the lower of the two trailing cloud image areas nicely all the way to 100 R_{Io}. The lower of the two trailing cloud image areas corresponds to the east-west sodium cloud profile when the directional feature is oriented either north or south (i.e., above or below the east-west line or null location). For this non-null condition, it is particularly noteworthy that the spatially-isotropic ejection of sodium from the exobase with a modified sputtering flux distribution with α=7/3 provides an excellent fit to the combined eclipse, emission, and forward/trailing sodium cloud image profile data from 1.4 R_{Io} to 100 R_{Io}.

The measured trailing data points in Figure 12b were, however, acquired at the null condition and are consistent with the upper of the two trailing cloud image areas also acquired at the null condition. In order to fit the trailing profile for the null condition, it is then clear that a flux distribution is required with an even more enhanced high-speed population than the modified sputtering flux distribution with α=7/3. Since the modified sputtering flux distribution for α=7/3 corresponds to the limit of a single collision cascade process described by a Thomas-Fermi cross section (see Smyth and Combi 1988b), reducing the value of α to a smaller value becomes somewhat physically questionable but may be done for practical purposes of illustrating the impact of an enhanced high-speed population in the model calculation.

For a modified sputtering flux distribution with α=2, a most probable speed of 0.4 km sec^{-1}, and an isotropic exobase source rate of 1.9 x 10^{26} atoms sec^{-1} (i.e., a total flux ϕ_0 of 4.7 x 10^8 atoms cm^{-2} sec^{-1}), the model-data comparison is shown in Figure 13 for the eclipse column density and in Figure 14 for the emission and sodium cloud east-west D_2 emission brightness profiles. In Figure 13, the sputtering flux distribution provides a reasonably good fit to the observed column density data points with only a small departure

very near the exobase and produces a column density profile beyond 10 R_{Io} that is significantly enhanced compared to the α=7/3 case in Figure 11b. In Figure 14, the calculated D_2 emission brightness profile for the forward profile is significantly above the measured data point both inside and outside the Lagrange radius and is above or in the very top of the forward cloud image area all the way to 100 R_{Io}. The additional enhanced high-speed population of the α=2 modified sputtering flux distribution is too large and therefore not consistent with the observed forward profile. In contrast for the trailing profile in Figure 14, the calculated D_2 emission brightness profile matches the measured data point inside and outside of the Lagrange radius very well and then threads the upper of the two trailing cloud image areas nicely all the way to ~90 R_{Io}. This demonstrates that the trailing cloud can be fitted with an enhanced high-speed population of sodium atoms in the flux distribution. It also immediately demonstrates that the flux distribution at the exobase must be nonisotropic with some of the enhanced high-speed population weighted more toward vector directions that will preferentially populate the trailing cloud rather than the forward cloud. This nonisotropic requirement for a flux distribution for speeds of ~20 km sec^{-1} is consistent with the conclusion reached by the modeling analysis of observations for the north-south oscillating directional features by Pilcher *et al.* (1984). In this analysis, their ~20 km sec^{-1} sodium was constrained to be initially directed at near right angles to Io's orbital motion and hence was angularly deficient in the forward direction of motion of the satellite and (more importantly) in the trailing apex direction, which preferentially populates the forward cloud.

4. DISCUSSION AND CONCLUSIONS

The composite spatial information for sodium obtained by combining the eclipse observations (radial distances from Io of 1.4 R_{Io} to ~10 R_{Io}), the emission observations (east-west distances of ± 4 R_{Io} to ± 40 R_{Io}) and the sodium cloud observations (east-west distances of ± 10 R_{Io} to ± 100 R_{Io}) has been analyzed to extract a basic description for the flux speed distribution at the satellite's exobase. An isotropic modified-sputtering flux speed distribution with α=7/3, a most probable speed of 0.5 km sec^{-1}, and a source strength of 1.7×10^{26} atoms sec^{-1} provided a very good fit to these composite observations when the directional feature is either north or south and hence not contributing to east-west profile of the trailing cloud. It is remarkable that these observations, acquired by a number of ground-based programs over very different spatial scales and at different times during the 1975-1985 decade, are so self consistent. Near Io, the two-dimensional sodium column density produced by this modified sputtering distribution as calculated by the sodium cloud model in the profile analysis above is shown in Figure 15 and can be seen at larger distances from Io to become nonspherical and more confined near the satellite plane. This flattening near the satellite plane is the merging of the near Io corona into the sodium cloud and is caused naturally by orbital dynamics beyond the satellite Lagrange sphere where the gravity of Jupiter is dominant. This merging and its spatial extension into the forward sodium cloud is reproduced very well by the isotropic modified sputtering distribution. The forward cloud portion of the east-west emission data profiles has a rather tightly confined slope that, in the absence of the trailing cloud enhancement at the null condition, is less steep and is brighter than the trailing cloud profiles. In order, however, to reproduce the extended east-west profile in the trailing sodium cloud when the directional feature is in the satellite plane (i.e., the null condition), additional nonisotropic high-speed

sodium is required and is generally consistent with the earlier modeling of the directional feature (Pilcher *et al.* 1984).

The sodium atoms ejected from Io's exobase as described above by the modified sputtering flux distribution have speeds primarily in the range from 0 to a few 10's km sec^{-1}. This neutral flux distribution represents the spatially integrated effect of the incomplete collisional cascade process that occurs from the collisional interactions of heavy-ions in the corotating plasma torus with neutrals in Io's atmosphere. This flux speed distribution can be alternatively described as a source rate speed distribution by multiplying it by the satellite surface area. In addition to these ion-neutral elastic collisional encounters, resonance charge exchange between plasma torus sodium ions and neutral sodium in Io's atmosphere (i.e., $Na + Na^+ \rightarrow Na^+ + Na$) is also responsible for producing sodium atoms with higher speeds relative to Io. These speeds are centered about the corotational ion speed (~60 km sec^{-1}) relative to Io's motion and have a dispersion reaching from several 10's km sec^{-1} to ~100 km sec^{-1}. This higher-speed source of sodium atoms together with some lower speed (~15-20 km sec^{-1}) sodium atoms associated with the nonisotropic source for the directional feature have been shown in modeling studies (Smyth and Combi 1991; Flynn *et al.* 1992) to accurately reproduce the image of sodium in the (D_1+D_2) emission line brightness measured on a radial scale of ± 400-500 planetary radii about Jupiter by Mendillo *et al.* (1990). This large scale distribution of sodium has been called the magneto-nebula or sodium zenocorona. Modeling studies for this image indicated that the higher-speed source was ~2 x 10^{26} atoms sec^{-1} while the lower speed source was ~1 x 10^{26} atoms sec^{-1}. More recent observations and analysis for the sodium zenocorona images (Flynn *et al.* 1993) have shown that the source strength for the higher-speed sodium source is time variable with values usually in the range ~2-4 x 10^{26} atoms sec^{-1}. In addition, a recent analysis by Wilson (1993, private communication) of images

for the narrow forward jet of sodium observed by Schneider *et al.* (1991) has shown that this spatially distributed source is time variable and typically contributes a few times 10^{25} atoms sec^{-1} to the higher speed sodium source for the zenocorona. A typical total source rate speed distribution for sodium at Io's exobase can therefore be constructed by combining the modified sputtering source rate distribution determined in this paper with the charge exchange source rate distribution for the zenocorona (see Smyth and Combi 1991). This total source rate speed distribution function is shown in Figure 16, where the lower (solid line) and upper (dashed line) curves correspond, respectively, to the sodium zenocorona higher-speed source rate of 2.2×10^{26} atoms sec^{-1} as determined by Smyth and Combi (1991) from January 1990 image data and 4×10^{26} atoms sec^{-1} as determined by Flynn *et al.* (1993) from February 1991 image data.

The total source rate speed distribution functions at Io's exobase expected for other atomic species, such as K, O, and S, can be constructed in a similar fashion to sodium by adopting the estimated source rates for the modified sputtering distribution and the charge exchange distribution given by Smyth and Combi (1991). The main differences in the total source rate speed distribution functions will arise from the relative importance of the source strengths for the modified sputtering and charge exchange processes. The relative importance of the higher speed source to the lower speed source would be much smaller than sodium for K, because of the smaller number of K^+ ions in the plasma torus, and would be significantly larger than sodium for O and S, because of the much larger number of O and S ions in the plasma torus.

Future studies for the sodium flux speed distribution at Io's exobase are anticipated using a much larger emission data set for sodium (~100 profiles) acquired in 1987 and recently reduced by Schneider (1993, private communication) to a form suitable for

analysis. Because of the much larger data base, it will be possible in these studies to analyze the combined spatial and spectral information in order to refine the nonisotropic nature of the flux distribution and also to search for possible east-west and System III modulations in the flux speed distribution. Once this information is determined for sodium, the implications for the more abundant species in Io's atmosphere will be particularly important in other related studies for the many faceted and complex phenomena in the Io-Jupiter system.

ACKNOWLEDGMENTS

We are grateful to N. M. Schneider for helpful discussions and for providing the numerical data for the 1985 emission observations. This research was supported by the Planetary Atmospheres Program of the National Aeronautical and Space Administration under grant NAGW-3585 to the University of Michigan and under contracts NASW-4416 and NASW-4471 to Atmospheric and Environmental Research, Inc.

REFERENCES

Bergstralh, J. T., D. L. Matson, and T. V. Johnson 1975. Sodium D-Line Emission from Io: Synoptic Observations from Table Mountain Observatory. *Astrophys. J. Lett.* **195**, L-131-L135.

Bergstralh, J. T., J. W. Young, D. L. Matson, and T. V. Johnson 1977. Sodium D-Line Emission from Io: A Second Year of Synoptic Observation from Table Mountain Observatory. *Astrophys. J. Lett.* **211**, L51-L55.

Brown, R. A., and Y. L. Yung 1976. Io, Its Atmosphere and Optical Emissions. In *Jupiter Studies of the Interior, Atmosphere, Magnetosphere, and Satellites* (T. Gehrels, Ed.), pp. 1102-1145. Univ. of Arizona Press, Tucson.

Flynn, B., M. Mendillo, and J. Bumgardner 1992. Observations and Modeling of the Jovian Remote Sodium Emission. *Icarus* **99**, 115-130.

Flynn, B., M. Mendillo, and J. Bumgardner 1993. The Jovian Sodium Nebula: Two Years of Ground-Based Observations. preprint.

Goldberg, B. A., Yu. Mekler, R. W. Carlson, T. V. Johnson, and D. L. Matson 1980. Io's Sodium Emission Cloud and the Voyager 1 Encounter. *Icarus* **44**, 305-317.

Goldberg, B. A., G. W. Garneau, and S. K. LaVoie 1984. Io's Sodium Cloud. *Science* **226**, 512-516.

Goldberg, B. A. and Smyth, W. H. 1993. The JPL Table Mountain Io Sodium Cloud Data Set. Paper in preparation.

Matson, D. L., B. A. Goldberg, T. V. Johnson, and R. W. Carlson 1978. Images of Io's Sodium Cloud. *Science* **199**, 531-533.

Mendillo, M., J. Baumgardner, B. Flynn and W. J. Hughes 1990. The Extended Sodium Nebula of Jupiter. *Nature*, **348**, 312-314.

Murcray, F. J. 1978. Observations of Io's Sodium Cloud, Ph. D. Thesis, Dept. of Physics, Harvard University.

Murcray, F. J. and R. M. Goody 1978. Pictures of the Io Sodium Cloud. *Ap. J.*, **226**, 327- 335.

Pilcher, C. B., W. H. Smyth, M. R. Combi, and J. H. Fertel 1984. Io's Sodium Directional Features: Evidence for a Magnetospheric-Wind-Driven Gas Escape Mechanism. *Ap. J.*, 287, 427-444.

Schneider, N. M. 1988. Sodium in Io's Extended Atmosphere. Ph.D. Thesis, Department of Planetary Sciences, Univ. of Arizona.

Schneider, N. M., D. M. Hunten, W. K. Wells, and L. M. Trafton 1987. Eclipse Measurements of Io's Sodium Atmosphere. *Science*, **238**, 55-58.

Schneider, N. M., D. M. Hunten, W. K. Wells, A. B. Schultz, and U. Fink 1991. The Structure of Io's Corona. *Ap. J.*, **368**, 298-315.

Smyth, W. H. and M. R. Combi 1987. Nature of Io's Atmosphere and its Interaction with the Planetary Magnetosphere. *BAAS*, **19**, 855.

Smyth, W. H. and M. R. Combi 1988a. A General Model for Io's Neutral Gas Cloud. I. Mathematical Description. *Ap. J. Supp.*, **66**, 397-411.

Smyth, W. H. and M. R. Combi 1988b. A General Model for Io's Neutral Gas Clouds. II. Application to the Sodium Cloud. *Ap. J.*, **328**, 888-918.

Smyth, W. H. and M. R. Combi 1991. The Sodium Zenocorona. *JGR*, **96**, 22711-22727.

Smyth, W. H. and B. A. Goldberg 1993. The Io Sodium Cloud: Space-Time Signatures of East-West and System III Longitudinal Asymmetries in the Jovian Magnetosphere. Paper presented at the Io: An International Conference, San Juan Capistrano, California, June 22-25.

Smyth, W. H., and M. B. McElroy 1978. Io's Sodium Cloud: Comparison of Models and Two-Dimensional Images. *Astrophys. J.* **226**, 336-346.

Table 1

1985 Io Eclipse and Emission Measurements

Date	UT Midpoint	Io Geocentric Phase Angle Range (deg)	Io System III Longitude Range (deg)	Spectrum ID	Type of Observation	
					Eclipse	Emission
August 27	0714	61.4 ± 0.7	29.9 ± 2.3	85g188		1
	0720	62.3 ± 11.0	32.9 ± 35.8	a	1	
	0830	72.2 ± 1.1	65.1 ± 3.4	85g196		2
September 13	0641	276.6 ± 0.7	194.7 ± 2.3	85h032		3
September 14	0245	87.7 ± 0.7	31.4 ± 2.3	85h102		4
	0326	93.5 ± 4.2	50.5 ± 13.7	b	2	
	0416	100.6 ± 0.4	73.6 ± 1.4	85h113		5
September 15	0316	294.7 ± 0.7	353.7 ± 3.0	85h152		6
	0500	309.4 ± 11.5	41.7 ± 37.4	c	3	
September 21	0604	100.5 ± 1.6	112.5 ± 5.2	d	4	
September 23	0230	117.2 ± 0.7	267.6 ± 2.3	85h433		7
	0301	121.6 ± 0.4	281.9 ± 1.2	85h436		8
	0356	129.3 ± 2.0	307.3 ± 6.7	e	5	
	0534	143.1 ± 0.7	352.9 ± 2.3	85h457		9

a. Eclipse 1 : 85g179, 85g181, 85g185, 85g188, 85g192, 85g193, 85g196

b. Eclipse 2 : 85h103, 85h104, 85h105, 85h106, 85h107, 85h108, 85h109, 85h110, 85h112

c. Eclipse 3 : 85h153, 85h154, 85h155, 85h157, 85h159, 85h162, 85h163

d. Eclipse 4 : 85h287, 85h288, 85h289, 85h290, 85h291, 85h292, 85h293, 85h294, 85h295

e. Eclipse 5 : 85h441, 85h442, 85h443, 85h444, 85h445, 85h446, 85h447, 85h448, 85h449, 85h450

Table 2. 1985 Emission Data

	Radial Distance From Io (satellite radii)	D_2 Intensity (kR)								
		Emission 1 61.4° 27 August (85g188)	Emission 2 72.2° 27 August (85g196)	Emission 4 87.7° 14 September (85h102)	Emission 5 100.6° 14 September (85h113)	Emission 7 117.2° 23 September (85h433)	Emission 8 121.6° 23 September (85h436)	Emission 9 143.1° 23 September (85h457)	Emission 3* 276.6° 13 September (85h032)	Emission 6 294.7° 15 September (85h152)
	-29.92					0.69	0.93	0.66		
	-29.65									1.12
	-24.48								1.40	
	-21.76					1.19	0.84	0.95		
	-16.32					1.38	2.10		2.22	
	-15.78							1.74		2.15
	-14.96				1.91					
	-10.88	3.16				2.90	3.29	3.38	4.40	
↑	-9.52			3.17						
West	-6.80	5.21	4.50	6.41		7.49	7.76		1.54	
	-4.08	14.65	11.29	14.71				7.54	28.69	
	-3.81									18.75
	-2.18	24.31	18.39	24.12		25.61	25.01	21.00	45.47	
	-1.09	27.46	19.99	27.14		29.95	28.72	23.89	48.61	
	-0.82									24.85
Io	0.00	27.44	19.19	27.14		27.90	30.16	23.97	45.56	
	0.27									25.27
	1.09	25.87	19.35	26.65	23.03	26.31	26.39	22.84	39.45	
	1.36									22.90
	2.18	25.19	16.87	25.68	19.60	22.42	23.91	20.21	33.60	
	3.26									11.53
	4.08	17.60	11.92	18.10	11.87	15.54	14.83	12.52	20.06	
	5.98									4.79
East	6.80	8.31	5.52	8.17	5.52	7.09	7.10	6.02	7.52	
↓	10.06									1.66
	10.88	3.40	1.94	3.84	3.21	2.47	2.47	2.26	2.73	
	15.50									0.77
	16.32			2.84	1.81	1.03	1.11	0.82	1.39	
	21.76			2.25		0.68	0.75	0.52		
	23.66									0.53
	24.48				1.24				1.06	
	27.20			1.39						
	35.36			1.27					1.00	
	46.24								0.83	

*calibration uncertain

Table 3

Power Law Fit to the D_2 Emission Profiles for Io East of Jupiter†

Date	Io Geocentric Phase Angle (deg)	Io System III Longitude (deg)	Exponent		Amplitude (kR)	
			East Profile	West Profile	East Profile	West Profile
August 27	61.4	29.9	1.67 (F)	1.57 (T)	191	124
	72.2	65.1	1.85 (S)	1.80 (S)	169	142
September 14	87.7	31.4	1.23 (S/T)	1.80 (S/F)	89	188
	100.6	73.6	1.27 (T)	--	66	--
September 23	117.2	267.6	2.05 (T)	1.57 (F)	342	135
	121.6	281.9	1.96 (T)	1.54 (F)	283	138
	143.1	352.9	2.16 (T)	1.64 (F)	374	165

† Profile points inside of 4 R_{Io} are excluded

F = forward cloud; S = symmetric turning point; T = trailing cloud.

Table 4
East-West D_2 Brightness Profiles for Sodium Cloud Image Data

LT Date	LT Time	Image ID Number	Io Geocentric Phase Angle (deg)	Io System III Longitude (deg)	East-West Distance from Io for Specified D_2 Brightness Level (satellite radii)							
					0.5 kR		1.0 kR		1.5 kR		2.0 kR	
					Forward	Trailing	Forward	Trailing	Forward	Trailing	Forward	Trailing
Image Data Set Reference: Murcray (1976)												
1976 Nov. 16	0806	ES 328B	256	262	--	--	51	29	46	24	28	14
1977 Jan 27	0024	ES 369A	86	193	60	38	50	22	44	19	32	16
	0217	ES 370D	102	245	>83	30	56	25	46	21	24	19
					0.2 kR		0.5 kR		1.0 kR		2.0 kR	
					Forward	Trailing	Forward	Trailing	Forward	Trailing	Forward	Trailing
Image Data Set Reference: Goldberg and Smyth (1993)												
1981 May 5	0819	SIP 418/31-33	102	300	78	69	63	40-66	45	37	24	21
May 12	0848	SIP 420/30-32	91	302	66	86	41	37	35	29	20	21
May 13	0346	SIP 421/21-23	253	108	74-103	73	70	41	41	27	29	20
	0555	SIP 421/32-33	271	168	124	65	112	44	51	30	26	19
June 6	0436	SIP 424/10-12	103	300	81	75	68	71	36	26	20	23
					0.3 kR		0.6 kR		0.9 kR		1.8 kR	
					Forward	Trailing	Forward	Trailing	Forward	Trailing	Forward	Trailing
Image Data Set Reference: Morgen (1984)												
1983 June 13	0714	I 8492	274	230	--	39	58	26	37	19	20	--
	0722	I 8494	275	233	--	35	52	22	40	20	20	--
	0729	I 8496	276	237	>93	36	52	22	37	17	22	--
	0827	I 8501	284	264	>93	39	61	25	42	19	23	--
	0949	I 8509	296	301	>93	47	63	26	44	17	24	--
	1010	I 8511	299	311	>93	41	63	23	44	16	19	--

Table 5

1985 Io Emission Measurements

Emission	Date	Io Geocentric Phase Angle Range (deg)	Io System III Longitude Range (deg)	Directional Feature Orientation	Dominant Spatial Profile	Enhanced Doppler Signatures
1	August 27	61.4 ± 0.7	29.9 ± 2.3	null	similar	trailing/forward
2		72.2 ± 1.1	65.1 ± 3.4	south	symmetric	no
3	September 13	276.6 ± 0.7	194.7 ± 2.3	null/north	similar	trailing
4	September 14	87.7 ± 0.7	31.4 ± 2.3	null	trailing	trailing
5		100.6 ± 0.4	73.6 ± 1.4	south	---	no
6	September 15	294.7 ± 0.7	353.7 ± 3.0	null	trailing	trailing
7	September 23	117.2 ± 0.7	267.6 ± 2.3	north	forward	no
8		121.6 ± 0.4	281.9 ± 1.2	north	forward	no
9		143.1 ± 0.7	352.9 ± 2.3	null	forward	no

FIGURE CAPTIONS

FIG. 1. 1985 Eclipse Data. The sodium column density is shown as a function of the radial distance from the center of Io for the five eclipse measurements acquired by Schneider *et al.* (1991). The position of the nominal exobase and the average Lagrange radius are indicated.

FIG. 2. 1985 Emission Data. The sodium D_2 emission brightness in units of kiloRayleighs is shown as a function of the east-west distance from the center of Io along the observing slit for the nine emission observations summarized in Table 3 and acquired by Schneider *et al.* (1991).

FIG. 3. Selected East and West Brightness Profiles for the 1985 Emission Data. The spatial profiles both east and west of Io for the sodium D_2 emission brightness in units of kiloRayleighs are shown as a function of the distance along the observing slit from the center of Io for five emission observations identified by their satellite geocentric phase angle. These five profiles occur when Io is east of Jupiter and just past the satellite phase angle where the forward cloud has its symmetric turning point so that the trailing cloud profiles are all to the east of Io and the forward cloud profiles are all to the west of Io. A power law fit to each profile is also shown. At larger distances from Io, an envelope for the east-west D_2 emission profile acquired from sodium image data is shown by the shaded area. For the trailing profile, the shaded area is divided into two parts, where the lower area corresponds to sodium cloud data where the directional feature is oriented either north or south and where the upper area corresponds to the directional feature oriented along the east-west direction (i.e., the null condition).

FIG. 4. System III Correlation for the North-South Orientation of the Sodium Cloud Directional Feature. The north and south orientation of the directional feature as determined by Goldberg and Smyth (1993) from a set of sodium D-line emission image observations is shown as a function of the System III longitude angle of Io. Note that image observations for Io east and west of Jupiter are identified, respectively, by open and filled squares.

FIG. 5. Io Sodium Cloud Images. Three calibrated D_2 emission images of the Io sodium cloud from the JPL Table Mountain Data Set are shown to proper scale with Jupiter and Io's orbit as viewed from earth in 1981 (Smyth and Goldberg 1993). The Io System III longitude and corresponding orientation of the trailing directional feature in image A are 247 degrees and north, in image B are 104 degrees and south, and in image C are 178 degrees and only very slightly north. An east-west spatial scale of ± 100 planetary radii about Io is shown for reference. Contour levels for the D_2 brightness, from outside to inside, are 0.2, 0.5, 1, 2, 4, 6, 8, and 10 kR.

FIG. 6. Monoenergetic Sodium Cloud Modeling of the 1985 Eclipse Data. The eclipse data points of Schneider *et al.* (1991) are shown by the open circles. The dots are calculated by the Io sodium cloud model of Smyth and Combi (1988b) for their case C description of the plasma torus with an east-west electric field of 2.8 mV m^{-1} in the Io frame and for an isotropic and radial ejection of 2.6 km sec^{-1} sodium atoms from an assumed exobase of 2600 km radius for a source strength of 6.2×10^{25} atoms sec^{-1}. The calculation was performed for an Io geocentric phase angle of 92.9 degrees and an Io System III longitude angle of 48.6 degrees. The sodium source used here is typical of that required for this monoenergetic calculation to fit the D_2 emission brightness of the sodium cloud images at larger distances from Io.

FIG. 7. Effect of Lifetime on the Sodium Column Abundance. Two model calculations for the column abundance are compared with the eclipse data points (shown by the open circles) of Schneider *et al.* (1991). The plasma torus description adopted in the Io sodium cloud model is described in Fig. caption 6. The eclipse data points are fit outside and somewhat inside the Lagrange radius by the model for the minimum lifetime case (filled circles), which occurs for an Io phase angle of 90 degrees (eastern elongation), an Io System III magnetic longitude angle of 179 degrees, and a sodium source rate of 0.96 x 10^{26} atoms sec^{-1}. The same source rate is assumed for the maximum lifetime case (filled squares), which occurs for an Io phase of 270 degrees (western elongation) and an Io System III magnetic longitude angle of 299 degrees.

FIG. 8. Flux Speed Distribution Functions for Sodium at Io's Exobase. Maxwell-Boltzmann flux speed distribution for sodium are shown for a most probable speed, v_m, of 1.3 km sec^{-1} (short dashed line) and 2.0 km sec^{-1} (longer dashed line). Modified sputtering flux speed distributions are also shown for α =3 and a most probable speed of 1.0 km sec^{-1} (dotted line) and for α =7/3 and a most probable speed of 0.5 km sec^{-1} (solid line). All of the flux speed distributions are normalized to unit area.

FIG. 9. Model Calculations for the Io Eclipse Data Using a Maxwell-Boltzmann Flux Speed Distribution. The atomic sodium column density profile near Io determined from the 1985 eclipse data by Schneider *et al.* (1991) is shown by the open circles. The model calculated column density profiles are shown by solid dots for the (cylindrically-averaged) corona, by solid triangles for the forward cloud along the east-west slit direction, and by solid squares for the trailing cloud along the east-west slit direction. These column density profiles were calculated using the Io sodium cloud model of Smyth and Combi (1988b) for their case C

description of the plasma torus (see Fig. caption 6) and for an Io geocentric phase angle of 92.9 degrees and an Io System III longitude angle of 48.6 degrees, which are similar to the emission 4 observation conditions in Table 1. Sodium was ejected uniformly from an assumed exobase of 2600 km radius with a velocity dispersion for a Maxwell–Boltzmann flux distribution, where in (a) v_m = 1.3 km sec^{-1} and ϕ_0 = 3.0 x 10^8 atom cm^{-2} sec^{-1}, and in (b) v_m = 2.0 km sec^{-1}, and ϕ_0 = 1.8 x 10^8 atom cm^{-2} sec^{-1}.

FIG. 10. Model Calculations for the East-West D_2 Brightness Profiles Using a Maxwell-Boltzmann Flux Speed Distribution. The east-west D2 brightness profile near Io in both the trailing and forward cloud directions as determined by the emission 4 data of Schneider *et al.* (1991) are shown by the open circles. The east-west profile envelopes in both the trailing and forward cloud directions as determined from the sodium cloud image data are shown by the shaded areas (see Fig. caption 3). The descriptions of the symbols for the calculated profiles, the sodium cloud model and plasma torus, and the Maxwell–Boltzmann flux distribution in (a) and (b) are the same as in Fig. caption 9.

FIG. 11. Model Calculations for the Eclipse Data Using a Modified Sputtering Flux Speed Distribution. The atomic sodium column density profile near Io determined from the 1985 eclipse data by Schneider *et al.* (1991) is shown by the open circles. The model calculated column density profiles are shown by solid dots for the (cylindrically-averaged) corona, by solid triangles for the forward cloud along the east-west direction, and by solid squares for the trailing cloud along the east-west direction. These column density profiles were calculated using the Io sodium cloud model of Smyth and Combi (1988b) for their case C description of the plasma torus (see Fig. caption 6) and for an Io geocentric phase angle of 92.9 degrees and an Io System III longitude angle of 48.6 degrees, which are similar to the emission 4 observation conditions in Table 1. Sodium was ejected uniformly from an assumed exobase

of 2600 km radius with a velocity dispersion for a modified sputtering flux distribution, where in (a) $\alpha = 3$, $v_m = 1.0$ km sec^{-1}, and $\phi_0 = 3.2 \times 10^8$ atom cm^{-2} sec^{-1}, and in (b) $\alpha = 7/3$, $v_m = 0.5$ km sec^{-1}, and $\phi_0 = 4.2 \times 10^8$ atom cm^{-2} sec^{-1}.

FIG. 12. Model Calculations for the East-West D_2 Brightness Profiles Using a Modified Sputtering Flux Speed Distribution. The east-west D_2 brightness profile near Io in both the trailing and forward cloud directions determined by the emission 4 data of Schneider *et al.* (1991) are shown by the open circles. The east-west profile envelopes determined from the sodium cloud image data are shown by the shaded areas (see Fig. caption 3). The descriptions of the symbols for the calculated profiles, the sodium cloud model and plasma torus, and the modified sputtering flux distribution used in (a) and (b) are the same as in Fig. caption 11.

FIG. 13. Model Calculations for the Eclipse Data Using a Modified Sputtering Flux Speed Distribution. The atomic sodium column density profile near Io determined from the 1985 eclipse data by Schneider *et al.* (1991) is shown by the open circles. The model calculated column density profiles are shown by solid dots for the (cylindrically-averaged) corona, by solid triangles for the forward cloud along the east-west direction, and by solid squares for the trailing cloud along the east-west direction. These column density profiles were calculated using the Io sodium cloud model of Smyth and Combi (1988b) for their case C description of the plasma torus (see Fig. caption 6) and for an Io geocentric phase angle of 92.9 degrees and an Io System III longitude angle of 48.6 degrees, which are similar to the emission 4 observation conditions in Table 1. Sodium was ejected uniformly from an assumed exobase of 2600 km radius with a velocity dispersion for a modified sputtering flux distribution, where $\alpha = 2$, $v_m = 0.4$ km sec^{-1}, and $\phi_0 = 4.7 \times 10^8$ atom cm^{-2} sec^{-1}.

FIG. 14. Model Calculations for the East-West D_2 Brightness Profiles Using a Modified Sputtering Flux Speed Distribution. The east-west D2 brightness profile near Io in both the trailing and forward cloud directions determined by the emission 4 data of Schneider *et al.* (1991) are shown by the open circles. The east-west profile envelopes determined from the sodium cloud image data are shown by the shaded areas (see Fig. caption 3). The descriptions of the symbols for the calculated profiles, the sodium cloud model and plasma torus, and the modified sputtering flux distribution are the same as in Fig. caption 13.

FIG. 15. Two-Dimensional Nature of the Sodium Column Density in Io's Corona. Contours for the two-dimensional column density in Io's corona are shown in the sky-plane of the earth as determined from the sodium cloud model calculation for the modified sputtering flux speed distribution described in Fig. 11(b). The vertical and horizontal directions are the projected directions that are, respectively, perpendicular and parallel to the semi-major axis of the Io's orbital ellipse on the sky plane. The scale is in kilometers, and the small tick marks are separated by 1000 km. Io's location and size are shown to scale by the black circle. The sodium column density contours in units of 10^{11} atoms cm^{-2} are, from inside to outside, 7, 5, 3, 2, 1, 0.7, 0.5, 0.3, and 0.2.

FIG. 16. Total Source Rate Speed Distribution Function for Sodium at Io's Exobase. The total source rate speed distribution function at Io's exobase, in units of 10^{26} atoms sec^{-1} $(km/sec)^{-1}$, is composed of three separate source rate speed distributions as discussed in the text and is shown for a smaller (solid line) and larger (dashed line) source strength for the higher-speed zenocorona source centered about 57 km sec^{-1}. The decomposition of the solid curve into its three separate source rate speed distributions is shown in the cutout and is determined by combining (1) the isotropic modified sputtering source rate distribution

(dotted line in the cutout) for $\alpha = 7/3$, $v_m = 0.5$ km sec^{-1} and a source strength of 1.75 x 10^{26} atom sec^{-1}, (2) the nonisotropic lower-speed source rate distribution (short dashed line in the cutout) for the sodium zenocorona centered about 20 km sec^{-1}, with a source strength of 1.1 x 10^{26} atoms sec^{-1} as determined by Smyth and Combi (1991), and (3) the nonisotropic higher-speed source rate distribution (longer dashed line in the cutout) for the sodium zenocorona centered about 57 km sec^{-1}, with a source strength of 2.2 x 10^{26} atoms sec^{-1} as determined by Smyth and Combi (1991). The source rate speed distribution (dashed line) with the larger source strength for the higher-speed zenocorona source is determined in the same fashion with the exception that the higher-speed zenocorona source is increased to 4.0 x 10^{26} atoms sec^{-1} , so as to exhibit the typical time-variable source range of 2-4 x 10^{26} atoms sec^{-1} reported by Flynn *et al.* (1993).

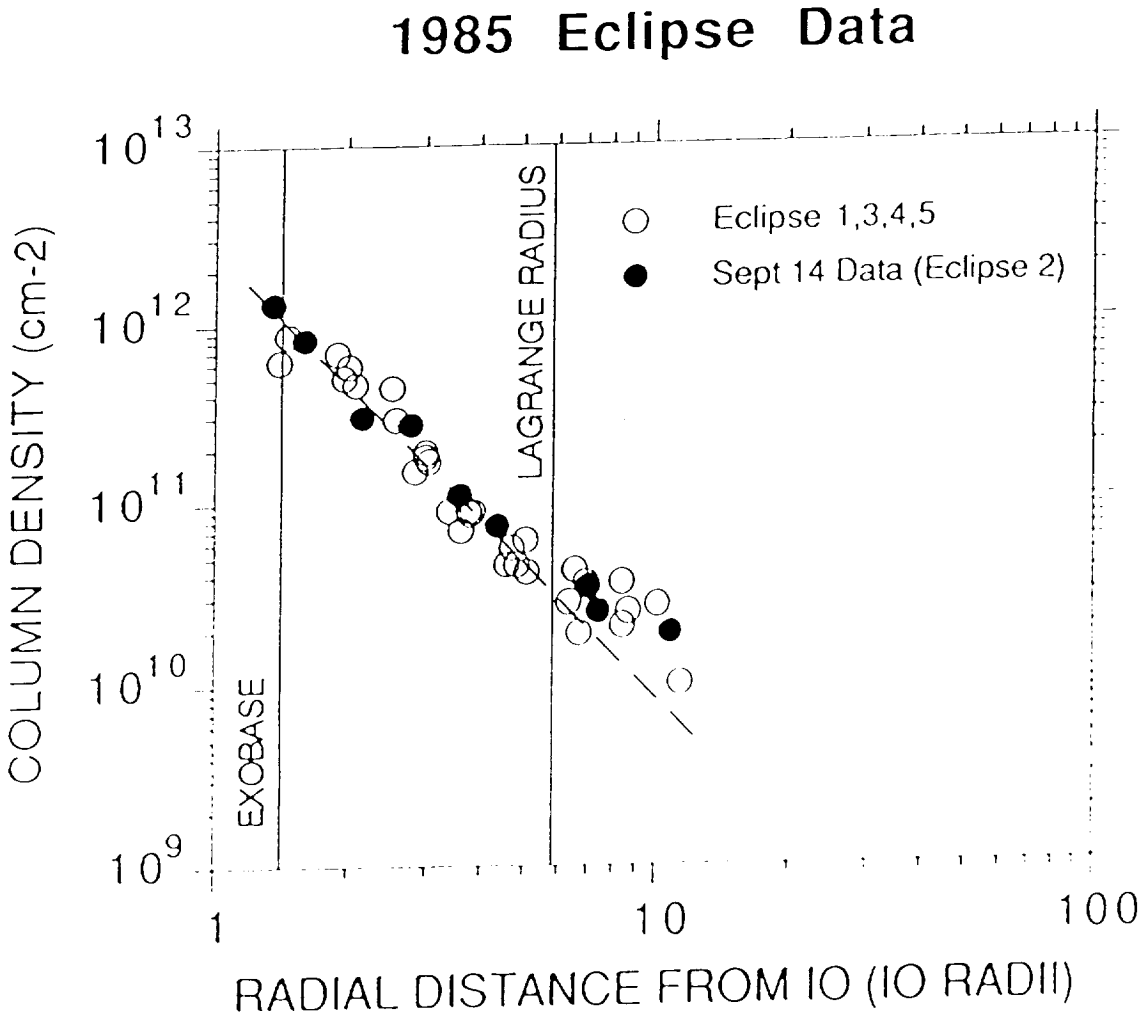
1985 Eclipse Data
COLUMN DENSITY (cm-2)
10^{13}
10^{12}
10^{11}
10^{10}
10^{9}
EXOBASE
LAGRANGE RADIUS
Eclipse 1,3,4,5
Sept 14 Data (Eclipse 2)
1
10
100
RADIAL DISTANCE FROM IO (IO RADII)

Figure 1

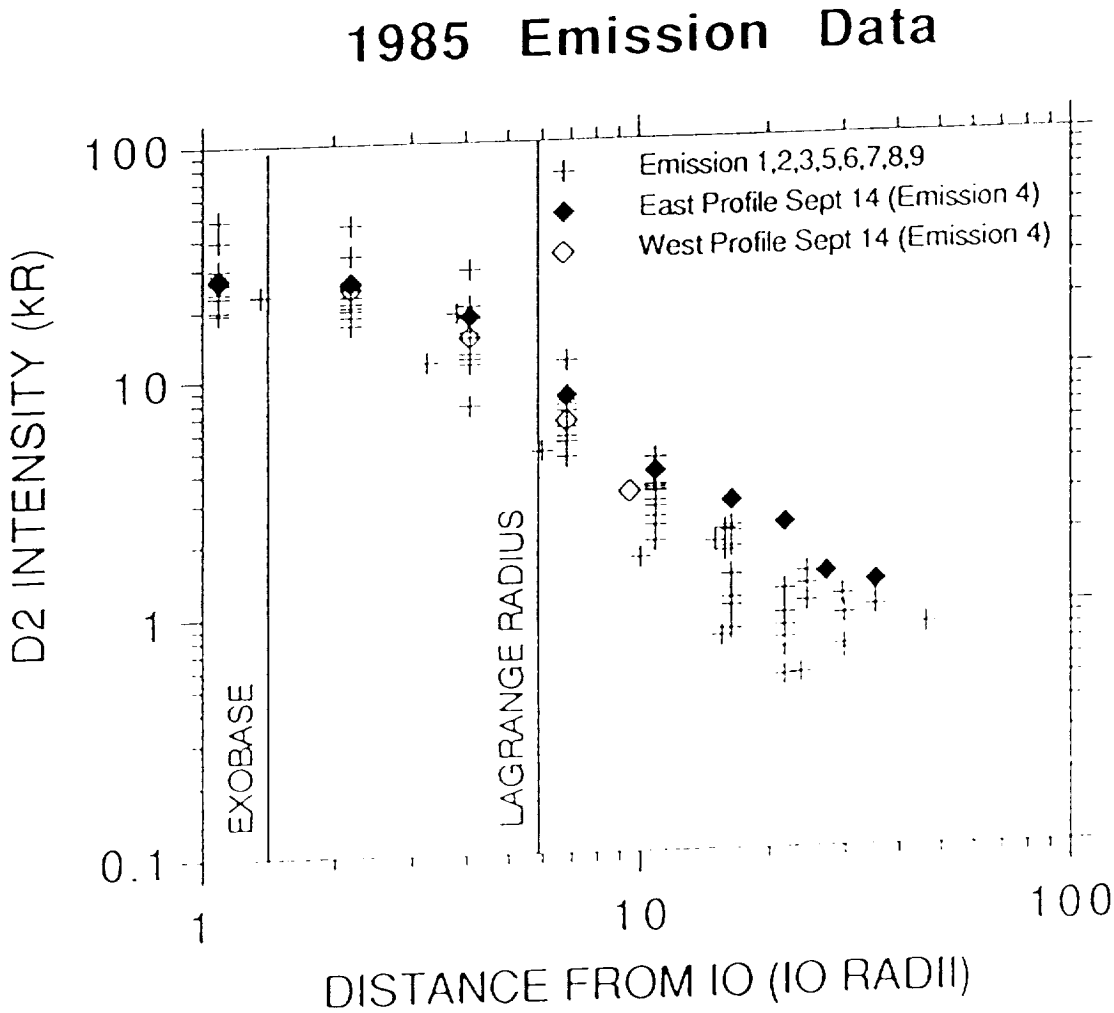
1985 Emission Data
Emission 1,2,3,5,6,7,8,9
East Profile Sept 14 (Emission 4)
West Profile Sept 14 (Emission 4)
D2 INTENSITY (kR)
100
10
1
0.1
EXOBASE
LAGRANGE RADIUS
1
10
100
DISTANCE FROM IO (IO RADII)

Figure 2

1985 EMISSIOM DATA

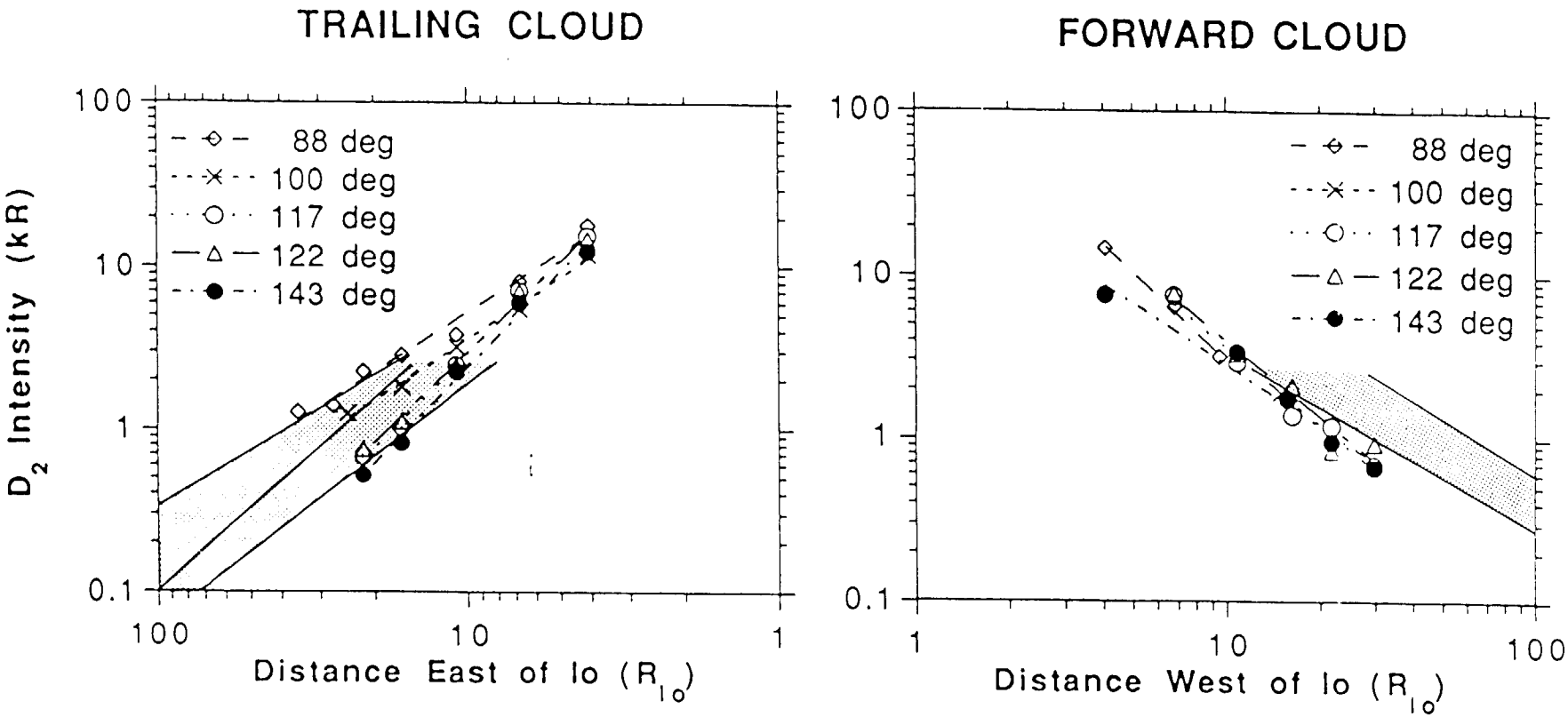

Figure 3

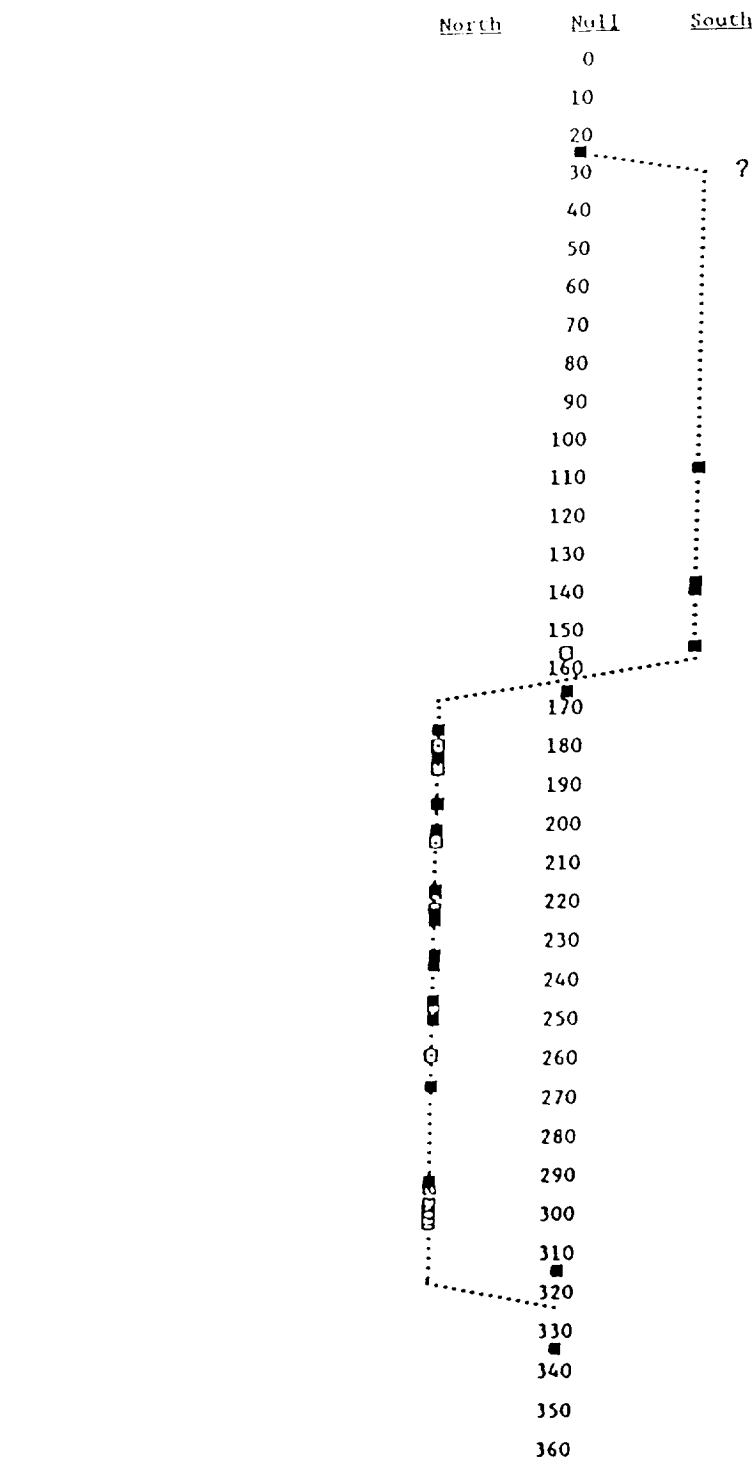
North
Null
South
0
10
20
30
40
50
60
70
80
90
100
110
120
130
140
150
160
170
180
190
200
210
220
230
240
250
260
270
280
290
300
310
320
330
340
350
360
?
East Cloud
West Cloud

Figure 4

IO SODIUM CLOUD 1981

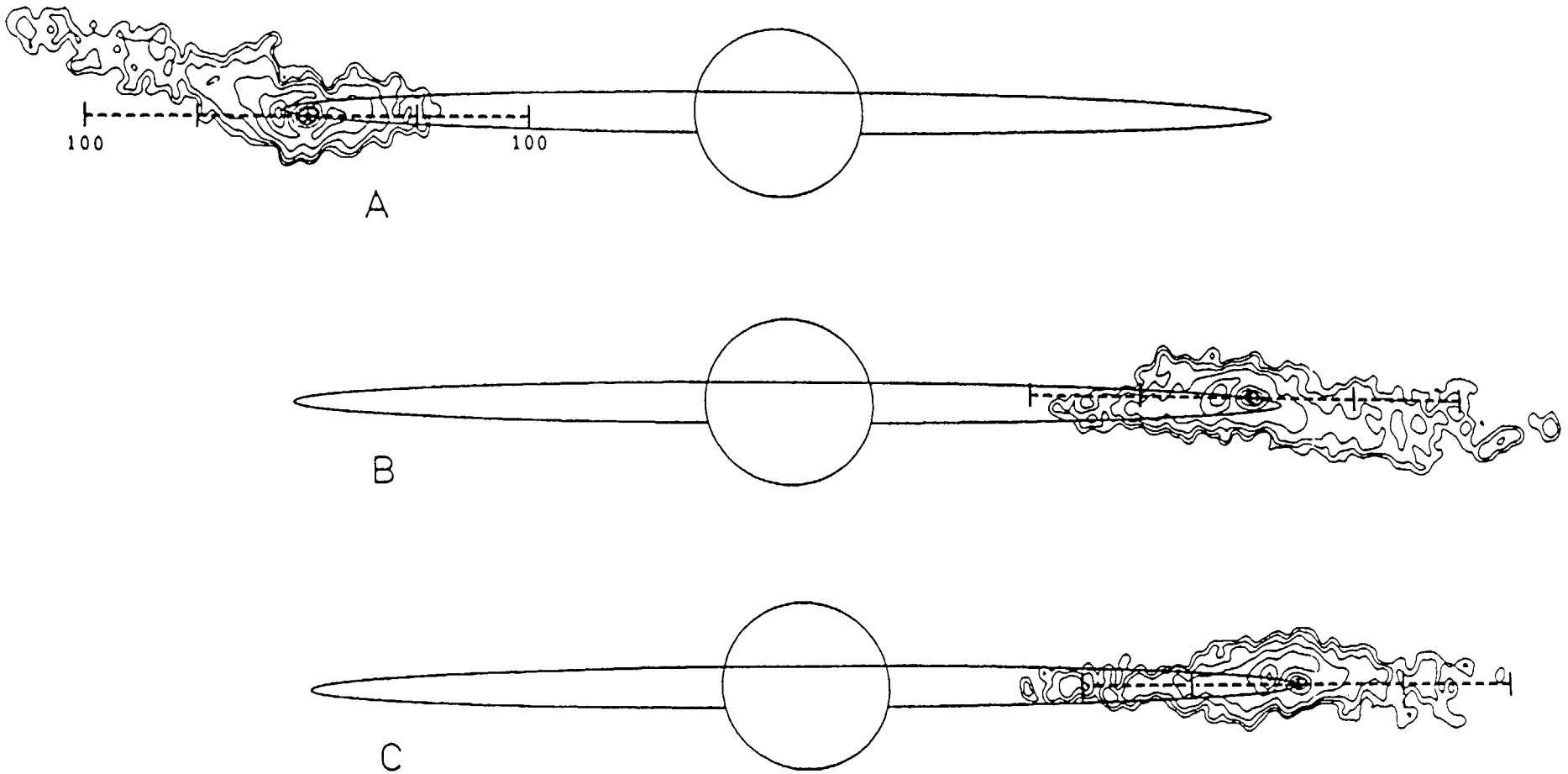

Figure 5

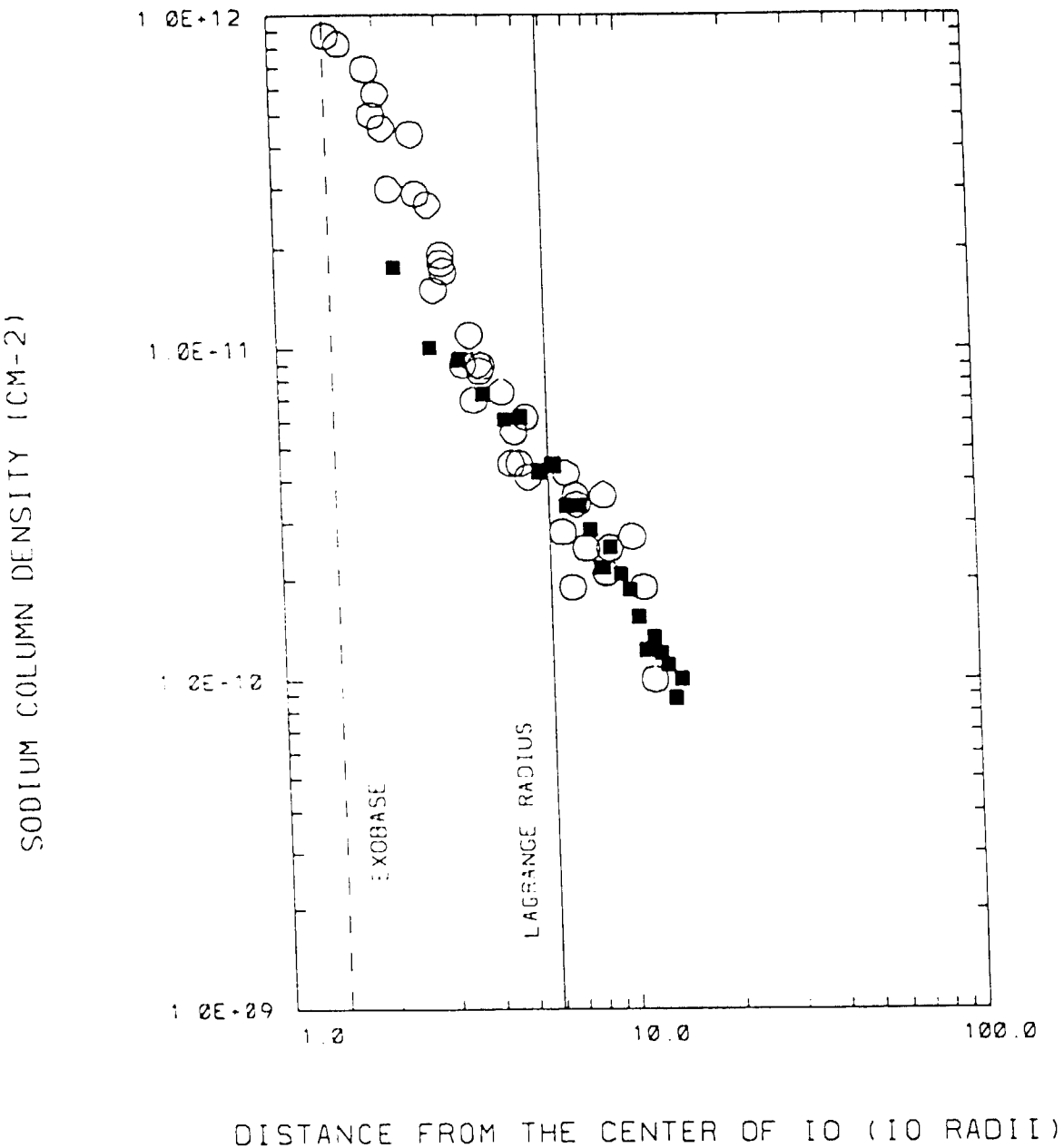
1.0E+12
1.0E-11
1.0E-10
1.0E-09
1.0
10.0
100.0
EXOBASE
LAGRANGE RADIUS
SODIUM COLUMN DENSITY (CM-2)
DISTANCE FROM THE CENTER OF IO (IO RADII)

Figure 6

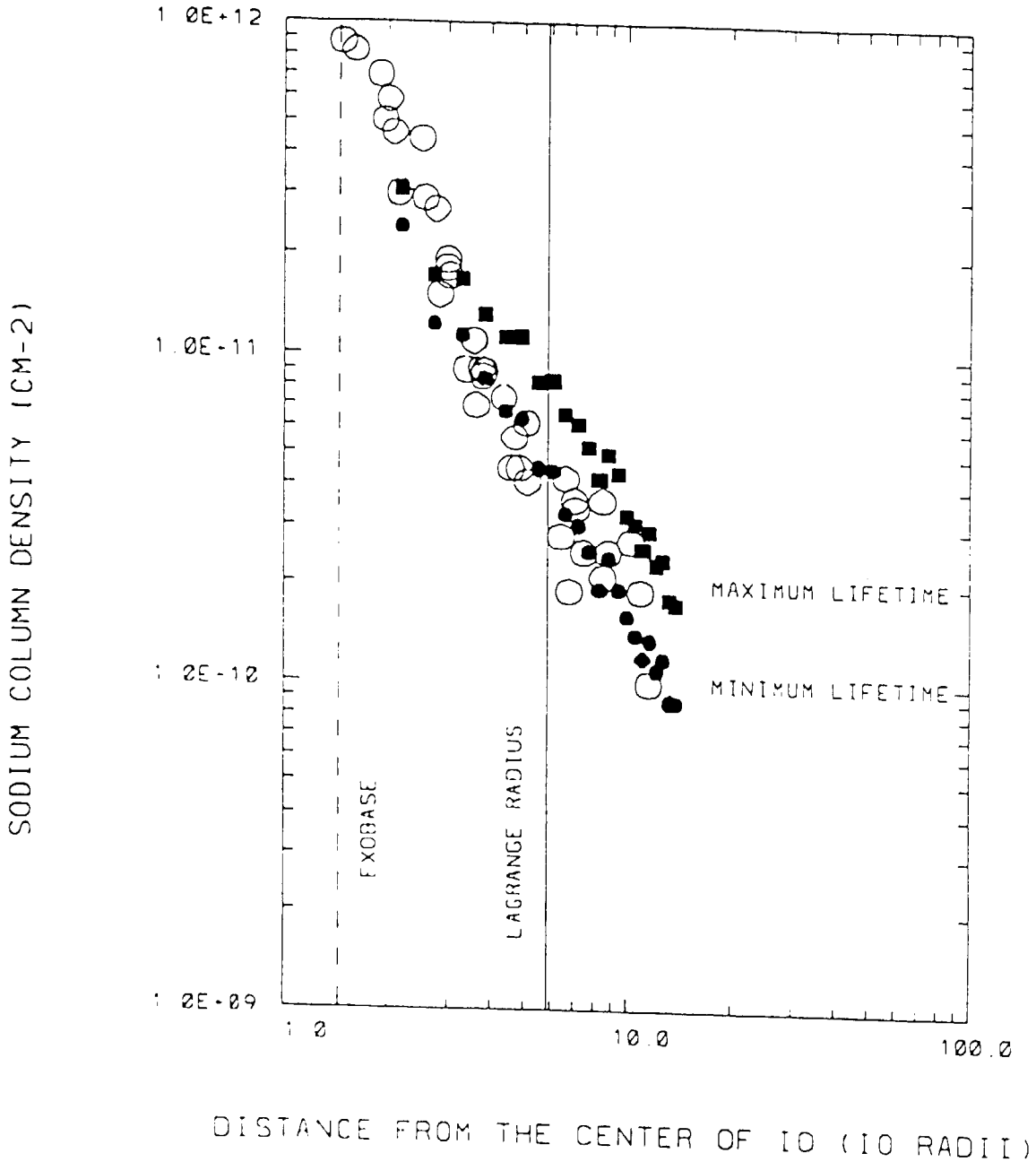
1.0E+12
1.0E-11
2E-10
2E-09
1.0
10.0
100.0
SODIUM COLUMN DENSITY (CM-2)
DISTANCE FROM THE CENTER OF IO (IO RADII)
EXOBASE
LAGRANGE RADIUS
MAXIMUM LIFETIME
MINIMUM LIFETIME

Figure 7

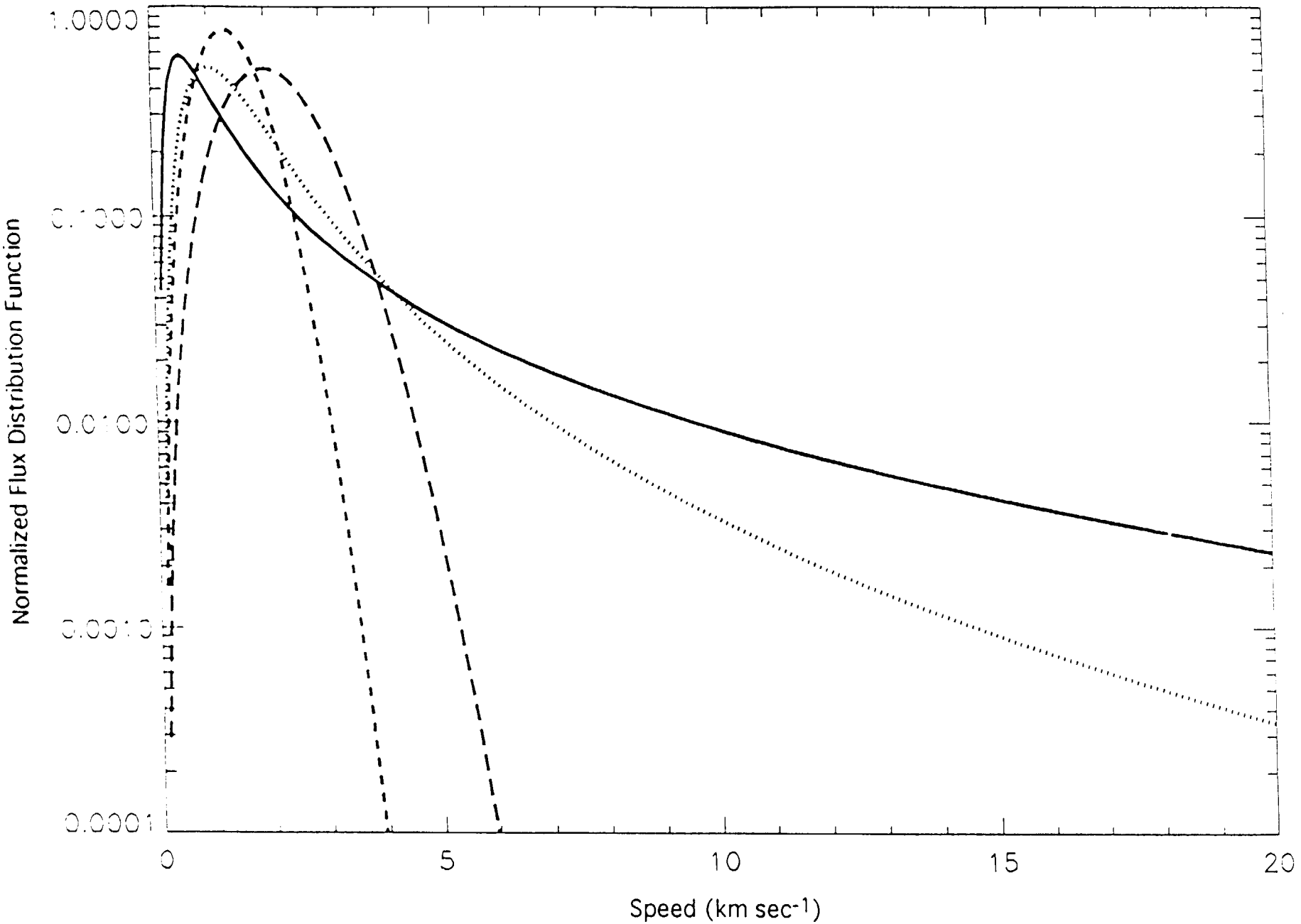
1.0000
0.1000
0.0100
0.0010
0.0001
Normalized Flux Distribution Function
0
5
10
15
20
Speed (km sec-1)

Figure 8

Maxwell-Boltzmann Flux Distribution

Most Probable Speed = 1.3 km/s
Isotropic Exobase Source Rate = 1.2×10^{26} atoms/s

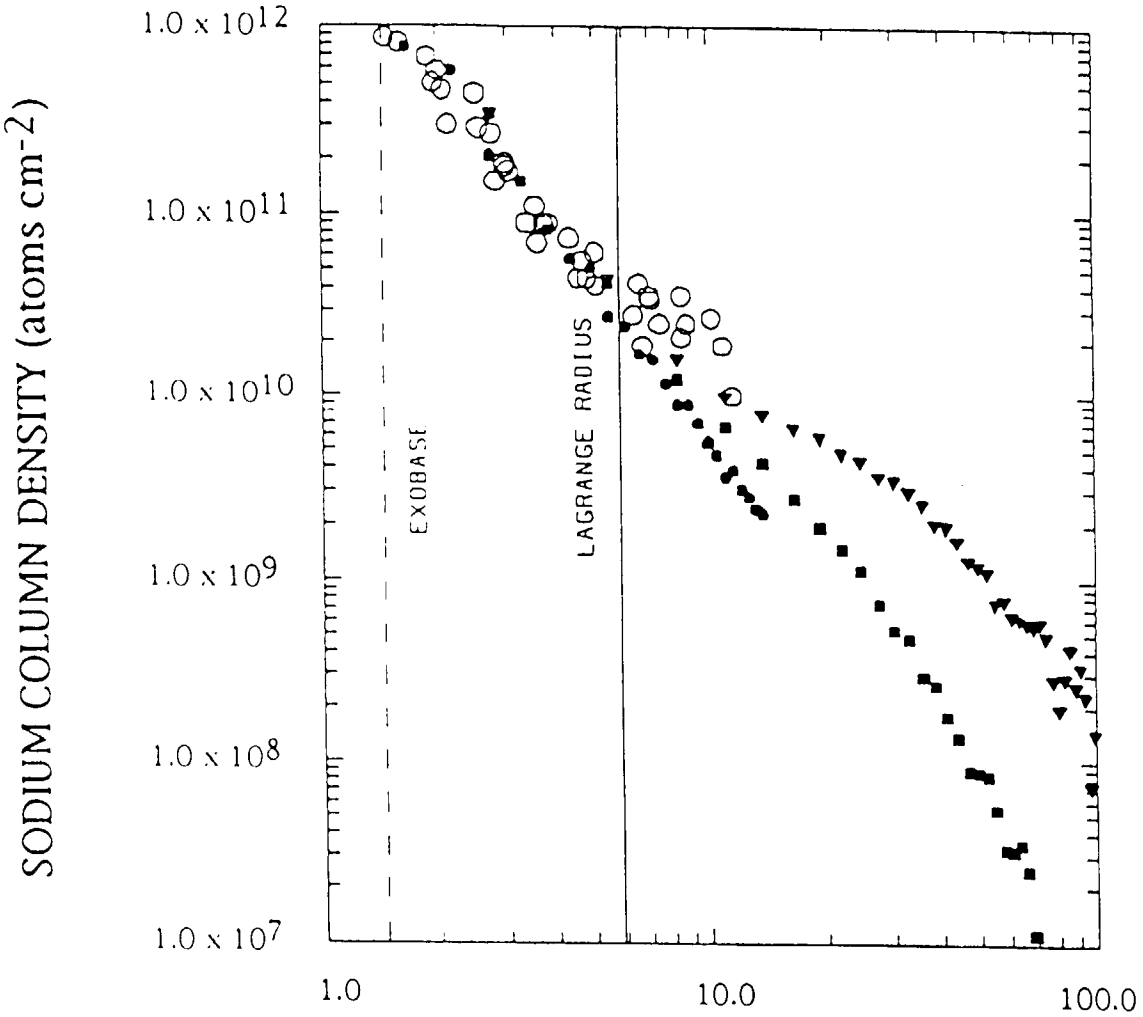

Figure 9a

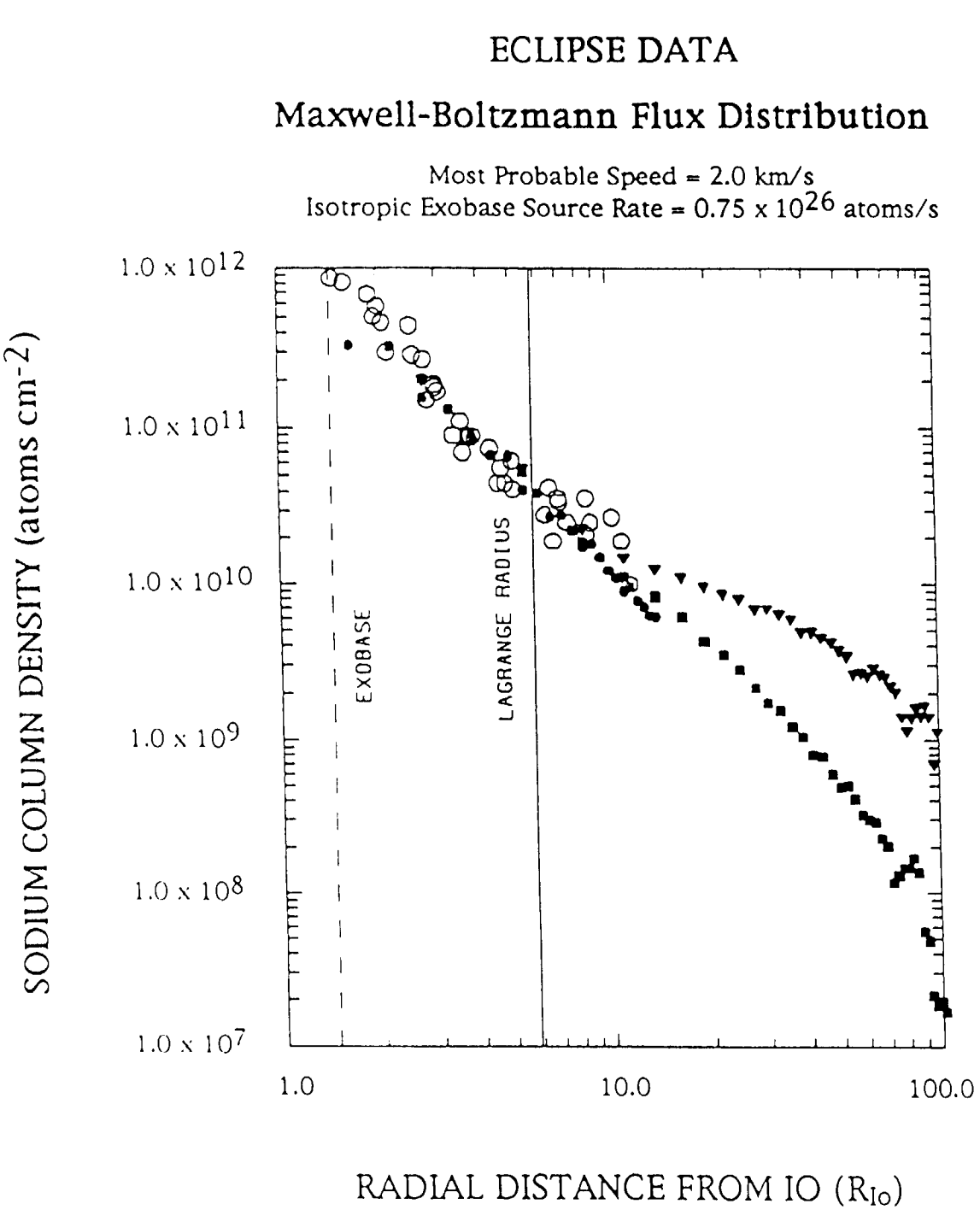
ECLIPSE DATA
Maxwell-Boltzmann Flux Distribution
Most Probable Speed = 2.0 km/s
Isotropic Exobase Source Rate = 0.75 x 10^26 atoms/s
SODIUM COLUMN DENSITY (atoms cm^-2)
1.0 x 10^12
1.0 x 10^11
1.0 x 10^10
1.0 x 10^9
1.0 x 10^8
1.0 x 10^7
EXOBASE
LAGRANGE RADIUS
1.0
10.0
100.0
RADIAL DISTANCE FROM IO (R_Io)

Figure 9b

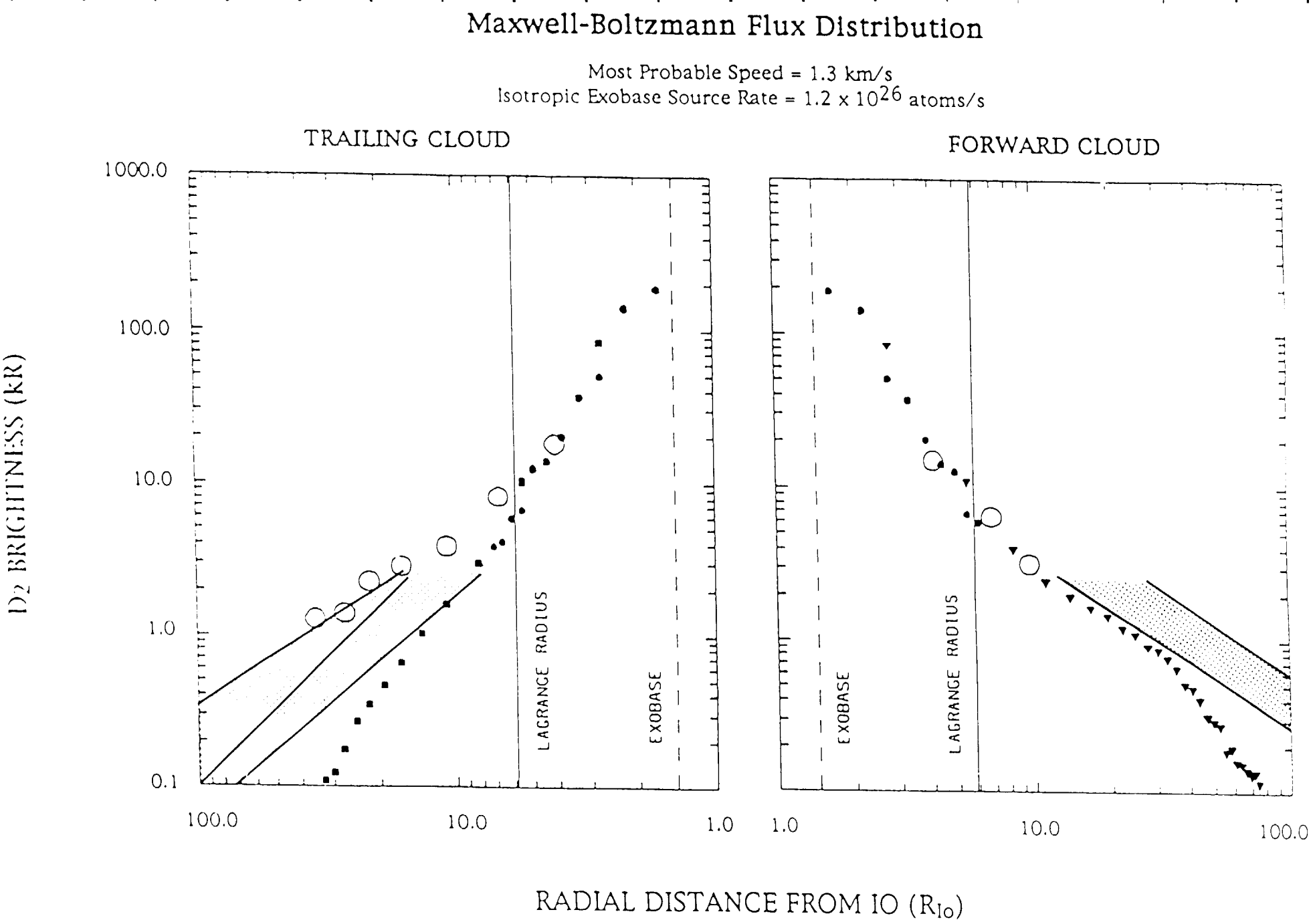
Maxwell-Boltzmann Flux Distribution
Most Probable Speed = 1.3 km/s
Isotropic Exobase Source Rate = 1.2 x 10^26 atoms/s
TRAILING CLOUD
FORWARD CLOUD
1000.0
100.0
10.0
1.0
0.1
D2 BRIGHTNESS (kR)
LAGRANGE RADIUS
EXOBASE
100.0
10.0
1.0
1.0
10.0
100.0
RADIAL DISTANCE FROM IO (RIo)

Figure 10a

EMISSION DATA

Maxwell-Boltzmann Flux Distribution

Most Probable Speed = 2.0 km/s
Isotropic Exobase Source Rate = 0.75 x 10^{26} atoms/s

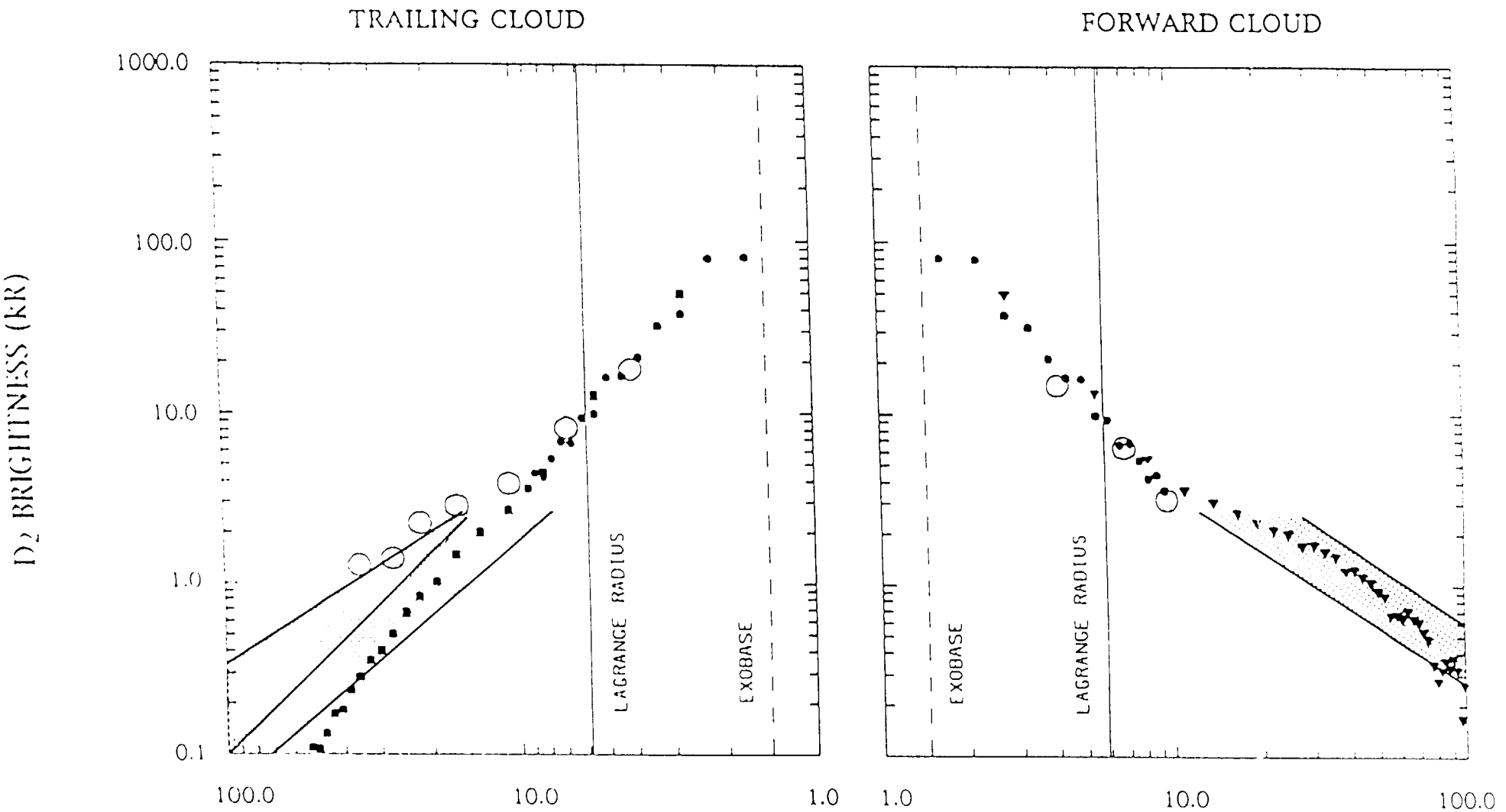

Figure 10b

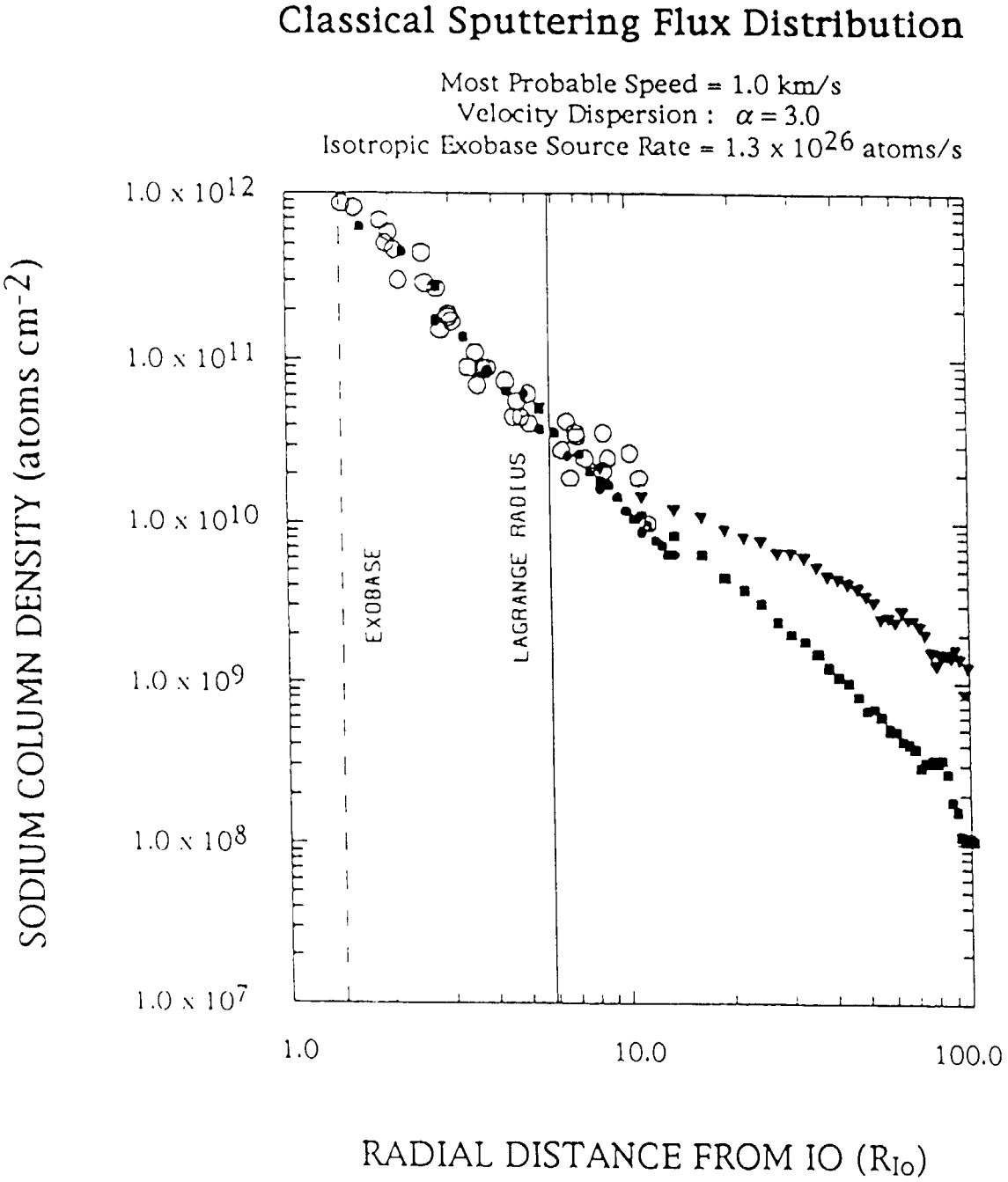
Classical Sputtering Flux Distribution
Most Probable Speed = 1.0 km/s
Velocity Dispersion : α = 3.0
Isotropic Exobase Source Rate = 1.3 x 10^26 atoms/s
SODIUM COLUMN DENSITY (atoms cm^-2)
1.0 x 10^12
1.0 x 10^11
1.0 x 10^10
1.0 x 10^9
1.0 x 10^8
1.0 x 10^7
EXOBASE
LAGRANGE RADIUS
1.0
10.0
100.0
RADIAL DISTANCE FROM IO (R_Io)

Figure 11a

ECLIPSE DATA

Modified Sputtering Flux Distribution

Most Probable Speed = 0.5 km/s
Velocity Dispersion : $\alpha = 7/3$
Isotropic Exobase Source Rate = 1.7×10^{26} atoms/s

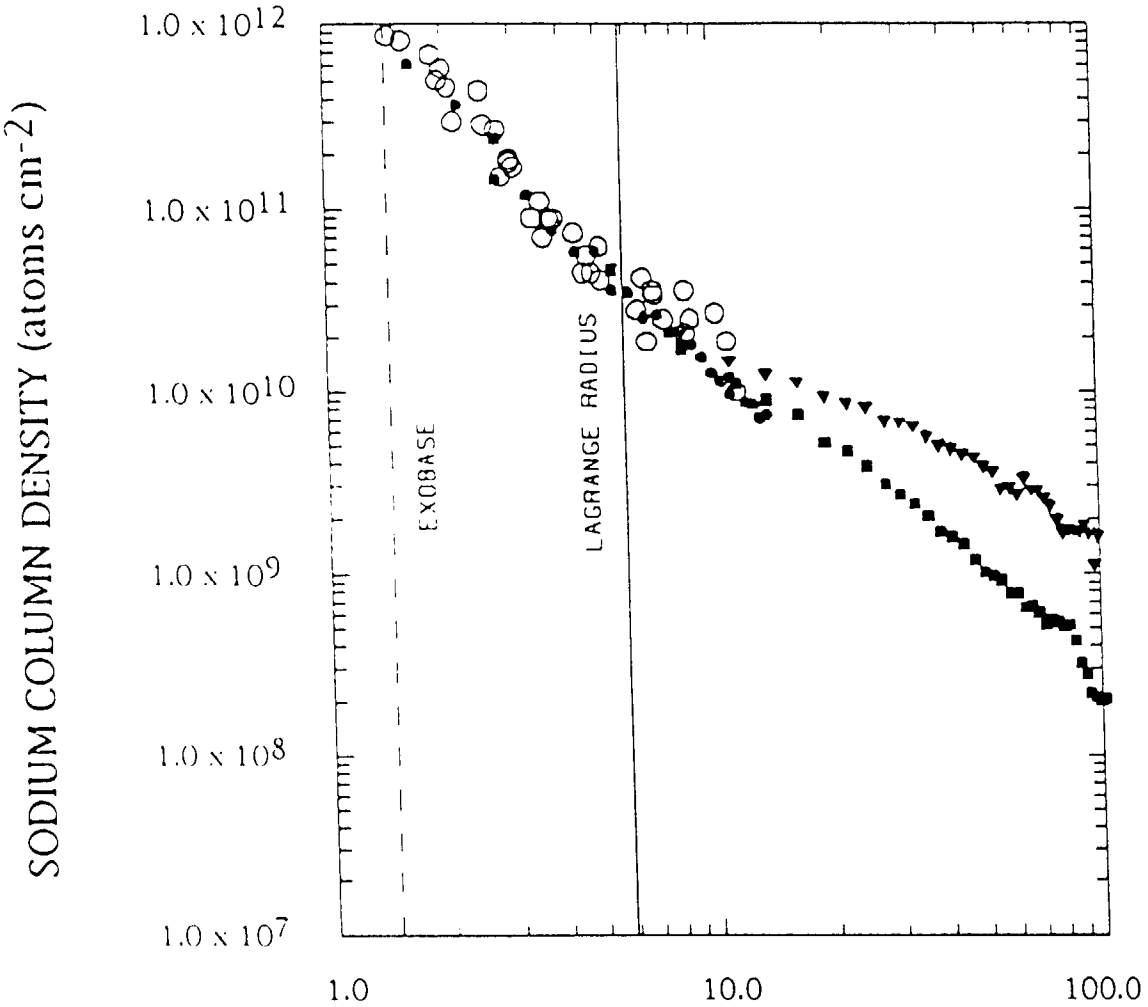

Figure 11b

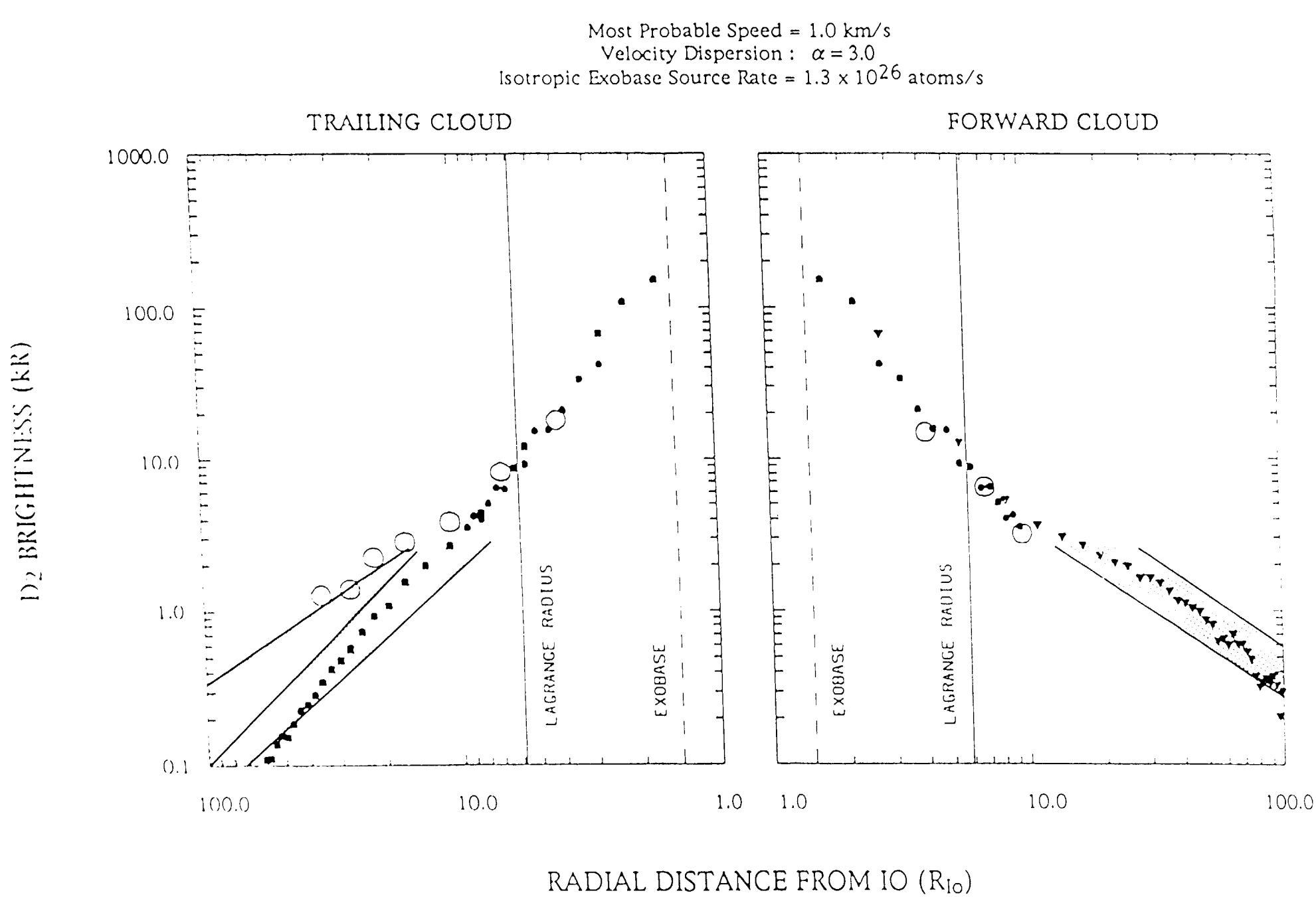
Classical Sputtering Flux Distribution
Most Probable Speed = 1.0 km/s
Velocity Dispersion : α = 3.0
Isotropic Exobase Source Rate = 1.3 x 10^26 atoms/s
TRAILING CLOUD
FORWARD CLOUD
1000.0
100.0
10.0
1.0
0.1
D2 BRIGHTNESS (kR)
LAGRANGE RADIUS
EXOBASE
100.0
10.0
1.0
1.0
10.0
100.0
RADIAL DISTANCE FROM IO (RIo)

Figure 12a

EMISSION DATA

Modified Sputtering Flux Distribution

Most Probable Speed = 0.5 km/s
Velocity Dispersion : $\alpha = 7/3$
Isotropic Exobase Source Rate = 1.7×10^{26} atoms/s

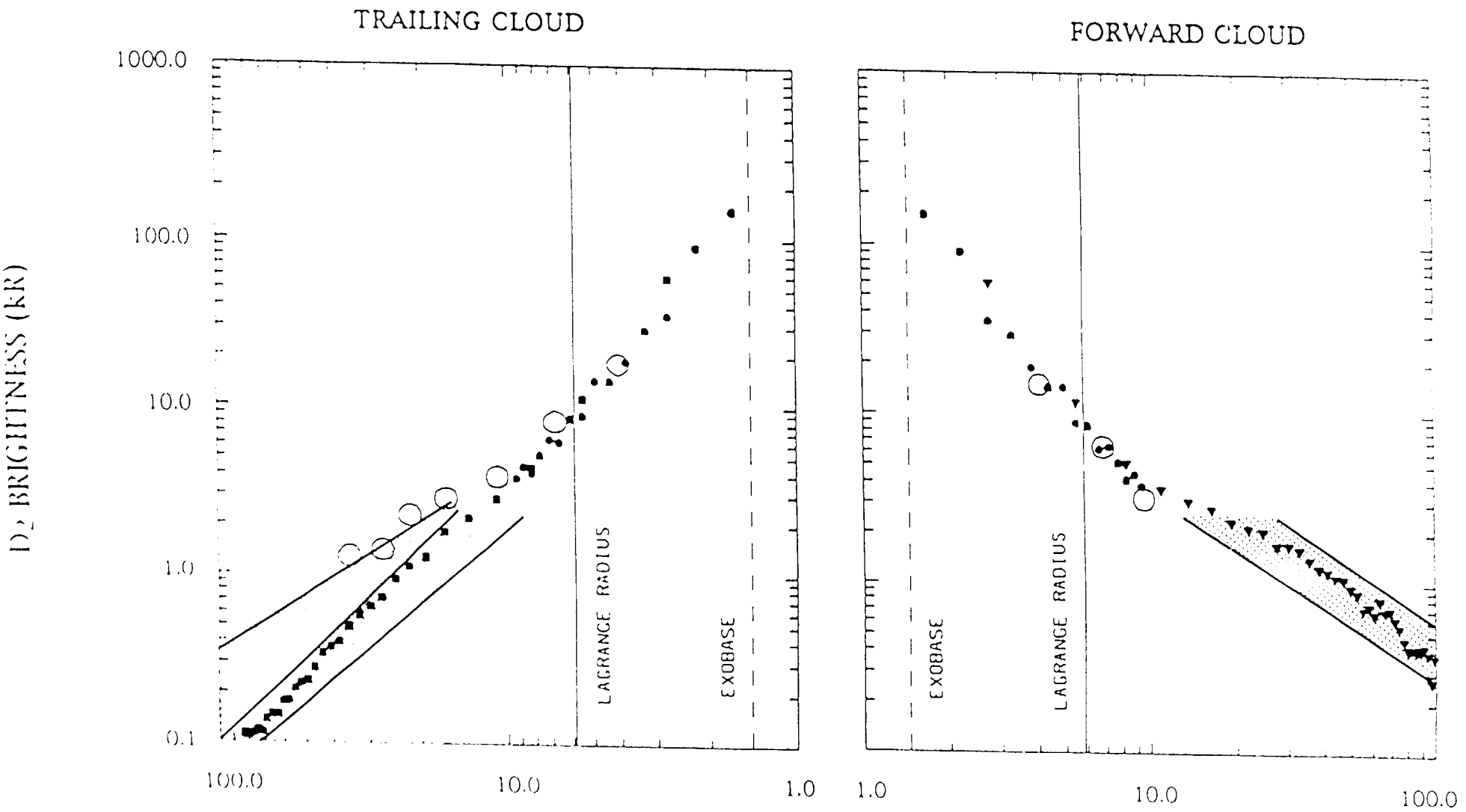

D₂ BRIGHTNESS (kR)

RADIAL DISTANCE FROM IO (R_{Io})

Figure 12b

ECLIPSE DATA

Modified Sputtering Flux Distribution

Most Probable Speed = 0.4 km/s
Velocity Dispersion : $\alpha = 2$
Isotropic Exobase Source Rate = 1.9×10^{26} atoms/s

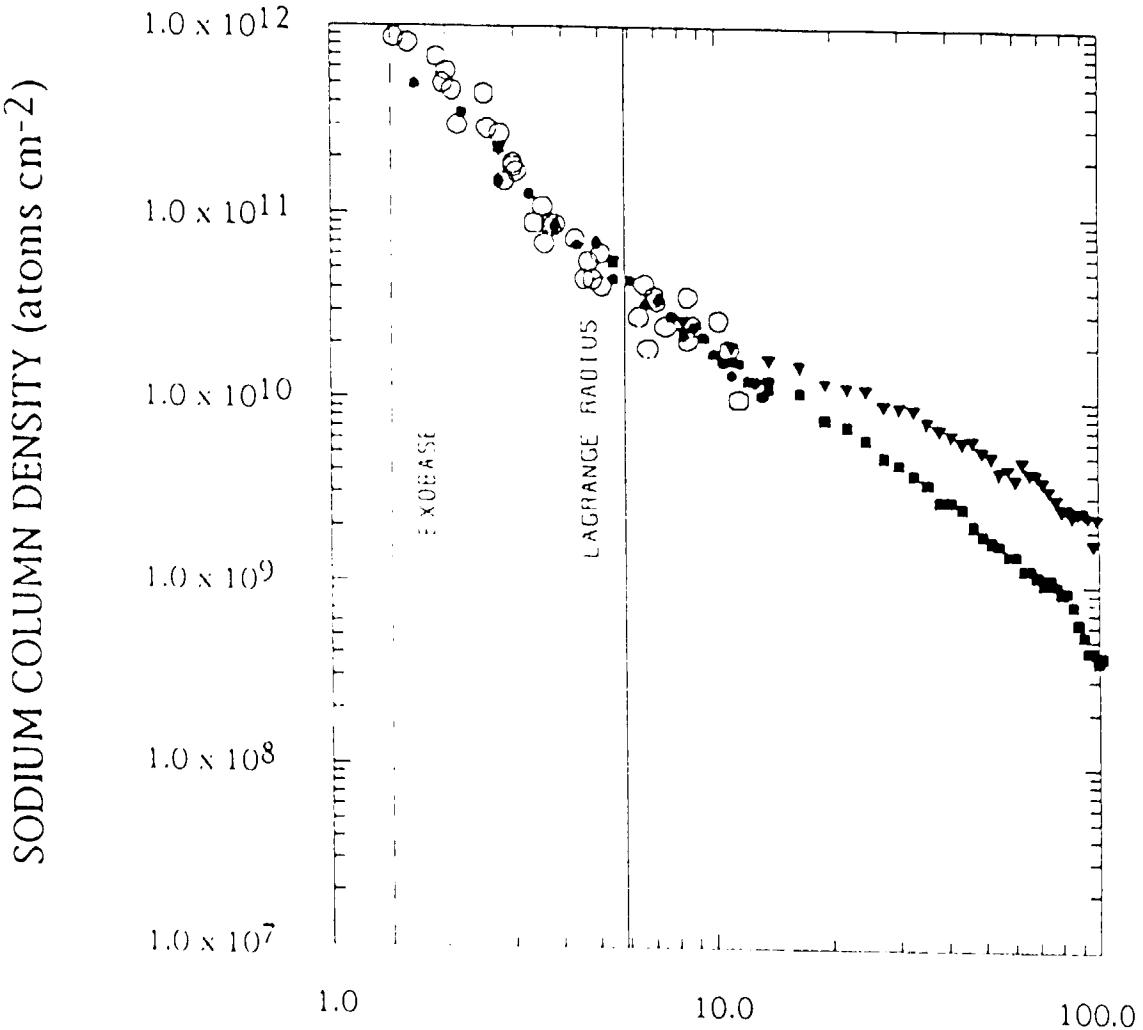

Figure 13

EMISSION DATA

Modified Sputtering Flux Distribution

Most Probable Speed = 0.4 km/s
Velocity Dispersion : $\alpha = 2$
Isotropic Exobase Source Rate = 1.9×10^{26} atoms/s

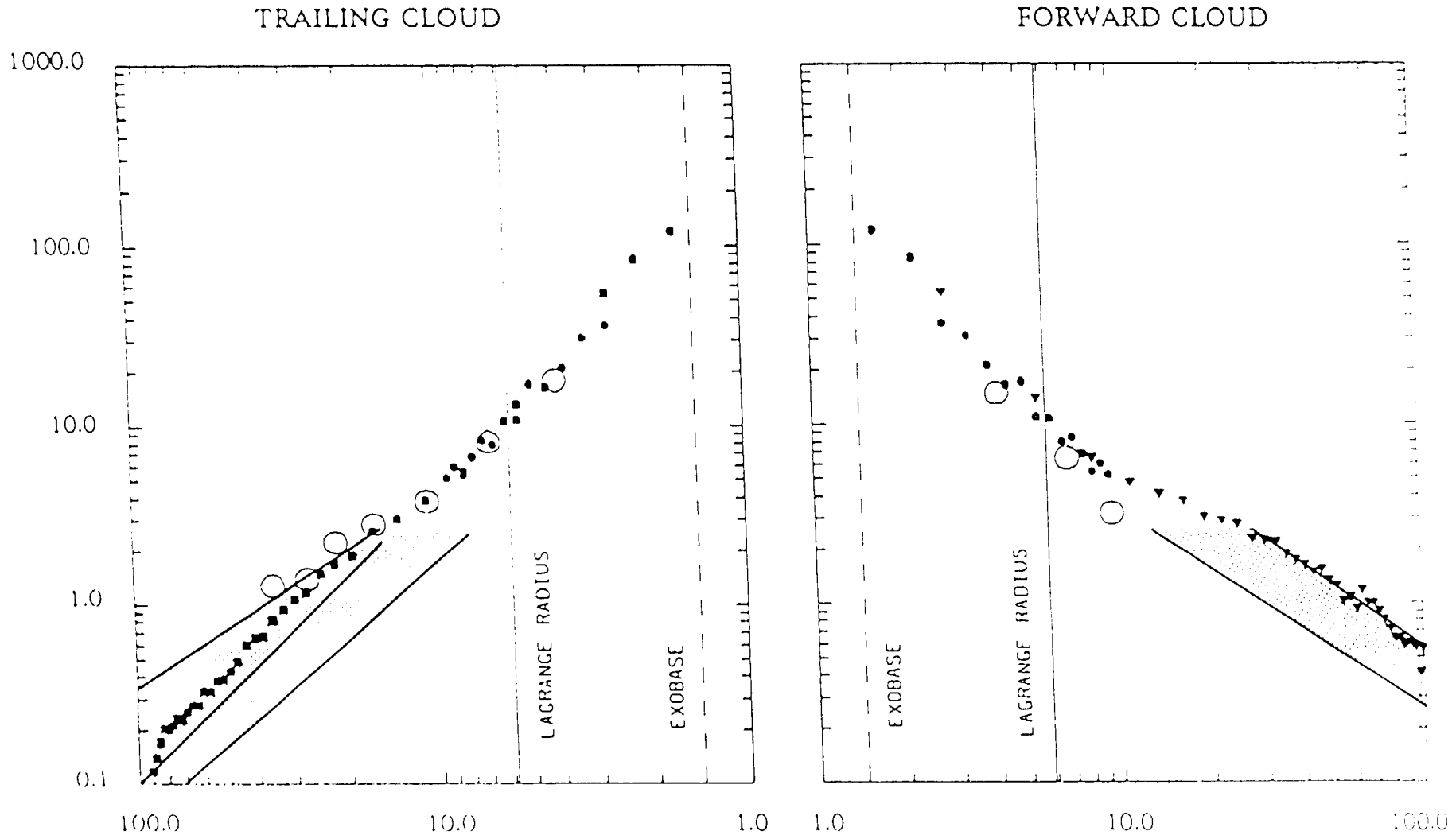

Figure 14

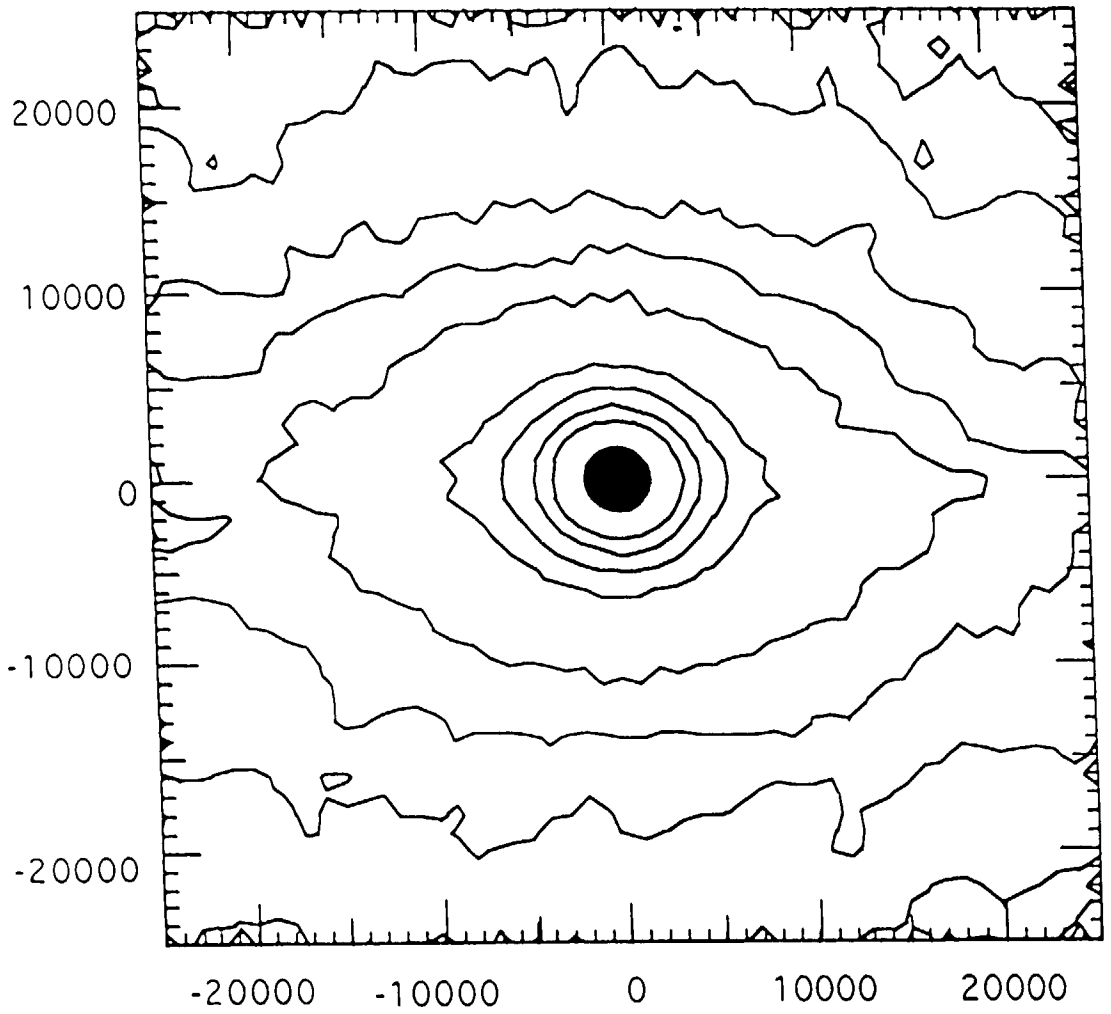

Figure 15

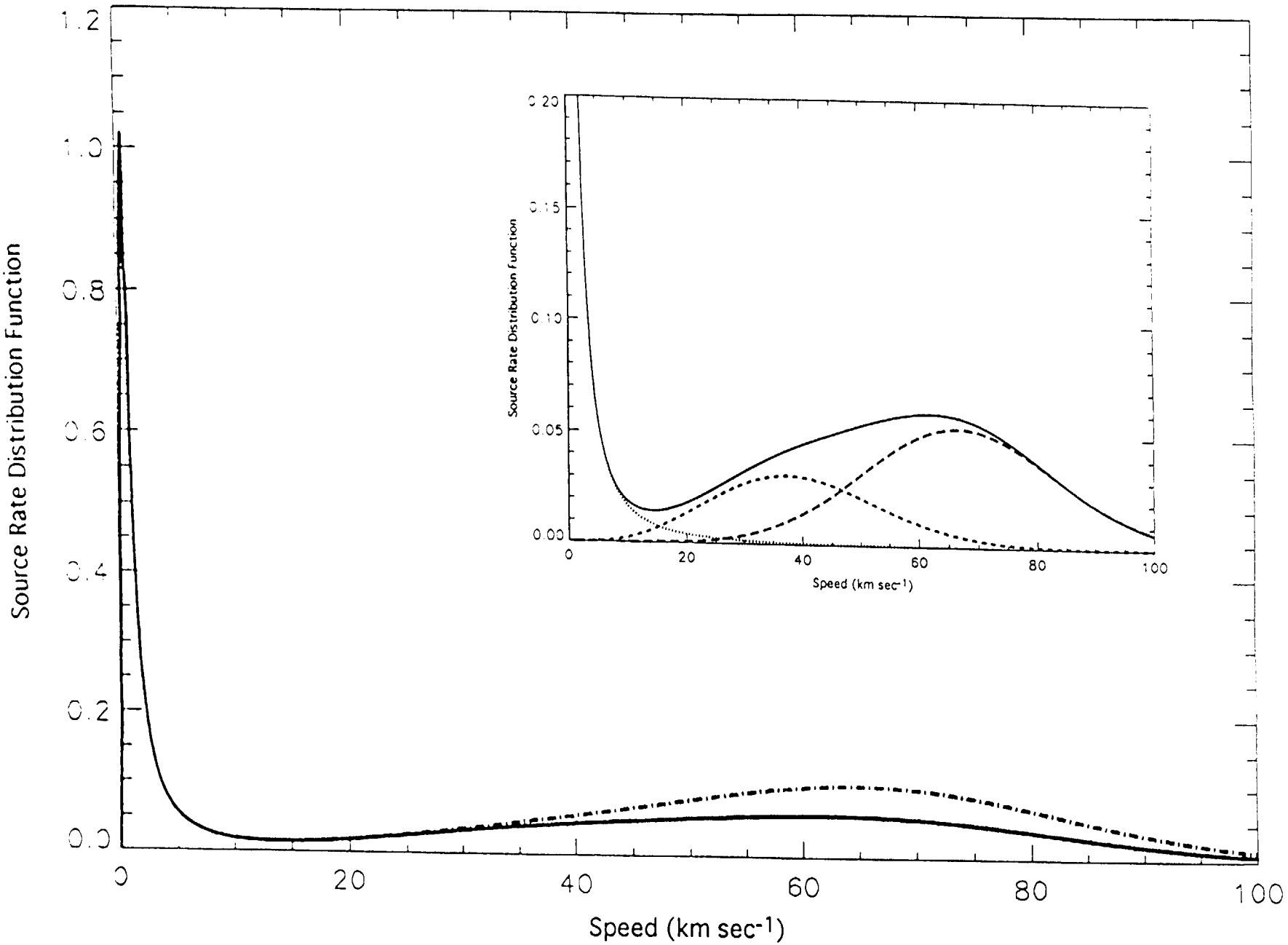
Source Rate Distribution Function
1.2
1.0
0.8
0.6
0.4
0.2
0.0
0
20
40
60
80
100
Speed (km sec-1)
Source Rate Distribution Function
0.20
0.15
0.10
0.05
0.00
0
20
40
60
80
100
Speed (km sec-1)

Figure 16

Appendix B

Correlating System III Longitudinal Asymmetries in the Jovian Magnetosphere and the Io Sodium Cloud

Correlating System III Longitudinal Asymmetries in the Jovian Magnetosphere and the Io Sodium Cloud

William H. Smyth[1]

Bruce A. Goldberg[2]

Preliminary Version

1. Atmospheric and Environmental Research, Inc., Cambridge, MA 02139

2. Jet Propulsion Laboratory, Pasadena, California 91103

Number of manuscript pages : 36

Number of Figures : 9

Number of Tables : 5

Key words : Io, satellite exosphere, gas tori, Jupiter's magnetosphere

Running heading : Correlating System III Longitudinal Asymmetries

For editorial correspondence and proofs please contact:

William H. Smyth

Atmospheric and Environmental Research, Inc.

840 Memorial Drive

Cambridge, MA 02139

Telephone number : (617) 547-6207

Fax number : (617) 661-6479

Internet : smyth@aer.com

ABSTRACT

An investigations is undertaken to study an observed space-time "bite-out" feature that occurs in the south portion of the Io sodium cloud when Io is near western elongation and is in the System III longitude angle interval between ~ 200° - 300° (i.e., in the so called "active sector"). This "bite-out" feature was discovered in the 263 images acquired in 1981 for the sodium cloud (Region B/C) by Goldberg et al. (1984). These sodium cloud images are a subset of the larger JPL Table Mountain Io Sodium Cloud Data Set obtained over the 1974 to 1981 time frame. Examination of the 1981 sodium cloud images shows, surprisingly, that the "bite-out" signature does not occur (with the exception of only an occasional hint of it) when Io is near eastern elongation and is in the active sector. At the time of the sodium observations, an inherent System III asymmetry in the plasma torus was documented independently through ground-based observations of plasma torus ion emission lines by Morgan (1985 a,b). This inherent System III asymmetry has been used to improve the description of the plasma torus in the sodium cloud model of Smyth and Combi (1988b). The improved sodium cloud model has been used to study the "bite-out" signature. The modeling studies show that the time evolution of this "bite-out" signature can be reproduced and that it reflects the space-time dependent electron-impact ionization sink for sodium produced by the combined east-west and System III asymmetries in the Jovian magnetosphere. In particular, the "bite-out" feature for Io near western elongation is correlated with an inherent System III asymmetry in the Io plasma torus in the presence of an east-west electric field. The presence of an east-west electric field in the planetary magnetosphere has been inferred from a number of different plasma torus ion and neutral emission line brightnesses and was incorporated earlier in the sodium cloud model (Smyth and Combi 1987; 1988b) to explain the east-west intensity asymmetry first discovered in the slit-averaged brightness data for the sodium emissions very near Io (a subset of the larger JPL Table Mountain Io Sodium Cloud Data Set) reported by Bergstralh et al. (1974, 1975). This east-west intensity asymmetry is also exhibited in the 1981 Region B/C image data set at larger distances from Io that are beyond the observational occulting mask centered on the satellite. The sodium cloud, because of its short electron impact ionization lifetime in the plasma torus, therefore provides an additional avenue to monitor and study these east-west and System III structures of the magnetosphere in past as well as in future observational data.

1. INTRODUCTION

Studies of observational data for the time-dependent morphology of the D-line emissions of Io's sodium cloud on the sky plane have provided an excellent remote sensing tool for probing the nature of the local and escaping atmospheres of the satellite and their manifold interactions with the planetary magnetosphere. In the two decades since the startling 1972 discovery by Brown (1974) of D-line emissions from Io, a large number of increasingly higher quality spectral and spatial observations of the sodium cloud have been obtained from ground-based facilities. The JPL Table Mountain Io Sodium Cloud Data Set, the most massive such data set acquired to date, was briefly summarized earlier by Goldberg et al. (1984) and more extensively in the companion paper (Goldberg and Smyth 1992, hereafter Paper I). This data set provides a valuable information base for three reasons. First, it documents various aspects of the nature and temporal variability of the sodium emission over a seven year time span from 1974 to 1981. Second, it provides a framework for the 1979 Jupiter-encounter data set acquired by the Voyager 1 spacecraft not only because of the time period covered, but also because images of the sodium cloud were acquired on and near the closest approach date of March 5, 1979. Third, it establishes a unique comparison data set for the more recent and higher spatial/time resolution images that have begun to be acquired over the last few years and are anticipated to be obtained with improved instrumentation in the next several years.

Observations described in Paper I may be divided into two major and spatially complementary regions: Region A and Region B/C. As used here, Region A includes spatial emission from Io's disk and from the satellite's gravitationally bound atmosphere (i.e., radius ~ 6 satellite radii or 0.15 Jupiter radii) and has a maximum brightness near the satellite of ~100 kiloRayleighs (kR). Region B/C includes sodium D-line emission that

extends several Jupiter radii from Io, that is characterized primarily by a forward cloud and that has a brightness which varies from many 10's of kR nearer the satellite to ~ 0.2 kR at the nominally measured outer cloud boundary. Observations for Region A were acquired by single slits in 1974-1979 and 1981, by multislits in 1976-1978, and two-dimensional images in 1981. Two-dimensional images for Region B/C were obtained in 1976-1979 and in 1981. As summarized in Table 1, the complete data has led to the identification and/or subsequent study of a number of the spatial features or characteristics of the sodium emission near Io, near Io's orbit, and far from Io's orbit.

Two entries in Table 1, the east-west asymmetry of the forward cloud and the System III asymmetry of the sodium cloud near western elongation, are the only features for which there are to date no modeling analysis studies. The east-west intensity asymmetry of the sodium cloud is documented in the JPL data set spatially beyond the gravitational confines of the near Io data of Bergstralh et al. (1975, 1977), which also exhibited an east-west asymmetry, and is almost certainty caused by the same mechanism, namely an east-west asymmetry of the plasma torus sink for sodium. The east-west intensity asymmetry of the sodium cloud will not be addressed here. The System III asymmetry observed in the shape of the sodium cloud when Io is near western elongation is also very well documented in the JPL data set. This asymmetry, a "bite-out" or zone of deficient sodium in the cloud which occurs south of the satellite and to the outside of its orbit when the Io System III longitude angle is between ~ 200° - 300°, was first described by Goldberg et al. (1984). The purpose of this paper is to analyze the observational data for this System III "bite-out" and to provide an explanation for this phenomenon. It will be shown that the "bite-out" is a long-term feature of the sodium cloud near western but not eastern elongation and that it may be explained by an inherent System III asymmetry in the Io plasma torus in the presence of an east-west electric field.

The remaining paper is organized into four sections. In section 2, observational data for the sodium cloud and plasma torus are discussed. In section 3, the sodium cloud model used in the analysis of the "bite-out" of the sodium cloud is described. An inherent System III asymmetry based upon independent 1981 plasma torus observations is incorporated in the model to describe the spacetime dependent lifetime for sodium. In section 4, select images are analyzed using the model. Discussion of the analyses and conclusions drawn in the paper are given in section 5.

2. OBSERVATIONAL DATA

2.1 Io Sodium Cloud

The "bite-out" of the sodium cloud near western elongation was discovered in the 1981 Region B/C data by Goldberg et al. (1984). The time evolution of this "bite-out" was excellently documented in a sequence of these images acquired on May 13, 1981 which were included in a 16 mm movie showing the changing D_2 cloud image on the sky plane as Io moved about Jupiter (Goldberg et al. 1982; Goldberg 1983). The entire 1981 Region B/C data set consists of 263 images of the sodium cloud which were recorded simultaneously in both the D_2 (5890Å) and D_1 (5896Å) wavelength emission lines over 14 nights with an image integration time of approximately 10 minutes. Three consecutive images were usually added to improve signal to noise. These co-added images produced a time–averaged picture of the sodium cloud over an Io geocentric phase angle of about 4° and an Io System III magnetic longitude angle of about 14° and, therefore, approximate reasonably well instantaneous snapshots of the Io sodium cloud. The range of the geocentric phase angles and System III magnetic longitude angles of Io covered by the

entire 1981 Region B/C data set is summarized graphically in Figure 1 and numerically in Table 2. Most of the 263 images comprising this coverage have undergone some type of partial data processing so that the time evolution of the cloud can be followed qualitatively. The dots and squares in Figure 1 show the midpoint conditions for 34 images that have undergone complete data reduction and calibration. Observational conditions and Image ID Numbers for these 34 images are summarized in Table 3. A more detailed discussion of the 1981 Region B/C data set may be found in Paper I.

The time evolution of the "bite-out" in the south portion of the sodium cloud near western elongation is illustrated in Figure 2 for a sequence of four of the completely processed images of Table 3 that were acquired on May 13, 1981. In the top image of Figure 2, for which Io has a System III magnetic longitude angles of about 168°, the "bite-out" was not present. For System III magnetic longitude angles of about 180°, the "bite-out" however, began to appear in the form of a deficiency of sodium south of Io and to the outside of its orbit that slices across the image at an angle of positive slope, as is illustrated in the second image of Figure 2. The "bite-out" became more pronounced as the System III longitudinal angle increases as can be seen in the third and fourth images of Figure 2.

Examination of a number of other sodium cloud images indicates that the "bite-out" is a long-term feature of the sodium cloud near western elongation. The same "bite-out" pattern is also present in a sequence of four images from Table 3 covering the time period in 1981 from April 29 to June 14, which have very nearly the same geocentric phase angle but which have an increasing Io System III longitude angle range similar to Figure 2. Examination of the partially and completely processed images acquired on June 14, which overlap 31 days later (see Figure 1 and Table 2) the observational conditions for some of the images acquired in the May 13 image sequence of Figure 2, also shows that this same

behavior is exhibited. In addition, examination of partially and completely processed images near western elongation acquired on May 6, 1981 (see Figure 1) again reveals the same "bite-out" behavior of the cloud south of Io. The south "bite-out" is also consistent with two 1977 images and one 1979 (Voyager 1 encounter) image acquired near western elongation which were included in a paper by Goldberg et al. (1980) describing the 1976-1979 Region B/C data set even though the integration times for these earlier images were ~ 1 - 2 hours (see Paper I). The south "bite-out" of the west cloud is also present in the very high quality, but unpublished sodium cloud images, acquired on 13 June 1983 and 16 August 1984 by J. S. Morgan (1984, private communication). The south "bite-out" of the west cloud would therefore appear to be a long-term and stable feature of the sodium cloud.

It is natural to ask if there is a sodium deficiency south of Io when the satellite is near eastern elongation and has the same System III longitude angle range for which the "bite-out" occurs in the west cloud. In Figure 1, east cloud images obtained on April 28, May 5 and May 12 (i.e., at seven day intervals and one day earlier than the west cloud images on April 29, May 6 and May 13) and on June 6 (i.e., two weeks before the west cloud images on June 14) are well suited to address this question. This comparison, which was undertaken in Paper I, is summarized here.

Select and fully processed east images of the sodium cloud from Table 3 acquired on April 28, May 5 and May 12 are shown in Figure 3 for an Io System III longitude angle in the range from 221.3 to 293.9 degrees. For April 28, the three fully processed images in Table 3 have a sodium cloud that is brighter north of Io (see first two images in Figure 3). The image at an Io System III angle of 221.3 degrees is much more asymmetric north to south than the latter two similar images (SIP 415/43-45 and SIP 415/49-46) at a larger Io System III longitude angles near 300 degrees. It is, however, difficult to determine if the

first image at 221.3 degrees has a "bite-out" feature, although it is clear that the latter image at 293.9 degrees does not have this feature. For May 5, the images are fairly symmetric north and south of Io for an Io System III angle of 204.2 degrees (i.e., image SIP 418/13-13 in Figure 3), are slightly enhanced north of the satellite for a longitude angle of 259.2° (i.e., image SIP 418/24-26 in Figure 3) , and are symmetric north and south of the satellite for a longitude angle of 299.6° (image SIP 418/31-33, not shown). Examination of a number of additional images on May 5 that have not been fully reduced reinforces this behavior and indicates that the cloud is symmetric for Io System III longitude angles of 210°, that it becomes brighter north of Io for larger angles, and that the asymmetry then decreases and is absent by an angle of 294°. This spatial morphology of the south deficient zone of sodium in the east cloud is, however, characterized by a steeper gradient in the brightness for the whole sodium cloud south of Io rather than a sharp and inclined boundary for the deficient zone as is present in the south "bite-out" of the west cloud. The June 6 image (SPI 424/10-12, not shown), which has almost identical Io phase and System III angles as the May 5 image (SIP 418/31-33), exhibits only a slight north brightness enhancement compared to no enhancement in the May 5 image. In contrast, the May 12 images in Figure 3 do not show the south zone of deficient sodium that is indicated in the May 5 images and perhaps suggested by the April 28 images. Examination of all processed images for May 12 and additional images that have not been fully reduced shows that the cloud brightness is essentially symmetric north and south of the satellite for Io System III longitude angles ranging from ~ 210° to 302° and does not show an inclined boundary for the deficient zone as is present in the south "bite-out" of the west cloud one day later.

The different north-south behavior of the east cloud images on May 5 and May 12 for the same range of Io System III longitude angles (~ 180° - 300°) is surprising in the light of the consistency and repeatability of the south "bite-out" signature that occur in the

west cloud on May 6 and May 13 over this same range of Io System III longitude angles. The apparent long-term stability of the "bite-out" in the west cloud south of Io and its complete absence or at best very slight presence in the east cloud, suggesting a temporal or more erratic behavior exists in the east, raise some very interesting questions about the properties of the plasma torus which are discussed below.

2.2 Io Plasma Torus

The observed south "bite-out" in the west sodium cloud occurs when Io is in a System III longitude range of ~ 180 to 290 degrees so that the centrifugal symmetry plane and hence the most dense portions of the plasma torus are south of the satellite. Because the excitation mechanism for sodium emission in the D-lines is solar resonance scattering, the deficiency of sodium brightness in the "bite-out" represents a deficiency in the sodium abundance. This suggests that the "bite-out" is caused by a longitudinally asymmetry in the "so-called" active sector of the plasma torus (Hill, Dessler and Goertz 1983) in which the electron-impact ionization lifetime of sodium would then have to be enhanced. Such an enhancement would require an increase in some combination of the electron density and temperature in the active sector. Any increase in electron density would increase the emission brightness in the plasma torus of the S^+ ions (6716 Å and 6731 Å) and the S^{++} ions (9531 Å) since their electron impact excitation mechanism is primarily sensitive to the electron density for the electron temperatures in the plasma torus near Io. The brightness of the sodium emission lines and ion emission lines would then be naturally anticorrelated.

A physically corresponding System III brightness enhancement in these plasma torus S^+ emission lines, which is anticorrelated with the "bite-out" sodium brightness, has indeed been observed in the active sector from ground-based telescopes since 1976. This

enhancement has also been observed on later dates in the S^{++} ion emission line. Pertinent S^{+} spectral data for this brightness asymmetry have been acquired from ground-based observations in 1976 (Trafton 1980; Trauger, Münch and Roesler 1980), in 1977 and 1978 (Trafton 1980; Pilcher and Morgan 1980), in 1979 (Trafton 1980; Morgan and Pilcher 1982) and in 1981 (Morgan 1983, 1985 a,b). Image data for S^{+} and/or S^{++} emissions exhibiting this System III brightness asymmetry were also obtained from ground-based observations in 1980 (Roesler et al. 1982), in 1981 (Trauger 1984; Pilcher and Morgan 1985; Oliversen, Scherb and Roesler 1991), in 1982 (Trauger 1984), in 1983 (Trauger 1984; Pilcher and Morgan 1985), in 1984 (J. S. Morgan 1984, private communication; J. T. Trauger 1985, private communication), in 1985 (J. T. Trauger 1985, private communication), in the 1988-89 apparition (F. Scherb 1990, private communication; J. T. Trauger 1991, private communication), in the 1989-90 and 1990-91 apparitions (J. T. Trauger 1991, private communications; N. Thomas 1991, private communication), and in 1992 (Rauer et al. 1993). Most of the image data acquired in the last five to ten years have, however, not been analyzed or published to date. There are indeed a number of interesting and outstanding questions about the time variability of the radial and longitudinal structure of the plasma torus for which these observations are well suited and, consequently, as we shall see, for which these observations have corresponding time varying counterparts in the sodium "bite-out".

A comparison of these plasma observations for the System III asymmetry indicates that generally two separate longitudinally asymmetric brightness components appear to exist in the torus. The first component is centered at ~170 to 200 degrees, with an angular width of ~ 90 degrees or more, and is a permanent feature of the torus. When compared to the normal brightness of the plasma torus at the diametrically opposite magnetic longitude angle, the first component is typically 2-5 times brighter (and at extremes, 10 times

brighter) with significant brightness changes occurring on a time scale of months to years. The second component is centered at ~280-290 degrees, has a comparable angular width to the first component, and is sometimes present and sometimes absence in the torus. The brightness of the second component may be comparable to or less than brightness of the first component.

The stability of the "bite-out" in the west sodium cloud and the complete absence or at best very slight and erratic behavior of deficient sodium south of Io in the east cloud suggest that east-west differences in the properties of the plasma torus, in addition to longitudinal asymmetries, also play an important role in shaping the Region B/C data summarized in Figure 1. The sense of this behavior is that a significant enhancement of the sodium lifetime in the active sector is always present near Io when the satellite is west of Jupiter (i.e., near western elongation at 270° Io geocentric phase angle) and never or at best only slightly present near Io when the satellite is east of Jupiter (i.e., near eastern elongation at 90° Io geocentric phase angle). As discussed in Paper I, the fully reduced sodium cloud images of Table 3 do, in fact, exhibit an east-west intensity asymmetry for the sodium brightness in a circular annulus centered on Io with an inner radius of 19,000 km and an outer radius of 21,000 km. The average D_2 brightness in the annulus for the sodium cloud images east of Jupiter was ~ 40% larger than the brightness for the sodium cloud images west of Jupiter. This behavior is consistent with the existence of a small east-west electric field in the magnetosphere (Barbosa and Kivelson 1983; Ip and Goertz 1983; Goertz and Ip 1984) which for a constant electric field simply displaces the plasma torus toward the east and produces a slightly hotter and more dense plasma at Io's orbit west of Jupiter.

The presence of such an east-west electric field was shown earlier to provide a consistent explanation (Smyth and Combi 1987) for the anticorrelation of the larger sodium D-line emission intensities east of Jupiter as measured even closer to Io in the discovery data of Bergstralh et al. (1975, 1977) and the larger intensities west of Jupiter of both the plasma torus S^+ optical emission line (6731Å) measured from a ground-based telescope (Morgan 1985 a,b) and the S^{++} extreme ultraviolet (EUV) emission line measured from the Voyager 1 spacecraft (Sandel and Broadfoot 1982). In the past several years, the documentation of this east-west intensity asymmetry has been expanded to include a number of additional emission lines and species as summarized in Table 4. Note in Table 4 that with the exception of neutral sodium, which is excited by solar resonance scattering, the west to east brightness ratio for all other emission lines is greater than unity as expected for electron impact excitation and the presence of an east-west electric field. More recent analysis (Sandel and Dessler 1988; Dessler and Sandel 1992) of the EUV plasma torus data acquired by the Voyager 1 and 2 spacecrafts suggests that the east-west electric field is, on the average, larger west of Jupiter than east of Jupiter and may also be dependent in magnitude on the System III longitude angle.

For our immediate purpose of understanding the "bite-out" in the Region B/C image data of Figure 1, the longitudinal structure and presence of an east-west electric field in the plasma torus is fortunately reasonably well documented in the winter to spring of 1981 by ground-based observations summarized in Table 5. Of these plasma torus observations, the extension amount of data acquired by Morgan (1983) and his analysis and modeling of these data (Morgan 1985 a,b) provide the most relevant information base for the bulk of the sodium observations in Figure 1 which occur in mid to late spring of 1981. An east-west asymmetry in the radial emission profiles of the optical SII (6716Å, 6731Å) and OII (3726Å) lines was documented in the observations of Morgan with higher intensities

measured on the west side of Jupiter. This east-west asymmetry in both the shape and intensity of the SII (6731Å) spectral data was independently verified (see Morgan 1985b) by 1981 image data of the SII (6731Å) emission acquired by Oliversen (1983; Oliversen et al. 1991). An adequate explanation of the east-west asymmetry of the ion data in the modeling analysis of Morgan (1985b) was obtained by a convective motion caused by an east-west electric field. The magnitude of the east-west electric field required to give a reasonable fit to the optical ion data was similar to that required to explain the east-west Voyager EUV (685Å) east-west intensity asymmetry and the anticorrelated east-west intensity asymmetry of the D-line emissions from the sodium cloud (see Smyth and Combi 1987). The System III longitudinal variation of the SII (6716Å, 6731Å) emissions was time dependent in the measurements of Morgan (1983; 1985 a,b). It changed from an ordered single peak ~ 2.5 times brighter in a broad region centered near 180° System III longitude in run 1 (Feb 14-17) and run 2 (Mar 20-23) to a double-peaked structure with peaks located near 180° and 290° in run 3 (April 21 - 24) and run 4 (May 2-4). In Figure 4, the longitudinal asymmetry for run 4 is shown and reveals that near 180° and 300° system III longitude the two intensity peaks west of Jupiter were brighter and vary by about a factor of 2 while the intensity peaks east of Jupiter were much dimmer and had a smaller amplitude variation. This double-peaked structure west of Jupiter was also independently verified in the April 1981 SII image data of Pilcher et al. (1985). In the modeling analysis of Morgan (1985b), intrinsic longitudinal intensity changes of about a factor of two were required to match the observed System III longitudinal asymmetries. The observations in the spring of 1981 of the System III longitudinal and east-west asymmetries in both the plasma torus and sodium cloud data suggest that these signatures are directly related. This relationship will be quantified and included in the sodium cloud model discussed in the next section.

3. MODEL DESCRIPTION

To study the time-variable signatures of the sodium cloud discussed in section 2, it is necessary to have a model that contains, to a reasonable level of accuracy, a description of the atom dynamics, the atom sink processes, the atom excitation mechanism, and the atom source velocity distribution at the satellite exobase. An improved version of the sodium cloud model of Smyth and Combi (1988b) using the framework of the more general model description in Smyth and Combi (1988a) is adopted here for this purpose. The orbital dynamics of sodium atoms in the cloud model are determined by the gravitational fields of both Io and Jupiter and by the acceleration of solar radiation pressure produced as atoms undergo resonance scattering in the D_1 and D_2 emission lines. All three factors were included in the earlier 1988 version of the sodium cloud model. The sink for sodium atoms in the circumplanetary magnetosphere near Io's orbit is determined by their spacetime dependent interactions with the plasma torus, which are dominated by electron impact ionization. In the earlier model, the sodium lifetime description was for electron impact ionization and was based upon a tilted and offset magnetic dipole field in the presence of a constant east-west electric field (~2.8 mV m^{-1} in Io's frame) for a heavy ion magnetospheric plasma with Voyager 1 encounter conditions. This plasma torus description, although spatially dependent upon three variables (i.e., radial L distance, magnetic latitude, and east-west angular location about Jupiter), was otherwise inherently longitudinally symmetric. The model of Smyth and Combi (1988b) has been improved here to include an inherently asymmetric plasma torus description. The description of the inherently asymmetric plasma torus is discussed below. The atom excitation mechanism for sodium, which is solar resonance scattering and depends upon the instantaneous atom-sun radial-velocity component because of the D_1 and D_2 Fraunhoffer features in the solar spectrum, was implemented in the earlier model. The sodium source at Io's exobase has recently been shown by Smyth and

Combi (1993) to be well represented by a modified sputtering flux speed distribution function which has its maximum value at ~0.5 km sec^{-1} (i.e., a sub-escape speed from Io's exobase). For atoms in the sodium cloud, of which all have already escaped from Io, previous modeling efforts (Smyth and Combi 1988b) have shown, however, that the basic nature of the forward cloud and also the escaped sodium within about one half Jupiter radii north and south of Io can be reasonably well reproduced by assuming a monoenergetic 2.6 km sec^{-1} source at a nominal Io's exobase of 2600 km, where the escape speed is ~2.0 km sec^{-1}. This source is quite adequate for our present purposes of investigating the "bite-out" feature but will understandably (see Pilcher et al. 1984) not reproduce the trailing-cloud directional feature due to its absences of higher-velocity components (i.e., ~10-20 km sec^{-1}) or the brightness gradient in the more distance portions of the forward cloud (Smyth and Combi 1993).

As discussed in section 2, an examination of the 1981 plasma torus data (Morgan 1985 a,b; Pilcher and Morgan 1985; Oliversen et al. 1991) indicated S^+ and S^{++} emission enhancements in the torus near Io's orbit in the System III longitudinal region of 180-300 degrees. The brightness enhancements appear to be attributed primarily to an increase in the electron density of the so-called S^+ "ribbon feature" (Trauger 1984) or "field-aligned feature" (Pilcher, Fertel and Morgan; 1985; Pilcher and Morgan 1985; Morgan and Pilcher 1982) that is located inside of Io's L-shell and also to a S^{++} plasma extension of this feature beyond Io's orbit. In 1981 during the time of the sodium cloud measurements, the longitudinal asymmetry in the torus had two components, the first one centered at a System III longitude angle $\lambda_m^{(1)}$ ~180-200 degrees and the second one centered at $\lambda_m^{(2)}$~280-290 degrees. The electron impact ionization lifetime of sodium will thus have an inherent longitudinal dependence.

The explicit functional dependence of the sodium lifetime, τ, on the System III longitude angle, λ_{III}, and the radial $\tilde{L}$ distance in the plasma torus coordinate frame of Smyth and Combi (1988b, see Appendix C) is given as follows:

$$\frac{1}{\tau} = \nu_0 \left\{ 1 + \left[\sum_{j=1}^{2} \alpha_j e^{-\left(\frac{\lambda_{III} - \lambda_{III}^{(j)}}{\sigma_j} \right)^2} \right] R(\tilde{L}) \right\} \qquad (1)$$

where

$$R(\tilde{L}) = \begin{cases} e^{-\left(\frac{\tilde{L} - \tilde{L}_0}{\sigma_{inner}} \right)^2} & \text{for } \tilde{L} - \tilde{L}_0 < 0 \\ e^{-\left(\frac{\tilde{L} - \tilde{L}_0}{\sigma_{outer}} \right)^2} & \text{for } \tilde{L} - \tilde{L}_0 > 0 \end{cases} \qquad (2)$$

and was suggested from the modeling of plasma torus spectra and image data by J. S. Morgan (1987, private communication). Here $\tau_0 = \nu_0^{-1}$ is the lifetime description for sodium determined by case C of Smyth and Combi (1988b). The lifetime τ_0 includes no inherent longitudinal asymmetry in the plasma torus. For the sodium lifetime τ, the parameters α_j determine the relative longitudinal strength of the two asymmetric plasma torus components while the parameters σ_j determine their angular widths. The radial dependence $R(\tilde{L})$ of the asymmetry is centered at $\tilde{L} = \tilde{L}_0$ and has an inner scale length σ_{inner} that differs from its outer scale length σ_{outer}. During the 1981 JPL observations of the sodium cloud, best estimated values for these parameters are given as follows:

$$\lambda_{III}^{(1)} = 180^\circ \qquad \lambda_{III}^{(2)} = 280^\circ \qquad \tilde{L}_0 = 5.65$$

$$\alpha_1 = 1 \qquad \alpha_2 = 1 \qquad \sigma_{inner} = 0.125 \qquad (3)$$

$$\sigma_1 = 45^\circ \qquad \sigma_2 = 45^\circ \qquad \sigma_{outer} = 1.0$$

where $\tilde{L}$, $\tilde{L}_0$, σ_{inner}, and σ_{outer} are understood to be measured in units of Jupiter radii.

Using the parameters values given by (3), the electron density is enhanced in the active longitudinal region by a factor of two (as in the best plasma torus model of Morgan 1985b) over the Voyager 1 value it has at the diametrically opposite longitudinal angle in the plasma torus. At Io's location, the sodium lifetime as a function of the satellite geocentric phase angle and System III longitude angle is correspondingly reduced over much of this angular domain by the same factor as is illustrated in Figures 5a and 5b, respectively, by comparison of the sodium lifetimes τ_0 and τ in the plasma torus. The plasma torus coordinate frame and its radial coordinate $\tilde{L}$ are defined so as to render the plasma torus description in a preferable frame where, for a given east-west angular location about Jupiter (e.g. eastern elongation), the two dimensional properties of the plasma torus (and hence also the sodium lifetime) are independent of the System III longitudinal angle, in the absence of an actual inherent System III asymmetry in the torus. This is illustrated in Figure 6, where the sodium lifetime τ_0 at eastern and western elongations are different because of east-west asymmetries in the plasma torus but are independent of the System III longitude angle. In contrast for τ, the sodium lifetimes at eastern and western elongations, although also different because of east-west asymmetries in the torus, are now different for each value of the System III longitude angle.

4. ANALYSIS OF OBSERVATIONS

To understand the importance of the plasma torus sink in the formation and time evolution of the "bite-out" feature, model calculations are first undertaken for the sequence of four D_2 emission images in Figure 2 observed on May 13 1981. Model calculations are shown in Figure 7 based upon the inherently asymmetric plasma torus sink illustrated in Figure 5b and in Figure 8 based upon the inherently symmetric plasma torus sink illustrated in Figures 5a and 6. The model calculations in Figure 8 provide a base-line case from which to identify in Figure 7 the effects of the inherently asymmetric plasma torus on the evolution of the "bite-out" feature. In Figures 7 and 8, the source is that for an isotropic and uniform monoenergetic (2.6 km sec^{-1}) flux of sodium atoms ejected radially from Io's exobase, where the atom flux is 2×10^8 cm^{-2} sec^{-1} referenced to Io's surface area in all cases. Comparison of Figures 7 and 2 indicates that both the basic character and the Io System III longitude evolution of the south "bite-out" feature are reasonably well simulate by the model. Indeed, this absence of the "bite-out" and its time evolution in Figure 8 shows that the "bite-out" is produced solely by the dependence of the sodium sink on the inherently System III asymmetry of the plasma torus. The excess length of the sodium cloud in model calculation compared to the observational data occurs because of the assumed constant and isotropic flux of sodium ejected from Io's exobase. A more realistic treatment of the source would provide a better match to the observational data but would not alter the conclusions determined for the time evolution of the "bite-out" feature.

To assess the impact of the east-west and inherently System III longitude asymmetries on the sodium cloud for Io near eastern elongation and the possible formation of a "bite-out" feature, two model calculations for the sodium cloud at an Io geocentric phase angle of 90.5° and an Io System III longitude angle of 221.3° are presented in Figure 9. In

the model calculations, the inherently asymmetric plasma torus is included in the sodium sink. For the monoenergetic 2.6 km sec^{-1} sodium source, both an isotropic (i.e., spherically symmetric on Io's exobase) and a more restrictive band source area (i.e., deficient in sodium ejected from the leading and trailing apex areas of Io's exobase) are assumed at a nominal exobase radius of 2600 km, where the escape speed is ~2.0 km sec^{-1}. The same flux is adopted as in Figure 7. The Io geocentric phase and Io System III longitude angles are those appropriate for the first April 28 image in Figure 3, and differ only appreciably for the latter angle from the second May 5 image in Figure 3 and the May 12 image at an Io geocentric phase angle of 91.2° and an Io System III longitude angle of 301.8°, not shown in Figure 3. The model images show no evidence of the "bite-out" feature in spite of the fact that Io was in the active sector of the plasma torus where the "bite-out" occurred when Io was near western elongation. Comparison of the two model images in Figure 9 illustrates how the band source reduces both the length and brightness of the forward cloud substantially from the symmetric source, but additional adjustments are required in the assumed constant source strength to match the brightness contours more exactly.

5. DISCUSSION AND CONCLUSIONS

The model images in Figure 9 show an east cloud that exhibits little or no asymmetric distribution of sodium north or south of Io when the satellite is in the active sector of the plasma torus, in contrast to the south "bite-out" feature in the model images in the west cloud in Figure 7. Additional model images (not shown) for May 5 east image (SIP 418/24-26) and the May 12 east image (SIP 420/30-32) that cover the Io System III longitude angle range of the asymmetric sink substantiate the results of Figure 9. The reason there is no deficient sodium signature south of Io in the east cloud model is because the east-west electric

field has displaced Io radially inward from the location of the asymmetric sink and thereby has literally removed the sodium from the spatial region of enhanced ionization. This is readily apparent by studying Figure 6 where the sodium lifetime in the plasma torus at eastern and western elongations is shown in relationship to Io's motion (dark oval) during one Io System III longitude period. The Io System III longitude angle on the oval in the centrifugal equator plane at the smaller radial displacement is 110° and increases as the satellite moves upward along the oval and reaches 200° at the top of the oval. The longitudinally asymmetric plasma torus sink for sodium is centered on the centrifugal plane at a radial distance of 5.65 planetary radii near the middle of the oval at eastern elongation (at the location of the black dot) and somewhat left of the oval at western elongation (at the location of the black dot). The small inner radial scale height σ_{inner} of the inherent System III enhancement causes the enhancement to decay so rapidly that it is unable to reach appreciably Io's location in the 110°- 290° sector in the east, while the outer radial scale height σ_{outer} of the inherent System III enhancement allows the enhancement to be felt at almost full force at Io's location in the 110°- 290° sector in the west.

The apparent time variability or erratic behavior of the east cloud and the stability of the west cloud regarding the zone of deficient sodium south of Io are therefore likely to be related to a difference (or time variability) in the strength of the east-west electric field east and west of Jupiter. It is clear from Figure 6 that the west cloud is in a rather stable relationship with the location of the inherently System III plasma torus enhancement for small modulations of the electric field strength west of Jupiter. This is not, however, true for the east cloud because of the very small scale height σ_{inner} and the rather close radial proximity of Io's orbit to the System III enhancement in the plasma torus. Small changes in the east-west electric field east and west of Jupiter can therefore modulate the radial inward displacement of Io relative to the radial location of longitudinally asymmetric plasma torus

sink and hence modulate the east cloud sodium population south of the satellite accordingly. More recent studies indeed suggest that the electric field may be time variable (Sandel 1985; Sandel and Dessler 1988; Dessler and Sandel 1992) and therefore provide a reasonably consistent explanation for the absence or erratic nature of the "bite-out" in the east cloud and the stable presence of the "bite-out" in the west cloud.

Additional studies of the 1981 sodium cloud observations (Region B/C) need to be undertaken by extending and refining the analysis initiated here. The complete set of 1981 calibrated images should be carefully modeled in order to determine the sodium source strength and its time variability and dependence on the Io geocentric phase and System III longitude. The analysis of the 1981 sodium cloud images (Region B/C) may also be readily applied to the 1976-1979 sodium cloud images (Region B/C). This would allow us to extend the time line and test the stability or time variability of various morphological features of the cloud and their corresponding physical properties and structures in the plasma torus. The 1976-1979 Region B/C data set includes two images on the Voyager 1 encounter day as well as a number of images around this encounter time. Studies of these images would be most valuable in linking the whole sodium cloud data set to the Voyager 1 encounter conditions determined by the spacecraft and providing a more solid base of understanding for the upcoming tours of the circumplanetary environment of Jupiter by the Galileo spacecraft.

ACKNOWLEDGMENTS

We are grateful to J. S. Morgan for many helpful discussions and for sharing with us his Io sodium cloud and plasma torus image data prior to publication. We also wish to thank M. L. Marconi for providing computational support for the model calculations. This research was supported by the Planetary Atmospheres Program of the National Aeronautical and Space Administration under contracts NASW-3949, NASW-4416, and NASW-4471 to Atmospheric and Environmental Research, Inc.

REFERENCES

Ballester, G. E. 1989. Ultraviolet observations of the atmosphere of Io and the plasma torus, Ph.D. thesis, The John Hopkins University.

Barbosa, D. D. and M. G. Kivelson 1983. Dawn-dusk electric field asymmetry of the Io plasma torus, *Geophys. Res. Lett.* **10**, 210-213.

Bergstralh, J. T., D. L. Matson, and T. V. Johnson 1975. Sodium D-line emission from Io: synoptic observations from table mountain observatory. *Ap. J. Lett.* **195**, L-131-L135.

Bergstralh, J.T., J. W. Young, D. L. Matson, and T. V. Johnson 1977. Sodium D-line emission from Io: A second year of synoptic observation from table mountain observatory. *Ap. J. Lett.* **211**, L51-L55.

Brown, R. A. 1974. Optical line emission from Io. In *Exploration of the Planetary System: Proceedings IAU Symp. No. 65* (A. Woszczyk, and C. Iwaniszewska, Eds.), pp. 527-531. D Reidel Publ. Co., Dordrecht.

Brown, R. A. and D. E. Shemansky 1982. On the nature of S II emission from Jupiter's hot plasma torus. *Ap. J.* **263**, 433-442.

Carlson, R. W., D. L. Matson, and T. V. Johnson 1975. Electron impact ionization of Io's sodium emission cloud. *GRL* **2**, 469-472.

Dessler, A.J. and B.R. Sandel 1992. System III variations in apparent distance of the Io plasma torus from Jupiter. *Geophys. Res. Lett.* **19**, 2099-2103.

Flynn, B., M. Mendillo, and J. Baumgardner 1992. Observations and modeling of the jovian remote neutral sodium emission. *Icarus* **99**, 115-130.

Goertz, C.K. and W.-H. Ip 1984. A dawn-to-dusk electric field in the Jovian magnetosphere, *Planet. Space. Sci.* **32**, 179-185.

Goldberg, B. A., R. W. Carlson, D. L. Matson, and T. V.Johnson 1978. A new asymmetry in Io's sodium cloud. *BAAS* **10**, 579.

Goldberg, B. A., Y. Mekler, R. W. Carlson, T. V. Johnson, and D. L. Matson 1980. Io's sodium emission cloud and the Voyager 1 encounter. *Icarus* **44**, 305-317.

Goldberg, B. A., R. W. Carlson, G. W. Garneau, T. V.Johnson, S. K. LaVoie, J. J. Lorre and D. L. Matson 1982. Dynamics of the Io sodium cloud. *BAAS* **14**, 762.

Goldberg, B. A. 1983. Dynamics of the Io sodium cloud, 16 mm movie produced for display at the National Air and Space Museum, Smithsonian Institute, Washington, D. C.

Goldberg, B. A., G. W. Garneau, and S. K. LaVoie 1984. Io's sodium cloud. *Science* **226**, 512-516.

Goldberg, B. A. and W. H. Smyth 1993. The JPL table mountain Io sodium cloud data set, companion paper.

Hill, T. W., A. J. Dessler and C. K. Goertz 1983. Magnetospheric models, In *Physics of the Jovian Magnetosphere*, (A. J. Dessler, Ed.), pp 106-156, Cambridge Press, N. Y.

Ip, W.-H. and C. K. Goertz 1983. An interpretation of the dawn-dusk asymmetry of UV emission from the Io plasma torus. *Nature* **302**, 232-233.

Matson, D. L. , B. A. Goldberg, T. V. Johnson, and R. W. Carlson 1978. Images of Io's sodium cloud. *Science* **199**, 531-533.

McGrath, M.A. and R. E. Johnson 1987. Magnetospheric plasma sputtering of Io's atmosphere. *Icarus* **69**, 519-531.

McGrath, M. A., H. W. Moos, D. F. Strobel and G. E. Ballester 1990. The Io plasma torus dawn-dusk brightness asymmetry, Paper presented at the Magnetospheres of the Outer Planets Fred Scarf Memorial Symposium, Annapolis, Maryland, August 20-24.

Mendillo, M., J. Baumgardner, B. Flynn, and W. J. Hughes 1990. The extended sodium nebula of Jupiter. *Nature* **348**, 312-314.

Morgan, J. S. 1983. Low resolution spectroscopy of the Io torus, Ph.D. thesis, Dept of Astronomy, Univ. of Hawaii.

Morgan, J.S. 1985a. Temporal and spatial variations in the Io torus, *Icarus* **62**, 389-414.

Morgan, J.S. 1985b. Models of the Io torus, *Icarus* **63**, 243-265.

Morgan, J. S. and C. B. Pilcher 1982. Plasma characteristics of the Io torus. *Ap. J.* **253**, 406-421.

Murcray, F. J. 1978. Observations of Io's sodium cloud. Ph.D. Thesis, Dept. of Physics, Harvard University, Cambridge, Massachusetts.

Murcray, F. J., and R. Goody 1978. Pictures of the sodium cloud. *Ap. J.* **226**, 327-335.

Oliversen, R. J. 1983. The Io plasma torus: its structure and sulfur emission spectra, Ph. D. thesis, Dept of Physics, Univ. of Wisconsin-Madison.

Oliversen, R. J., F. Scherb and F. L. Roesler 1991. The sulfur torus in 1981. *Icarus* **93**, 53-62.

Pilcher, C. B. 1980. Transient sodium ejection from Io. *BAAS* **12**, 675.

Pilcher, C. B. and W. V. Schempp 1979. Jovian sodium emission from region C_2. *Icarus* **38**, 1-11.

Pilcher, C. B. and J. S. Morgan 1980. The distribution of [SII] emission about Jupiter. *Ap. J.* **238**, 375-380.

Pilcher, C. B. and J. S. Morgan 1985. Magnetic longitude variations in the Io torus. *Adv. Space Res.* 5, 337-345.

Pilcher, C.B., W. H. Smyth, M. R. Combi, and J. H. Fertel 1984. Io's sodium directional features: Evidence for a magnetospheric-wind-driven gas escape mechanism. *Ap. J.* **287**, 427-444.

Pilcher, C. B., J. H. Fertel and J. S. Morgan 1985. [SII] images of the torus. *Ap. J.* **291**, 377-393.

Rauer, H., T. Bonev, K. Jockers, and N. Thomas 1993. Low resolution spectra of the Io plasma torus two days after ULYSSES encounter. Preprint.

Roesler, F. L., R. J. Oliversen, F. Scherb, J. Lattis, T. B. Williams, D. G. York, E. G. Jenkins, J. L. Lowrance, P. Zucchino and D. Long 1982. Fabry-Perot/CCD observations of [SIII] and [SII] emissions from the Jupiter plasma torus. *Ap. J.* **259** 900-907.

Sandel, B. R. and A. L. Broadfoot 1982. Io's hot torus- a synoptic view from Voyager, *J. Geophys. Res.* **87**, 212-218.

Sandel, B.R. and A.J. Dessler 1988. Dual periodicity of the Jovian magnetosphere. *J. Geophys. Res.* **93**, 5487-5504.

Scherb, F. and W. H. Smyth 1993. Variability of [OI] 6300 Å emission near Io. *J. Geophys. Res.* **98**, 18729-18736.

Schneider, N. M. 1988. Sodium in Io's extended atmosphere. Ph.D. Thesis, Department of Planetary Sciences, University of Arizona.

Schneider, N. M., D. M. Hunten, W. K. Wells, A. B. Schultz and U. Fink 1991a. The structure of Io's corona, *Ap.J.* **368**, 298-315.

Schneider, N. M., J. T. Trauger, J. K. Wilson, D. I. Brown, R. W. Evans, and D. E. Shemansky 1991b. Molecular origin of Io's fast sodium. *Science* **253**, 1394-1397.

Sieveka, E.M. and R. E. Johnson 1985. Nonisotropic coronal atmosphere on Io. J. *Geophys. Res.* **90**, 5327-5331.

Smyth, W.H. 1979. Io's sodium cloud: Explanation of the east-west asymmetries. *Ap. J.* **234**, 1148-1153.

Smyth, W. H. 1983. Io's sodium cloud: Explanation of the east-west asymmetries. II. *Ap. J.* **264**, 708-725.

Smyth, W.H., and M. R. Combi 1987. Correlating east-west asymmetries in the jovian magnetosphere and the Io sodium cloud. *Geophys. Res. Lett.* **14**, 973-976.

Smyth, W.H. and M.R. Combi 1988a. A general model for Io's neutral gas cloud. I. Mathematical description. *Ap. J. Supp.* **66**, 397-411.

Smyth, W.H., and M. R. Combi 1988b. A general model for Io's neutral gas cloud.

II. Application to the sodium cloud. *Ap. J.* **328**, 888-918.

Smyth, W.H. and M. R. Combi 1991. The sodium zenocorona. *JGR* **96**, 22711-22727.

Smyth, W.H. and M. R. Combi 1993. Io's sodium corona and spatially extended cloud: a consistent flux speed distribution. *Icarus*, submitted.

Smyth, W. H. and B. A. Goldberg 1993. Correlating system III longitudinal asymmetries in the jovian magnetosphere and the Io sodium cloud. Paper in preparation.

Smyth, W. H., and M. B. McElroy 1978. Io's sodium cloud: Comparison of models and two-dimensional images. *Ap.J.* **226**, 336-346.

Trafton, L. 1980. The Jovian SII torus: its longitudinal asymmetry. *Icarus* **42**, 111-124.

Trafton, L., T. Parkinson, and W. Macy, Jr. 1974. The spatial extent of sodium emission around Io. *Ap. J.* **190**, L85-L89.

Trafton, L., and W. Macy, Jr. 1978. On the distribution of sodium in the vicinity of Io. *Icarus* **33**, 322-335.

Trauger, J. T. 1984. The Jovian nebula: A post-Voyager prespective. *Science* **226**, 337-341.

Trauger, J. T., G. Münch and F. L. Roesler 1980. A study of the Jovian [SII] nebula at high spectral resolution. *Ap. J.* **236**, 1035-1042.

Wehinger, P. A., S. Wyckoff, and A. Frohlich 1976. Mapping of the sodium emission associated with Io and Jupiter. *Icarus* **27**, 425-428.

Wilson, J. K. and N. M. Schneider 1993. Io's fast sodium: Implications for molecular and atomic escape. preprint.

Table 1. Spatially Observed Characteristics of the Io Sodium Emission in the Jupiter System

	Observed Characteristic	Identification	Modeling Studies	Explanation
1.	Io Corona			
	Discovery	Brown (1974)		
	East-West Asymmetry Spatial Structure	Bergstralh et al. (1975, 1977)	Smyth (1979; 1983) Sieveka and Johnson (1985) McGrath and Johnson (1987)	Plasma Torus Sink
		Schneider et al (1991a)	Smyth and Combi (1993)	Plasma Impact Source
2.	Predominate Forward Cloud	Trafton et al. (1974) Murcray (1978) Matson et al. (1978) Murcray and Goody (1978) Goldberg et al. (1980)	Carlson et al. (1975) Matson et al. (1978) Smyth and McElroy (1978) Smyth (1983) Smyth and Combi (1988b)	Radial Structure of the Plasma Torus
3.	Dependence on Forward Cloud on Satellite PhaseAngle	(same as above)	(same as above)	Primarily a Changing Geometric Viewing Perspective
4.	Forward Cloud East-West Asymmetries			
	Intensity Asymmetry	Goldberg and Smyth (1993)	---	Plasma Torus Sink
	Phase Lag Asymmetry	Goldberg et al. (1978, 1984)	Smyth (1979; 1983) Smyth and Combi (1987, 1988b)	Solar Radiation Pressure
5.	Trailing Directional Features	Pilcher et al. (1984) Goldberg et al. (1984) Goldberg and Smyth (1993)	Pilcher et al. (1984)	High Speed Sodium and Oscillating Plasma Torus
6.	System III Asymmetry of the Sodium Cloud near Western Elongation	Goldberg et al. (1984) Goldberg and Smyth (1993)	(This Paper)	System III and East-West Plasma Torus Asymmetries
7.	Forward Jet	Pilcher (1980); Pilcher et al. (1984) Schneider (1988) Schneider et al. (1991b)	Wilson and Schneider (1993)	High Speed Spatially-Distributed Sodium Source
8.	Magneto-nebula or Zenocorona	Wehinger et al. (1976) Trafton and Macy (1978) Pilcher and Schempp (1979) Mendillo et al. (1990)	Smyth and Combi (1991) Flynn et al. (1992)	High Speed Io and Spatially-Distributed Sodium Source

Table 2
1981 Region B/C Images: Observing Chronology

Date of Observations	Start Conditions			End Conditions		
	Time (UT)	Io Phase Angle (deg)	Magnetic Longitude of Io† (deg)	Time (UT)	Io Phase Angle (deg)	Magnetic Longitude of Io† (deg).
25 March	7:03	25.2	275.3	8:23	36.5	312.7
5 April	5:18	89.6	365.0	7:40	109.5	70.9
6 April	4:33	287.3	290.7	5:52	298.5	327.3
6 April	6:38	305.1	348.5	7:44	314.4	19.1
28 April	4:21	84.0	200.2	8:50	121.9	324.9
29 April	3:18	279.2	117.5	7:15	312.9	227.1
4 May	3:10	215.4	209.2	9:50	272.4	34.1
5 May	3:17	60.0	159.4	9:25	111.7	330.2
6 May	3:07	262.5	101.4	8:27	307.9	249.5
12 May	3:15	44.5	147.5	9:07	93.9	310.8
13 May	3:20	248.9	96.6	9:00	297.2	253.8
4 June	3:34	47.2	377.3	5:48	66.0	79.5
5 June	3:38	251.7	325.6	4:07	255.8	339.1
5 June	5:27	267.2	16.0	5:55	271.1	29.0
6 June	3:48	95.8	278.0	5:56	113.9	337.3
14 June	3:38	282.7	208.4	5:20	297.1	255.7

† System III (1965)

Table 3
1981 Region B/C Images: Fully Processed by MIPL

Date of Observations	Start Conditions Time (UT)	Start Conditions Io Phase Angle (deg)	Start Conditions Magnetic Longitude of Io† (deg)	End Conditions Time (UT)	End Conditions Io Phase Angle (deg)	End Conditions Magnetic Longitude of Io† (deg)	Mid-Point Conditions Io Phase Angle (deg)	Mid-Point Conditions Magnetic Longitude of Io† (deg)	Image ID Number (Tape/frames)
5 April	5:00	291.1	303.2	5:36	296.3	319.8	293.7	311.5	SIP 410/13-15
8 April	4:49	88.0	213.1	5:24	92.9	229.4	90.5	221.3	SIP 415/27-29
	7:28	110.3	286.9	7:58	114.5	300.8	112.4	293.9	*SIP 415/43-45
	7:39	111.9	292.0	8:07	115.8	305.0	113.9	298.5	*SIP 415/44-46
9 April	3:48	283.5	131.3	4:19	287.9	145.6	285.7	138.5	SIP 416/4-6
	4:22	288.3	147.0	4:53	292.7	161.4	290.5	154.2	SIP 416/7-9
4 May	3:25	217.6	216.2	3:55	221.8	230.0	219.7	223.1	SIP 417/8-10
	4:20	225.4	241.6	4:53	230.1	256.8	227.8	249.2	SIP 417/13-15
	4:56	230.5	258.2	5:33	235.8	275.3	233.2	266.8	SIP 417/16-18
	5:49	238.1	282.7	6:28	243.6	300.7	240.9	291.7	SIP 417/20-22
	7:19	250.9	324.3	7:52	255.6	339.5	253.3	331.9	SIP 417/27-29
	9:06	266.1	13.7	9:50	272.4	34.1	269.3	23.9	SIP 417/36-39
5 May	3:59	65.9	178.9	4:30	70.3	193.3	68.1	186.1	SIP 418/10-12
	4:32	70.5	194.2	5:15	76.6	214.2	73.6	204.2	SIP 418/13-16
	6:34	87.7	250.9	7:10	92.7	267.6	90.2	259.3	SIP 418/24-26
	8:03	100.2	292.2	8:35	104.7	307.0	102.5	299.6	SIP 418/31-33
6 May	5:36	283.6	170.4	6:10	288.5	186.1	286.1	178.3	SIP 419/19-21
	6:11	288.6	186.6	6:43	293.2	201.4	290.9	194.0	SIP 419/22-24
2 May	3:28	46.4	153.5	3:55	50.2	166.0	48.3	159.8	SIP 420/6-8
	4:10	52.3	173.0	4:40	56.5	186.9	54.4	180.0	SIP 420/10-12
	5:05	60.0	198.5	6:28	71.6	237.0	65.8	217.8	SIP 420/15-20
	6:30	71.9	238.0	7:09	77.4	256.1	74.7	247.1	SIP 420/21-23
	8:28	88.5	292.7	9:07	93.9	310.8	91.2	301.8	SIP 420/30-32
13 May	3:28	250.1	100.3	4:03	255.1	116.4	252.6	108.4	SIP 421/21-23
	4:43	260.8	134.9	5:04	263.7	144.6	262.3	139.8	SIP 421/27-28
	5:42	269.1	162.2	6:07	272.7	173.8	270.9	168.0	SIP 421/32-33
	6:09	273.0	174.7	6:47	278.4	192.3	275.7	183.5	SIP 421/34-36
	6:49	278.7	193.2	7:23	283.5	208.9	281.1	201.1	SIP 421/37-39
	7:25	283.8	209.8	7:58	288.5	225.1	286.2	217.5	SIP 421/40-42
	8:00	288.7	226.0	8:35	293.7	242.2	291.2	234.1	SIP 421/43-45
	8:25	292.3	237.6	9:00	297.2	253.8	294.8	245.7	SIP 421/45-47
June	4:19	100.2	292.4	4:53	105.0	308.1	102.6	300.3	SIP 424/10-12
14 June	3:47	284.0	212.6	4:28	289.8	231.5	286.9	222.1	SIP 425/6-9
	4:17	288.2	226.5	5:05	295.0	248.7	291.6	237.6	SIP 425/9-12

† System III (1965)
* images processed are redundant

Table 4
Observed East-West Brightness Asymmetries in the Jupiter System

Species	Observational Mode	Emission Line (Å)	West/East Brightness Ratio	Reference
Na	Ground based	5889, 5895	~ 0.8	Bergstralh et al. (1975, 1977)
S^{++}	Voyager 1	685	~ 1.3	Sandel and Broadfoot (1982)
S^{+}	Ground based	4069	~ 2	Morgan (1985a,b)
		6731	~ 1.8	
O^{+}	Ground based	3726	~ 2.2	Morgan (1985a,b)
O	IUE	1356	~ 1.4	Ballester (1989)
S	IUE	1479	~ 1.7	Ballester (1989)
		1814	~ 1.5	
		1900, 1914	~ 1.3	
S^{+}	IUE	1256	~ 1.8	McGrath et al. (1990)
S^{++}	IUE	1729	~ 1.3	McGrath et al. (1990)
O	Ground based	6300	~ 1.5	Scherb and Smyth (1993)

Table 5
1981 Observations of the Io Plasma Torus

Reference	Observing Dates	O II (3726Å)	O II (3729Å)	S II (4069Å)	S II (4076Å)	S II (6716Å)	S II (6731Å)	S III (9531Å)
Brown and Shemansky (1982)	Feb 23, 24					✓	✓	
	April 25, 26, 27					✓	✓	
Morgan (1985 a, b)	February 14, 15, 16, 17	✓	✓	✓	✓	✓	✓	
	March 20, 21, 22, 23	✓	✓	✓	✓	✓	✓	
	April 21, 22, 23, 24	✓	✓	✓	✓	✓	✓	
	May 2, 3, 4	✓	✓	✓	✓	✓	✓	
Pilcher et al. (1985)	Mar 10, 11, 12, 13						✓	
	April 10, 11, 13						✓	
Oliversen et al. (1991)	Feb 16					✓	✓	✓
	Mar 25					✓	✓	✓
	Mar 26					✓	✓	

FIGURE CAPTIONS

FIG. 1. Observing Parameters for the 1981 Io Sodium Cloud Image Data for Table Mountain Observatory. The solid lines show the complete angular coverage for the data as listed in Table 1. The dots and squares show the mid-point conditions for the 34 completely reduced images listed in Table 2.

FIG. 2. 1981 May 13 Region B/C Image West Cloud Sequence. Four D_2 emission images of the sodium cloud in Table 3 as measured on the sky plane are shown in contour plot format and in proper spatial relationship to Jupiter, Io's location, and Io's circular orbit which appears as a thin ellipse. Contour brightness levels in kiloRayleighs, from outside to inside, are spaced as follows: 0.2, 0.5, 1.0, 2.0, 5.0, 10.0, 20.0.

FIG. 3. 1981 Region B/C Images East of Jupiter. Six D_2 emission images of the sodium cloud in Table 3 as measured on the sky plane east of Jupiter in 1981 are shown in contour plot format and in proper spatial relation to Jupiter, Io's location, and Io circular orbit. Contour brightness levels in kiloRayleighs, from outside to inside, are spaced as follows, 0.1, 0.2, 0.5, 1.0, 2.0, 5.0, 10.0 and 20.0.

FIG. 4. System III Variability of the Io Plasma Torus East and West of Jupiter. The intensity of the Io plasma torus in the 6731 Å emission line of S^+ measured near 5.5 Jupiter radii from the planet's center by Morgan (1985b) in Run 4 (May 2 - 4, 1981) is shown as a function of the System III longitude angle. Lines connect data points taken on the same night. Open symbols were taken to the east of Jupiter and filled symbols to the west of Jupiter.

FIG. 5. Lifetime of Sodium at Io's Location. The sodium lifetime at Io's location in units of hours is shown as a function of the Io System III magnetic longitude angle and the Io geocentric phase angle for a plasma torus description that is in (a) inherently symmetric and in (b) inherently asymmetric in the System III longitude angle.

FIG. 6. Lifetime of Sodium in the Plasma Torus at Eastern and Western Elongation. The sodium lifetime , in units of hours, is shown in the coordinate frame of the plasma torus for a plasma torus description that is inherently symmetric in System III longitude. The location of Io in the coordinate frame of plasma torus for these two elongation pictures varies periodically as a function of the System III magnetic longitude of the satellite and is shown by the dark oval. The radial location where the peak enhancement of the inherently System III longitude asymmetry occurs is indicated by the black dot.

FIG. 7. West Sodium Cloud Model Calculations for a Longitudinally Inherently Asymmetric Plasma Torus Sink. Model calculations for the D_2 emission brightness of the four images in Figure 2 are shown with the same adopted contour levels. An inherently asymmetric plasma torus description in System III longitude and a monoenergetic (2.6 km sec^{-1}) uniform and isotropic sodium source ejected from an exobase radius of 2600 km are assumed. The sodium flux, referenced to Io's surface area, is 2×10^8 atoms cm^{-2} sec^{-1}.

FIG. 8. West Sodium Cloud Model Calculations for a Longitudinally Inherently Symmetric Plasma Torus Sink. Model calculations for the D_2 emission brightness of the four images in Figure 2 are shown with the same adopted contour levels but for an inherently symmetric plasma torus description in System III longitude. The sodium source is the same as in Figure 7.

FIG. 9. East Sodium Cloud Model Calculations for a Longitudinally Inherently Asymmetric Plasma Torus Sink. Two model calculations for the D_2 emission brightness of the first April 28 image of Figure 3 are shown on the sky plane with the same adopted contour levels of Figure 3. The plasma torus sink for sodium is the same as in Figure 7. For both the isotropic and band sources, a monoenergetic (2.6 km sec^{-1}) ejection of sodium was assumed with the same exobase radius and uniform flux as adopted in Figure 7.

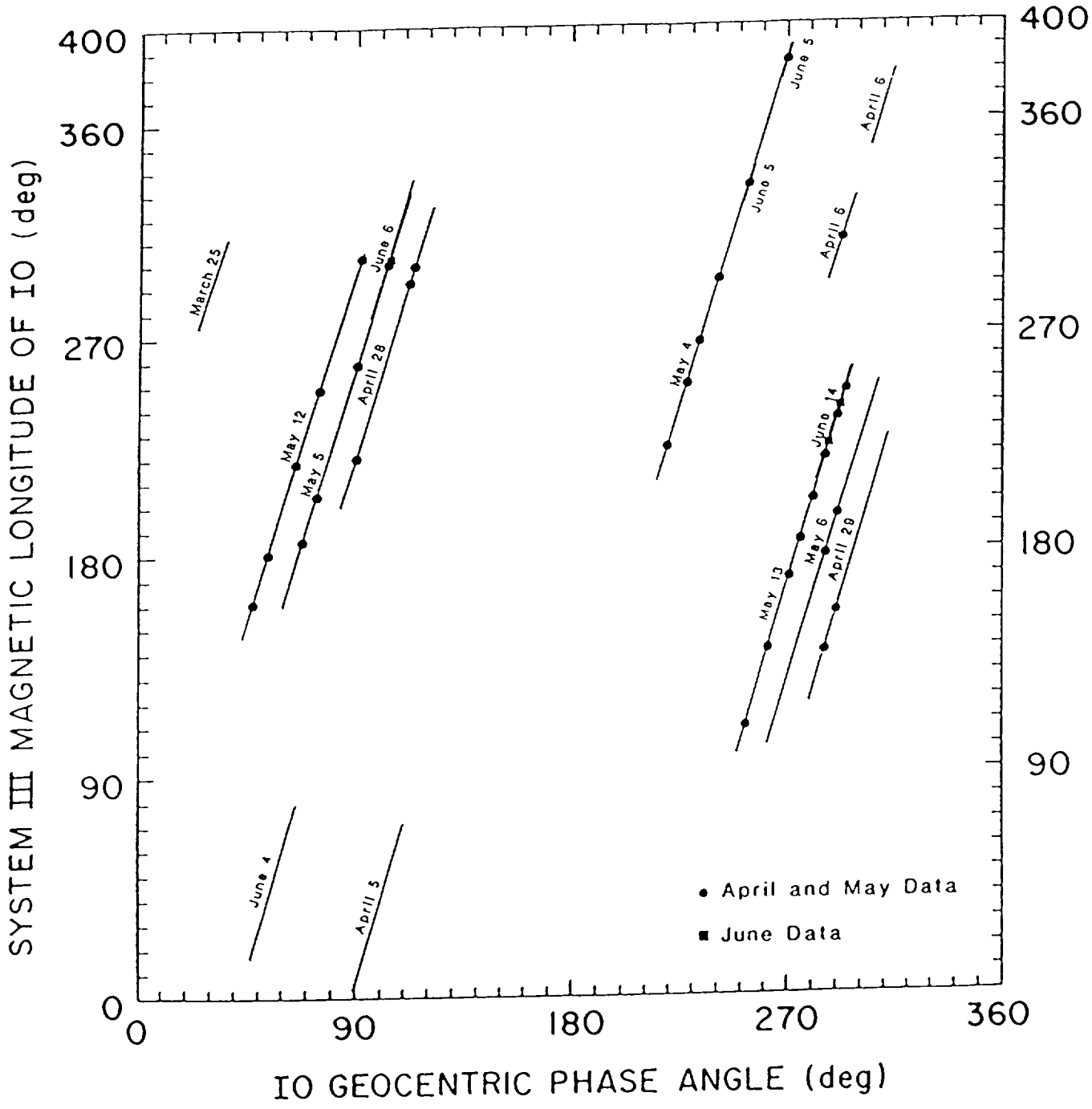
SYSTEM III MAGNETIC LONGITUDE OF IO (deg)
IO GEOCENTRIC PHASE ANGLE (deg)
0
90
180
270
360
400
March 25
June 6
May 12
May 5
April 28
June 4
April 5
June 5
June 5
April 6
April 6
May 4
June 14
May 13
May 6
April 28
• April and May Data
■ June Data

Figure 1

D_2 BRIGHTNESS OF THE SODIUM CLOUD

(JPL IMAGE DATA: MAY 13, 1981)

(CONTOUR LEVELS: 0.2, 0.5, 1, 2, 5, 10, kR)

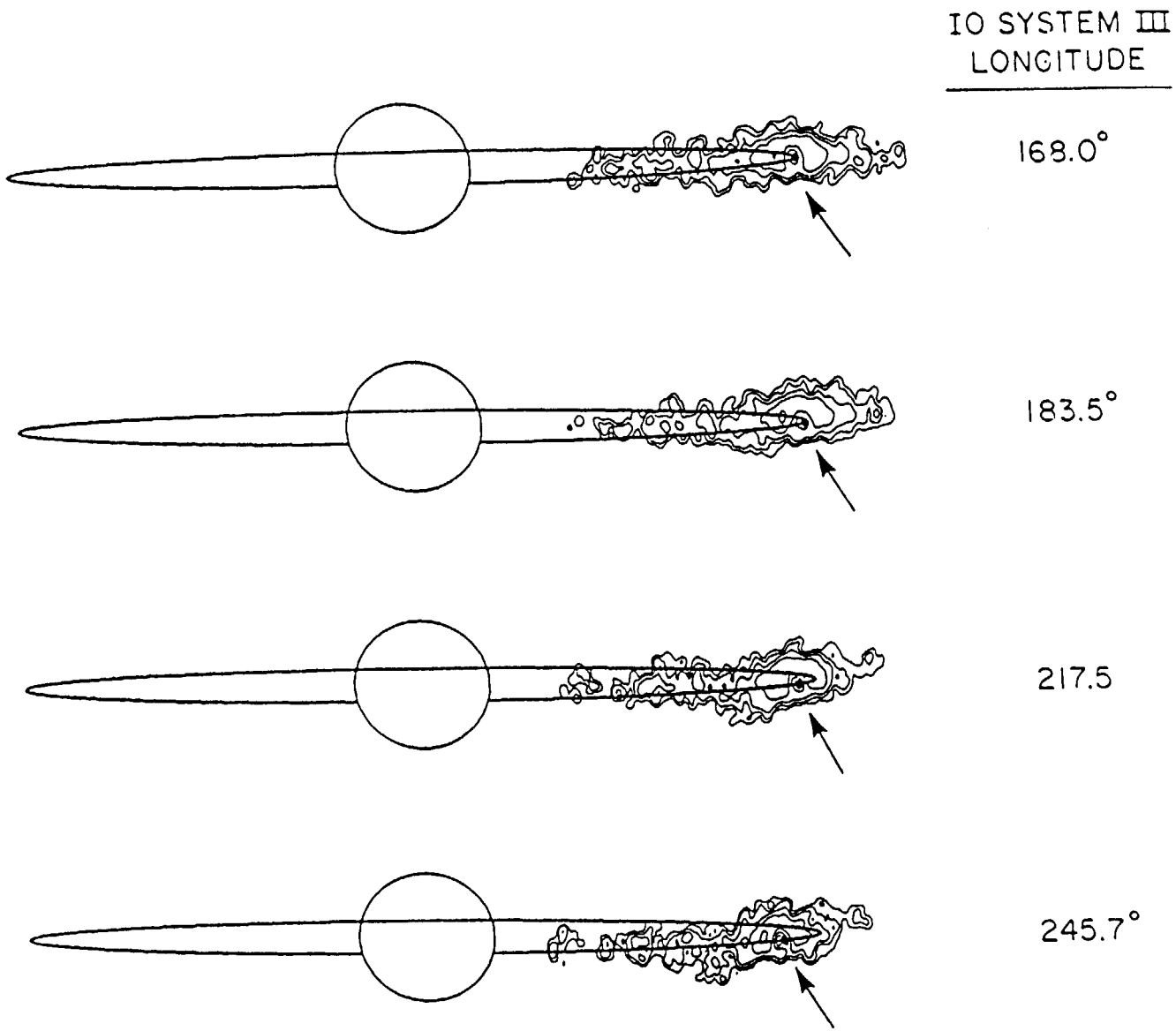

Figure 2

D2 BRIGHTNESS OF THE SODIUM CLOUD

(JPL IMAGE DATA)

(CONTOUR LEVELS : 0.2, 0.5, 1, 2, 5, 10 kR)

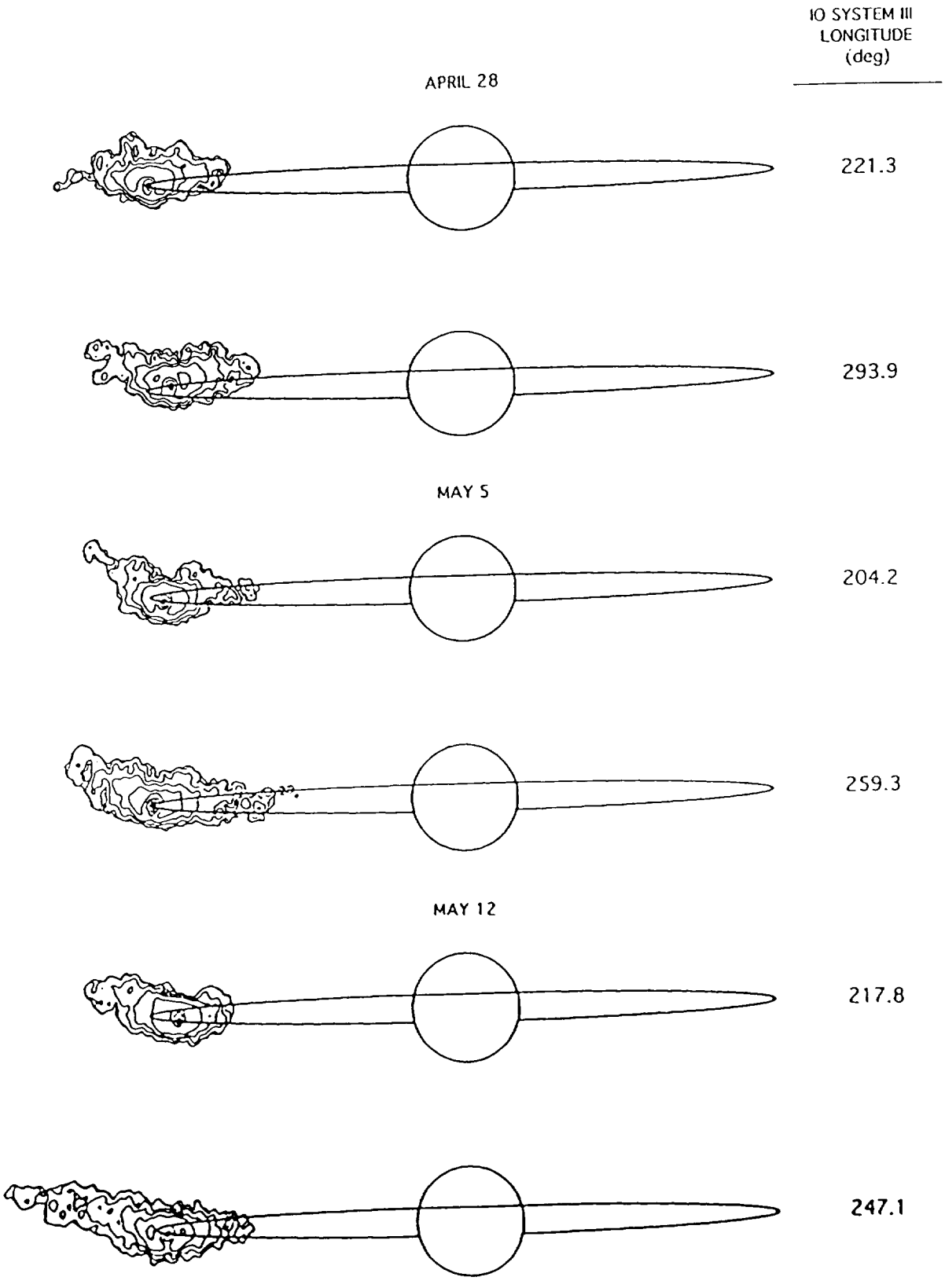

Figure 3

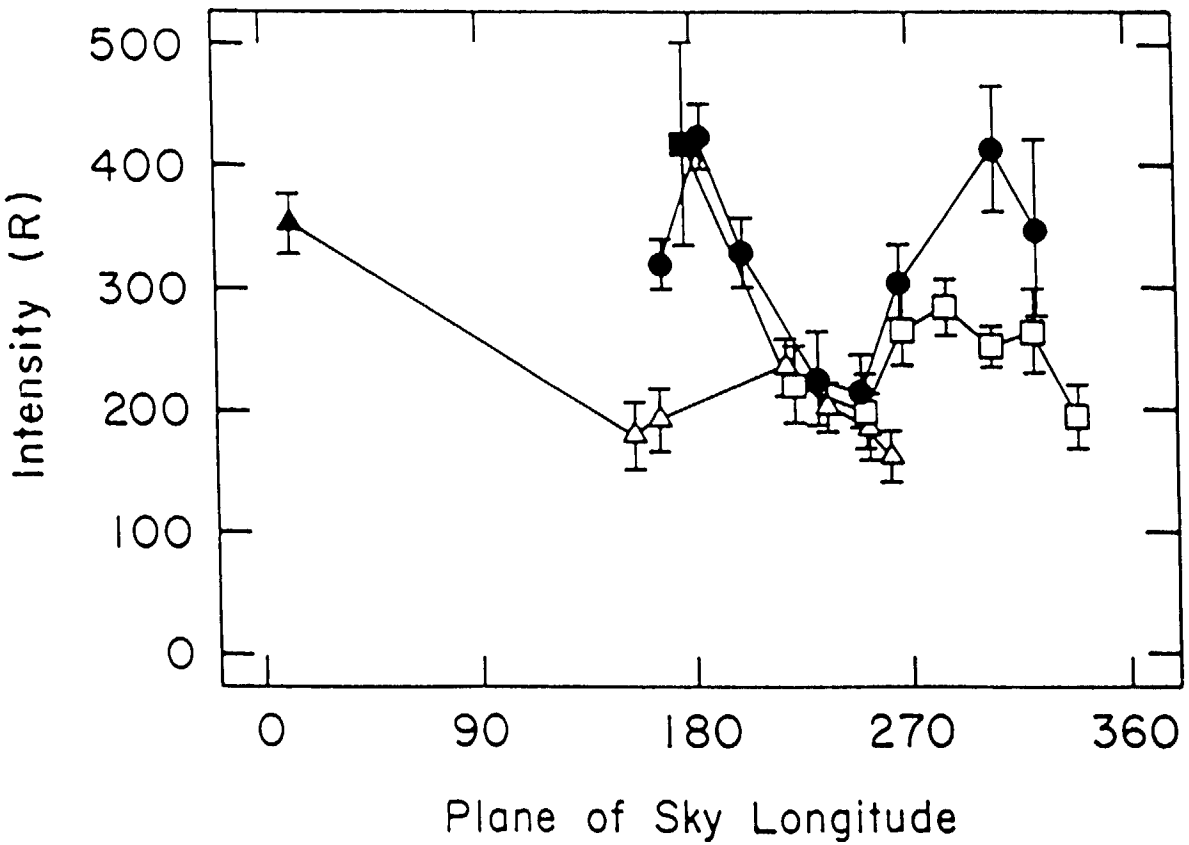
500
400
300
200
100
0
Intensity (R)
0
90
180
270
360
Plane of Sky Longitude

Figure 4

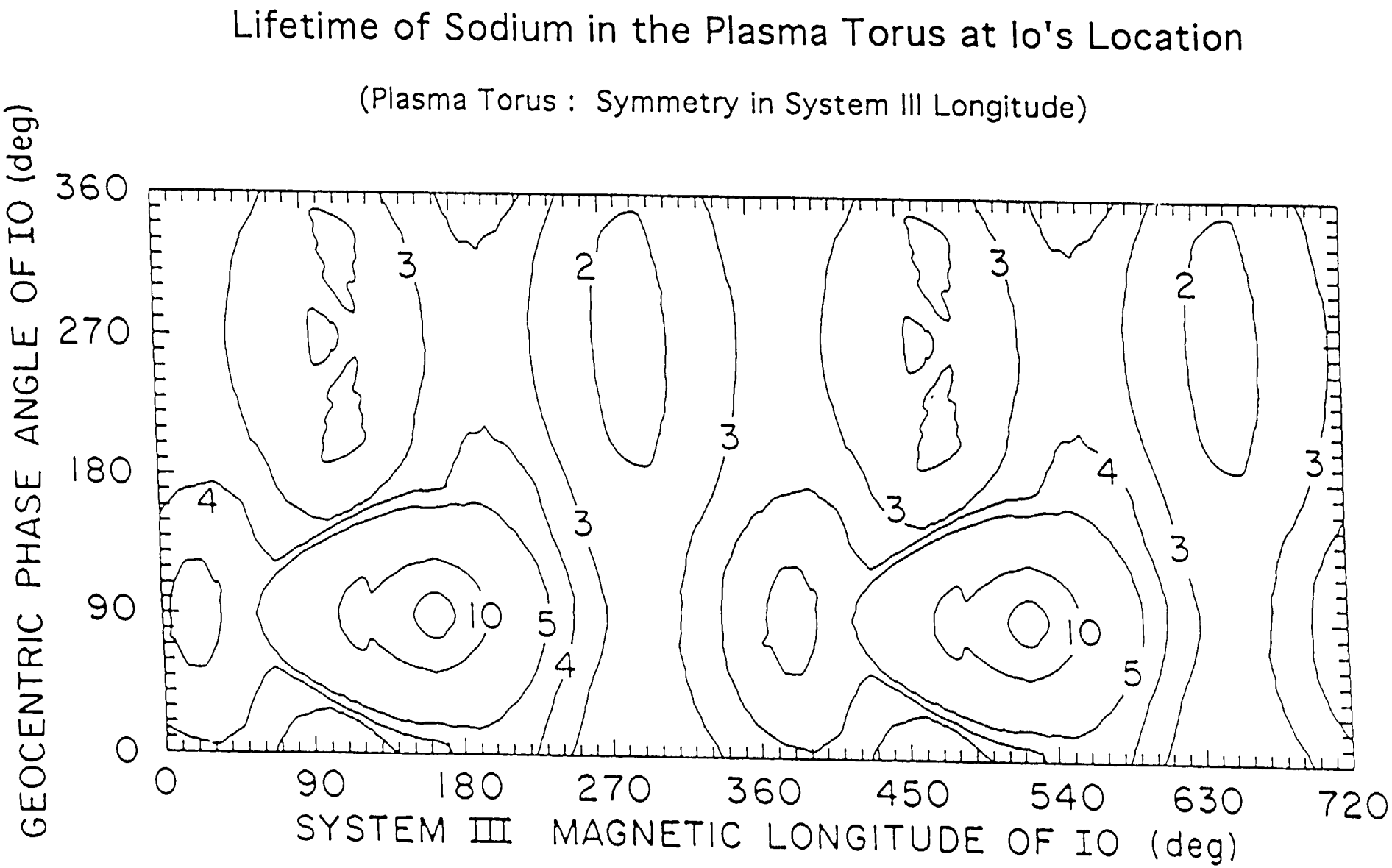
Lifetime of Sodium in the Plasma Torus at Io's Location
(Plasma Torus : Symmetry in System III Longitude)
GEOCENTRIC PHASE ANGLE OF IO (deg)
360
270
180
90
0
0
90
180
270
360
450
540
630
720
SYSTEM III MAGNETIC LONGITUDE OF IO (deg)
2
3
4
5
10

Figure 5a

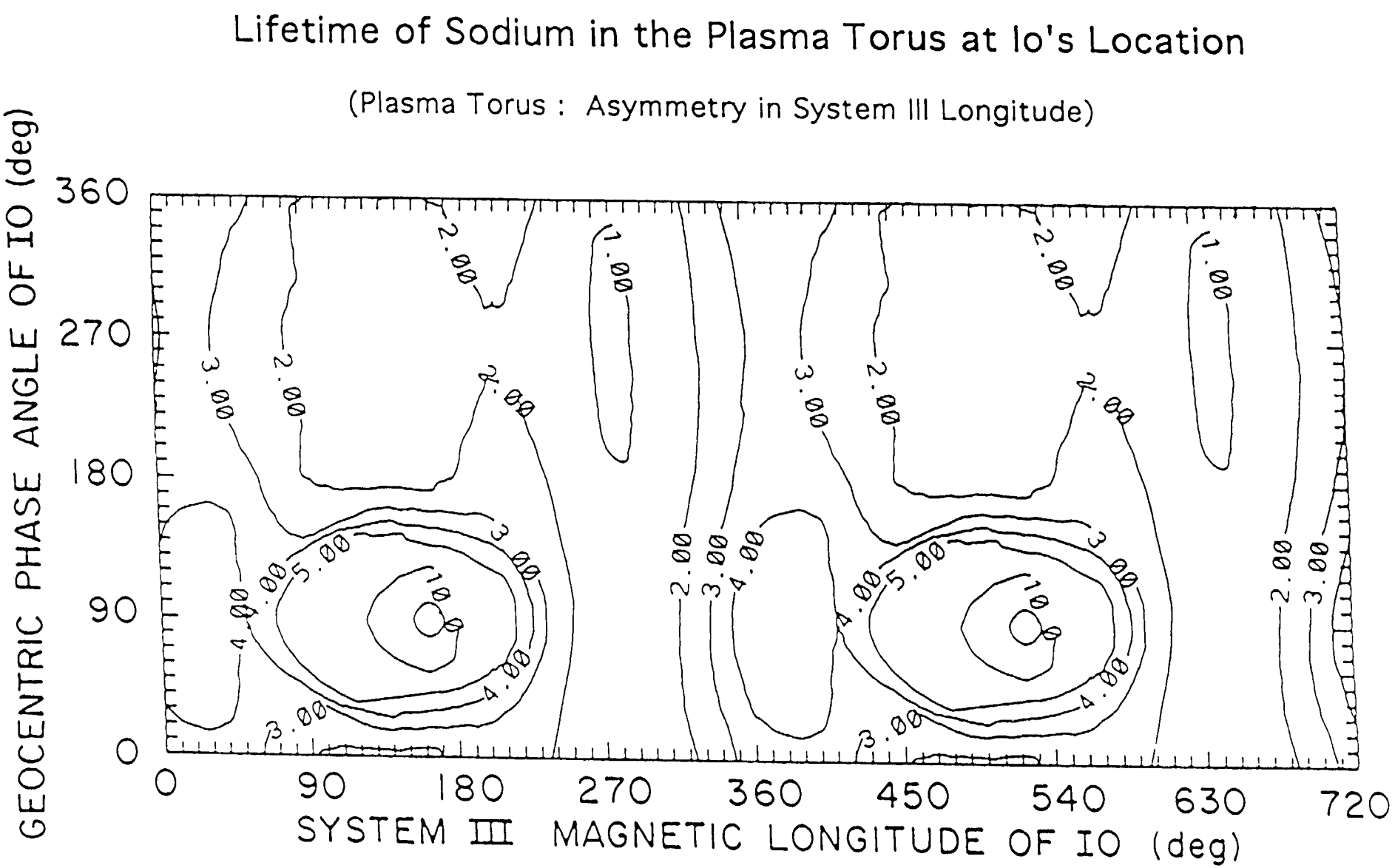
Lifetime of Sodium in the Plasma Torus at Io's Location
(Plasma Torus : Asymmetry in System III Longitude)
GEOCENTRIC PHASE ANGLE OF IO (deg)
360
270
180
90
0
0
90
180
270
360
450
540
630
720
SYSTEM III MAGNETIC LONGITUDE OF IO (deg)
1.00
2.00
3.00
4.00
5.00
10.00

Figure 5b

ELECTRON IMPACT LIFETIME OF SODIUM IN THE PLASMA TORUS
(HOURS)

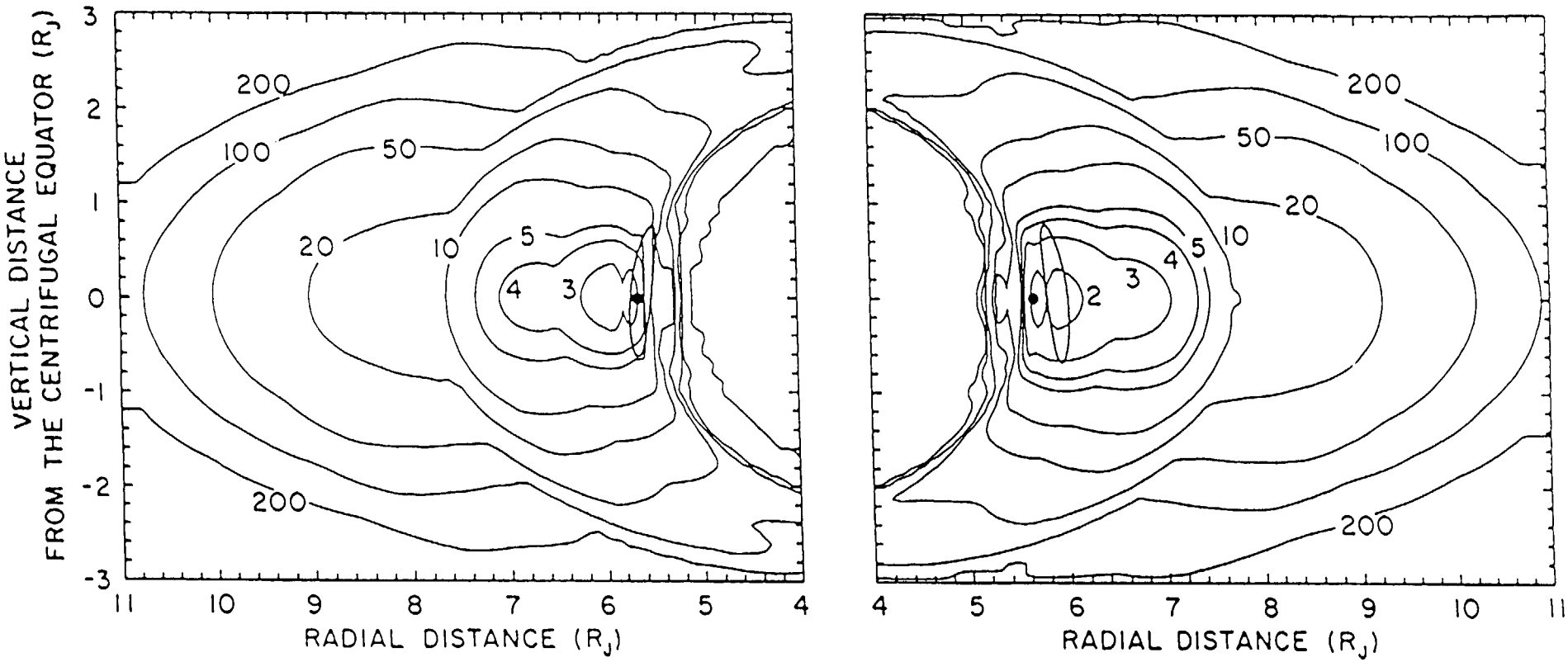

Figure 6

D_2 BRIGHTNESS OF THE SODIUM CLOUD
(MODEL)

SINK : LONGITUDINALLY ASYMMETRIC
SOURCE : ISOTROPIC, MONOENERGETIC

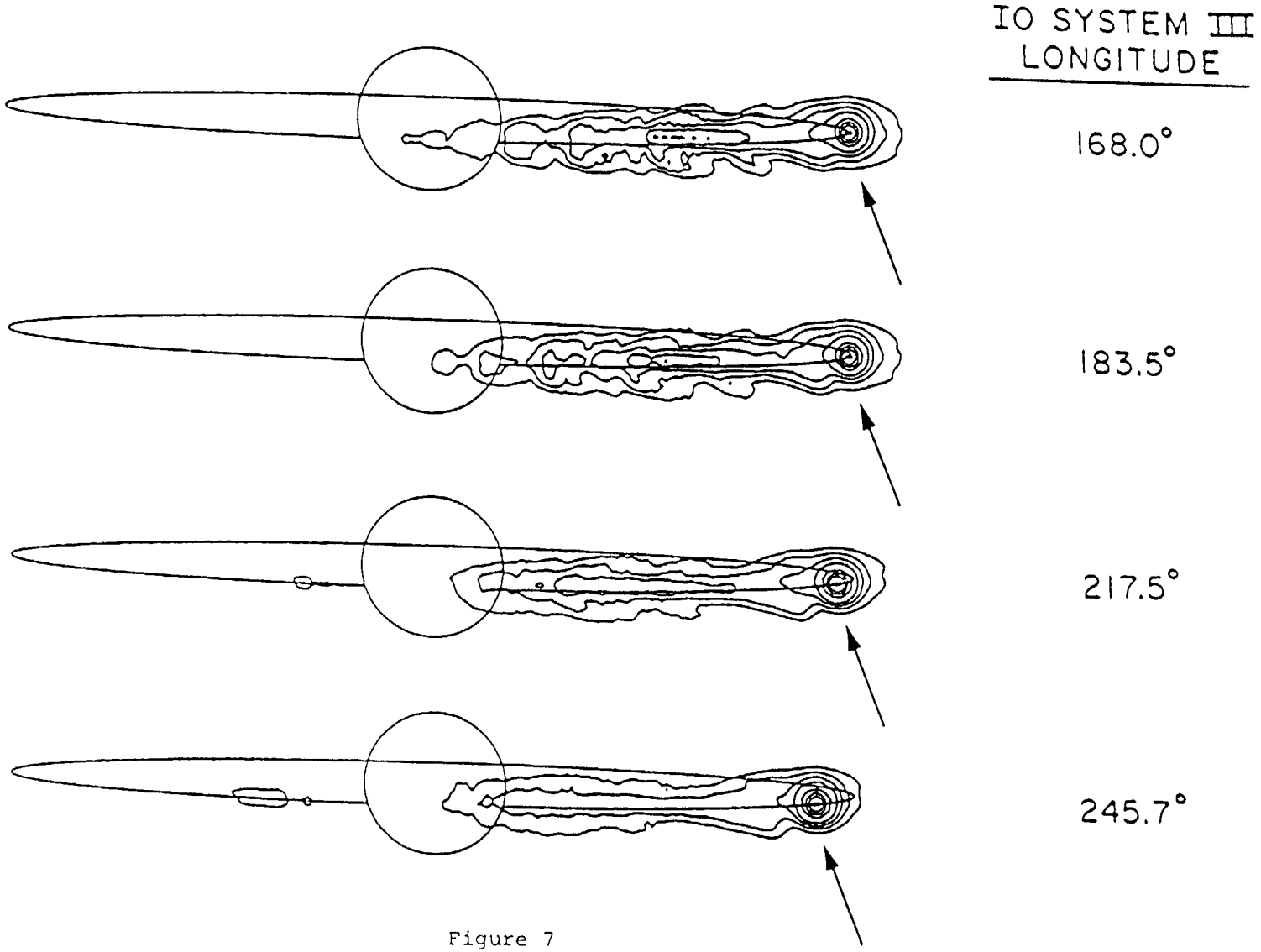

Figure 7

D_2 BRIGHTNESS OF THE IO SODIUM CLOUD

(MODEL)

SINK : LONGITUDINALLY SYMMETRIC

SOURCE : ISOTROPIC, MONOENERGETIC

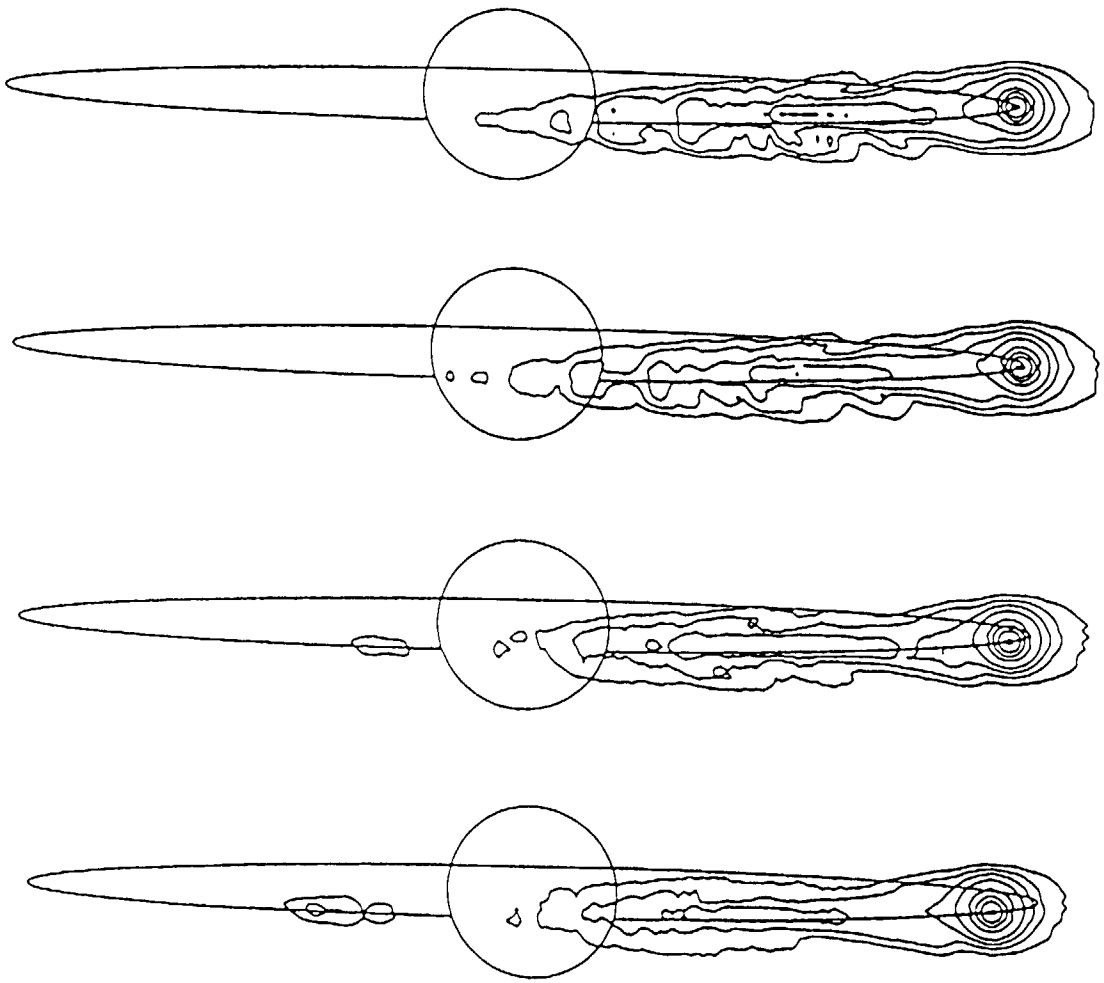

IO SYSTEM III LONGITUDE

168.0°

183.5°

217.5°

245.7°

Figure 8

D_2 BRIGHTNESS OF THE SODIUM CLOUD
(MODEL)

SINK : LONGITUDINALLY ASYMMETRIC

SOURCE		IO SYSTEM III LONGITUDE
SYMMETRIC	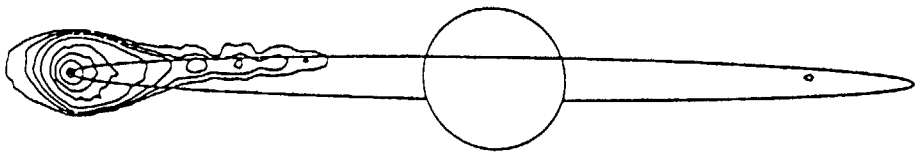	221.3°
BAND	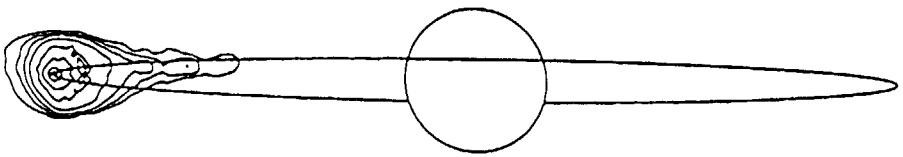	221.3°

Figure 9